Keele
University

Localized bulging in an inflated hyperelastic tube: the effects of rotation, multi-layering and torsion

Ali Abdullah Althobaiti

Submitted in partial fulfilment of the requirements of the degree of
Doctor of Philosophy

Keele University
School of Computing and Mathematics

June 2020

I certify that this thesis submitted for the degree of Doctor of Philosophy is the result of my own research, except where otherwise acknowledged, and that this thesis has not been submitted for a higher degree to any other university or institution.

Acknowledgements

Abstract

In this thesis, we start by considering a hyperelastic circular solid cylinder or tube that is rotating about its axis of symmetry with angular velocity ω. If the resultant axial force F is fixed, it is shown that the bifurcation condition for a solid cylinder or a tube that is shrink-fitted to a rigid circular cylindrical spindle is simply given by $d\omega/d\lambda_z = 0$, where λ_z is the axial stretch. When the spindle is absent (the case of unconstrained rotation), we also allow for the possibility that the tube is additionally subjected to an internal pressure P. It is shown that with P fixed, and ω and F both viewed as functions of the circumferential stretch λ_a and λ_z, the bifurcation condition for localized bulging is that the Jacobian of ω and F should vanish.

The second part of the thesis studies localized bulging in an inflated bilayer tube under inflation and axial extension. Firstly, bulging prevention in a hyperelastic bilayer tube composed of the Gent material is investigated. We determine several critical parameter regimes where localized bulging disappears, when one layer (layer I) of the tube cannot bulge whereas the other part (layer II) can. Surprisingly, we find that localized bulging still occurs if the proportion of layer II exceeds a critical value, no matter whether it occupies the inner layer or outer layer. Secondly, we focus on the effect of modulus ratio between two layers on the bulge formation. If the thickness of the bilayer tube is specified, the composite tube is more stable when the stiffer part occupies the outer layer. Moreover, the critical volume ratio v_{cr} as a function of the interfacial radius D has a maximum if $s > 1$ but a minimum if $s < 1$, where s is the ratio of the shear modulus of the outer layer to that of the inner layer.

Finally, we turn our attention to study the effect of torsion on the onset of localized bulging. When the twisting moment M is fixed, the bifurcation condition for localized bulging is that the Jacobian of the internal pressure P and the resultant axial force F should vanish. It is found that the onset of localized bulging can be delayed or removed when a torsion is applied to the tube.

Contents

List of Figures

List of Tables

Chapter 1

Introduction

When a hyperelastic tube is inflated by an internal pressure, the tube first expands cylindrically until the pressure reaches a critical value. Subsequently, a localized bulge appears at one point of the tube, and this state is known as the initiation stage. As inflation is continued into the tube, the pressure drops while the bulge grows until it reaches a maximum size (the growth stage). With continued inflation, the bulge propagates axially along the tube at a constant propagation pressure (the propagation stage); see Figure (1.1). This process has been illustrated by several authors. The earliest study of localized bulging in an inflated isotropic tube seems to have been by Mallock (1891), although the material was modelled by a linear constitutive law. Yin (1977) studied the propagation stage and made some assumptions on the strain-energy function. Therefore, he studied the progression of the bulge in cylindrical membranes
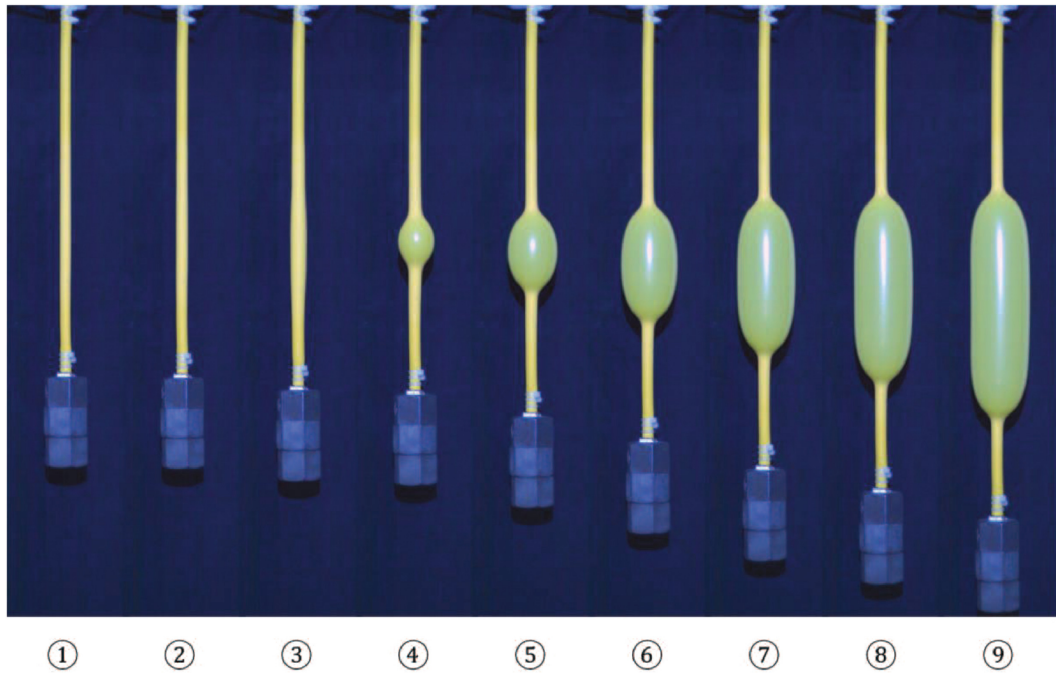
Figure 1.1: Representation of the whole bulging process (Wang et al., 2019). (1) apply a dead weight (2) inflation (3)-(4) the initiation stage (5)-(6) the growth stage (7)-(9) the propagation stage.

using Mooney and Hard-Smith models at small and large strains, respectively. Chater and Hutchinson (1984) show that the propagation pressure can be obtained by the use of Maxwell's equal-area rule.

One of the most important applications of localized bulging is in the mathematical modelling of aneurysm initiation in human arteries. An aneurysm is a bulge in a blood vessel due to the weakness of its wall; see Figure (1.2). Localized bulging in inflated tubes is similar to aneurysm formation. Thus, the study of bulge formation could provide useful insights into aneurysm formation in human arteries; see Seshaiyer
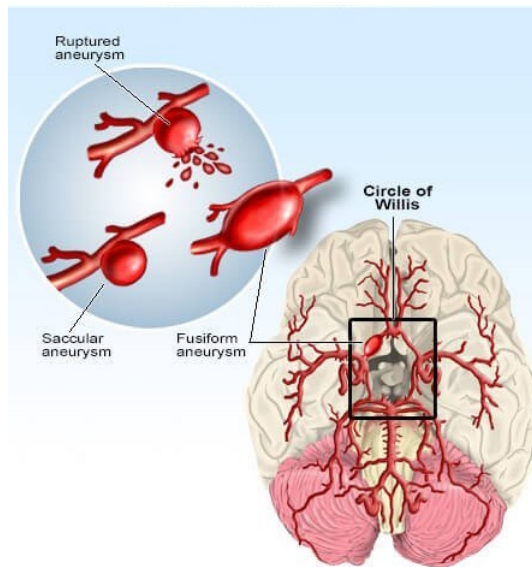
Figure 1.2: Brain aneurysm (https://www.medicinenet.com).

and Humphrey (2001), Pamplona and Mota (2012), Fu et al. (2012), Alhayani et al. (2014), Fu and Il'Ichev (2015), Varatharajan and DasGupta (2017) and Varatharajan and DasGupta (2018).

There are three distinct stages during the evolution of localized bulging: initiation, growth, propagation, as illustrated previously. These stages are commonly observed in other localization problems, such as propagating buckles in metal tubes (Kyriakides and Babcock, 1981), propagating necks in materials under tension (Hutchinson and Neale, 1983). Also, localized bulging is related to the so-called limiting point instability, which refers to the existence of a pressure maximum in uniform inflation, for more details see, Alexander (1971); Kanner and Horgan (2007); Mao et al. (2014); Hornỳ et al. (2015); Wang et al. (2018). Therefore, the understanding of bulging behavior

can shed light on many other localization problems, for instance, localized necking in dielectric membranes (Fu et al., 2018). Furthermore, the accuracy of hyperelastic material models, especially for moderate values of strains, can be examined by studying localized bulging in inflated tubes; see Zhou et al. (2018).

The problem of an inflated tube and the related issue of bifurcation is a classical subject in nonlinear elasticity, which has been investigated by many researchers; see, for instance, Adkins and Rivlin (1952), Green and Adkins (1960) and Kydoniefs (1969). In the bifurcation analysis of a hyperelastic tube under combined internal inflation and axial stretching/compression, early efforts were dedicated to studying periodic perturbations (Haughton and Ogden, 1979a,b), and the zero mode in the axial direction was believed to be another uniform state such that it was excluded. It was recognized recently by Fu et al. (2008) and Pearce and Fu (2010) that it is not the periodic mode but the zero mode that corresponds to localized bulging in a membrane tube. Meanwhile, a weakly nonlinear analysis was also carried out in Fu et al. (2008). In addition, the stability of bulging solutions was further studied by Fu and Xie (2010); Il'Ichev and Fu (2012), and the imperfection sensitivity has been examined in Fu and Xie (2012). On the other hand, Rodríguez and Merodio (2011) considered the equilibrium of different infinitesimal volume elements for a membrane tube subjected to internal pressure and axial loading. They rederived the bifurcation criteria for three bifurcation modes, including a prismatic mode, a bulging mode, and a composite mode. Under the membrane assumption, the effect of constitutive models on the bulge initiation was studied by Pearce (2012) for the cases of fixed axial force and fixed axial

length.

It is worth mentioning that in most of the above-mentioned theoretical works, the tube is modeled as a membrane, such that there is no bending stiffness. Fu et al. (2016) started from the exact theory of nonlinear elasticity to study bulging behavior in a tube of arbitrary thickness. Also, the accuracy of the membrane theory was examined. Most importantly, they derived an explicit bifurcation condition for localized bulging, and the effects of tube thickness and different constitutive models were discussed in detail. Indeed, the explicit bifurcation condition derived by Fu et al. (2016) makes it possible to explore the bulging behavior in double-fiber reinforced or layered tubes in the framework of finite elasticity. Using the bifurcation condition derived in the latter paper, Wang and Fu (2018) investigate the effects of fibre reinforcement on localized bulging of an inflated hyperelastic tube of arbitrary thickness. Furthermore, the applicability of the bifurcation condition derived by Fu et al. (2016) to layered structures is also validated by direct numerical evidence in Liu et al. (2019).

In practice, two different loading types are usually adopted for a tube under combined internal inflation and uniaxial tension, i.e., either the resultant axial force or the axial length is fixed. The former case can be achieved by suspending an object on one end and inflating the tube from the other end; see Figure (1.1). In this case, the movement of one end of the tube is unrestricted, and a distinctive feature is that the pressure against the volume (or the circumferential stretch) curve has an N shape if localized bulging occurs at a critical pressure. Furthermore, bifurcation leading to localized bulging is a result of the limit-point instability. Also, the propagation pressure can
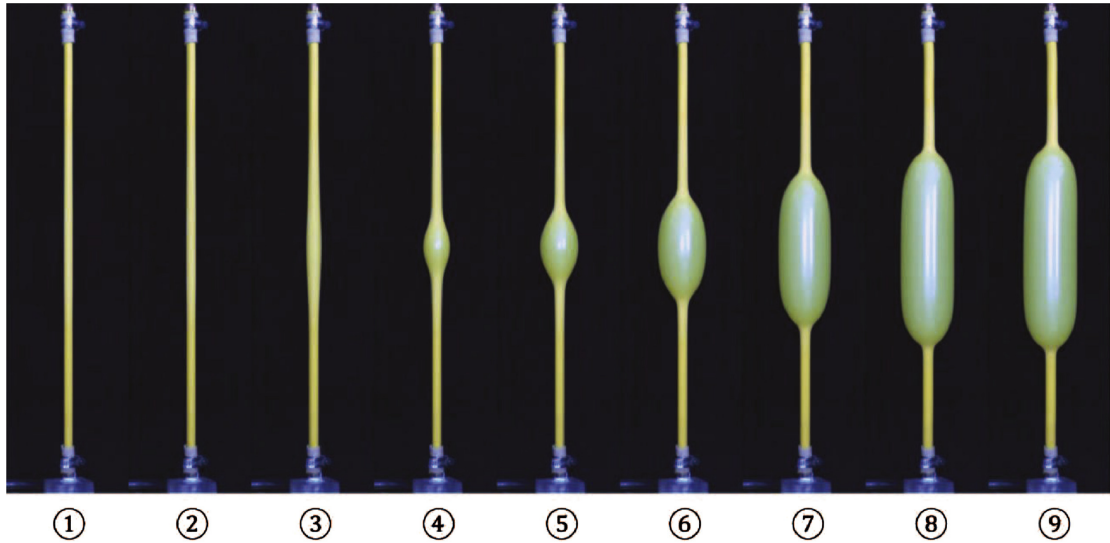
Figure 1.3: Localized bulging in the case of fixed axial length (Wang et al., 2019).

be determined by Maxwells equal-area rule. For the other loading type, a tube is first stretched to a prescribed value, and then the length is fixed; see Figure (1.3). In this situation, the behavior of pressure against volume might be monotonic. In this case, localized bulging also occurs if the internal pressure P exceeds a critical value, which provides a correspondence between the artery aneurysm and mechanical bifurcation.

Experimentally, pioneering works by Kyriakides and Chang (1990, 1991) explained many features of localized bulging such as pressure drop after bulge initiation in the case of fixed resultant axial force. Then, the inflation experiment was extended to textured tubes by Guo et al. (2016) and the case of fixed axial length was studied by Pamplona et al. (2006); Gonçalves et al. (2008) where comparisons with numerical solutions were also presented. Recently, Wang et al. (2019) carried out a new set of experiments guided by the newly emerged analytical results to evaluate the

imperfection sensitivity of the initiation pressure and the robustness of the propagation pressure. Since bulging bifurcation is subcritical, the experimentally measured initiation pressure is around 15% below the theoretical prediction.

Deformation of a rotating hyperelastic cylinder or tube is one of the first problems solved using the continuum mechanics theory; see for example Green and Zerna (1992) with results used to test the validity of constitutive assumptions. The question of an axisymmetric bifurcation for a rotating cylinder was studied by Patterson and Hill (1977) using the neo-Hookean material model. A significant generalization was subsequently made by Haughton and Ogden (1980a,b,c), who considered all the possible periodic buckling modes (prismatic, axisymmetric, or asymmetric) for a rotating cylinder or tube without restricting the material model in their general formulation although numerical results were presented only for the Ogden material model. In the last three studies, it was observed that the rotation speed, when viewed as a function of a stretch measure, may reach a maximum beyond which the primary deformation no longer exists. However, the connection between the limiting point instability and localized bulging bifurcation was not fully understood at that time. It is shown in Chapter 3 that under a certain loading condition, the existence of such an angular speed maximum is closely associated with axisymmetric bulging localized in the axial direction, a phenomenon rather similar to localized bulging in circular cylindrical tubes that are inflated by an internal pressure.

A common ground in Bucchi and Hearn (2013) and Wang and Fu (2018) to prevent

bulging is to reduce the extensibility of the reinforced fibers. However, in some engineering applications, for instance, the Anaconda wave energy extraction device, a very stiff tube is not applicable (Bucchi and Hearn, 2013). Consequently, we need to balance the stability and extensibility of a tube, and this is one of the motivations for the current study. Indeed, there are many kinds of constitutive models of rubber in continuum mechanics, such as the neo-Hookean model, MooneyRivlin model (Mooney, 1940), Ogden model (Ogden, 1972), Gent model (Gent, 1996) and Gent-Gent model (Pucci and Saccomandi, 2002), etc. Among them, the Gent model was proposed based on the finite extensibility of the polymeric chains in rubber, and a significant material parameter J_m represents the extension limit. In Chapter 4, we are concerned with the effect of the extension limit on bulging prevention, and thus we still adopt the Gent model. So, we want to determine the critical parameters to avoid localized bulging and then extend the current studies to layered tubes. We aim at offering an alternative to bulging prevention by using a tube that cannot bulge to cover the inside or outside of the original one.

It is well known that human arteries have a multilayer structure and they can be modeled as a bilayer tubular structure (Holzapfel et al., 2000; Gasser et al., 2005). In particular, strong evidence suggests that arteries stiffen with age (Kohn et al., 2015). Hence, in Chapter 5, we study localized bulging of an inflated bilayer tube to understand the effect of modulus ratio between two layers on the bulge formation and maximum radius at the center of the bulge. Moreover, we apply the Gent model and Ogden model to demonstrate the model insensitivity of the qualitative bifurcation

features. We wish to provide useful insight into aneurysm formation in human arteries and offers a possible way to control bulge initiation using a bilayer tube.

The deformation of a cylindrical tube under the combined action of internal inflation, extension and torsion has been studied by Rivlin (1948, 1949), Gent and Rivlin (1952), Balbi and Ciarletta (2015), Merodio and Ogden (2016) amongst others. Ren et al. (2011) found a critical thickness in a three-layered fiber-reinforced above which the limit-point instability becomes impossible. The problem of an inflated tube subject to axial extension and torsion was examined by Hamdaoui et al. (2014) for an incompressible transversely isotropic material (or a standard reinforcing model). The previous investigations are related to localized bulging only in the case of fixed axial force. The situation of fixed axial length corresponds to what human arteries are in vivo (Hornỳ et al., 2014). Thus, we wish to fill this gap in the literature in Chapter 6.

The results of Chapters 3,4 and 5 have been published in three journal articles, Wang et al. (2017); Liu et al. (2019); Ye et al. (2019).

Chapter 2

Mathematical Preliminaries

2.1 Introduction

In this Chapter we provide the basic theory of continuum mechanics which is needed for our research, including kinematics, balance laws and field equations, constitutive equations, hyperelastic materials, and strain energy functions. The fundamental concepts of continuum mechanics are presented in many books; see Ogden (1997), Taber (2004), Holzapfel (2000), and Fu and Ogden (2001). We also provide a summary of incremental equations, Stroh formulation, and the surface-impedance matrix method.

2.2 Summary of Continuum Mechanics

2.2.1 Kinematics

A body $\mathcal{B}$ can be defined as a set of particles or material points that can be put into a one-to-one correspondence with triplets of real numbers. In order to know the changes in geometric characteristics of the body, we shall call $\mathcal{B}_r$ a reference configuration or undeformed configuration and $\mathcal{B}_t$ a current configuration or deformed configuration. For our purpose, we shall use capital and small letters to indicate quantities in $\mathcal{B}_r$ and $\mathcal{B}_t$, respectively. Therefore, we have a mapping $\chi : \mathcal{B}_r \to \mathcal{B}_t$ which takes particles, associated with a position vector $\mathbf{X}$, in the reference configuration to particles in the current configuration. Then, we have

$$\mathbf{x} = \chi(\mathbf{X}, t), \quad \mathbf{X} \in \mathcal{B}_r, \tag{2.1}$$

where $\mathbf{x}$ is the position vector of $\mathbf{X}$ in $\mathcal{B}_t$ and t is time. For all coordinate systems, the differential of the position vector $\mathbf{X}$ can be written as

$$d\mathbf{X} = \frac{\partial \mathbf{X}}{\partial S_A} dS_A = \mathbf{G}_A dS_A, \tag{2.2}$$

where S_A are any set of coordinates. We also define another set of vectors $\mathbf{G}^B$ associated with $\mathbf{G}_A$ such that

$$\mathbf{G}_A . \mathbf{G}^B = \delta_{AB}, \tag{2.3}$$

where

$$\delta_{AB} = \begin{cases} 1 & \text{if } A = B \\ 0 & \text{if } A \neq B \end{cases}, \tag{2.4}$$

denotes the Kronecker delta.

In Kinematics, we are interested in how things move from the reference configuration to the current configuration. Thus, the deformation gradient tensor $\mathbf{F}$ is defined by

$$\mathbf{F} = \text{Grad } \mathbf{x} = \frac{\partial \mathbf{x}}{\partial S_A} \otimes \mathbf{G}^A, \tag{2.5}$$

where Grad is the gradient operator in $\mathcal{B}_r$ and $\otimes$ denotes the tensor product of an ordered pair of vectors. We shall use two orthonormal basis vectors $(\mathbf{E}_i)$ and $(\mathbf{e}_i)$ associated with the reference configuration and the current configuration, respectively. In rectangular coordinate systems, the deformation gradient tensor $\mathbf{F}$ can be defined as

$$\mathbf{F} = \text{Grad}\mathbf{x} = \frac{\partial(x_i \mathbf{e}_i)}{\partial X_j} \otimes \mathbf{E}_j = \frac{\partial x_i}{\partial X_j} \, \mathbf{e}_i \otimes \mathbf{E}_j, \quad i, j = 1, 2, 3. \tag{2.6}$$

If cylindrical coordinate systems are used for both $\mathbf{x}$ and $\mathbf{X}$, then

$$\mathbf{F} = \frac{\partial}{\partial R}(r\mathbf{e}_r + z\mathbf{e}_z) \otimes \mathbf{E}_R + \frac{1}{R}\frac{\partial}{\partial \Theta}(r\mathbf{e}_r + z\mathbf{e}_z) \otimes \mathbf{E}_\Theta + \frac{\partial}{\partial Z}(r\mathbf{e}_r + z\mathbf{e}_z) \otimes \mathbf{E}_Z. \tag{2.7}$$

In this case, the deformation gradient tensor can be written in matrix form as

$$\mathbf{F} = \begin{pmatrix} \dfrac{\partial r}{\partial R} & \dfrac{1}{R}\dfrac{\partial r}{\partial \Theta} & \dfrac{\partial r}{\partial Z} \\[2ex] r\dfrac{\partial \theta}{\partial R} & \dfrac{r}{R}\dfrac{\partial \theta}{\partial \Theta} & r\dfrac{\partial \theta}{\partial Z} \\[2ex] \dfrac{\partial z}{\partial R} & \dfrac{1}{R}\dfrac{\partial z}{\partial \Theta} & \dfrac{\partial z}{\partial Z} \end{pmatrix}. \tag{2.8}$$

We now consider two infinitesimal line elements $d\mathbf{X}$ and $d\mathbf{x}$ in the reference and current configurations, respectively. The relation between these elements under the deformation is then given by

$$d\mathbf{x} = \mathbf{F}d\mathbf{X}. \tag{2.9}$$

Let dV and dv be the infinitesimal volume elements in the reference and current configurations, respectively. According to the basic tensor theory (Spencer, 1980), the relationship between the two volume elements is given by

$$dv = JdV, \tag{2.10}$$

where J denotes the determinant of the deformation gradient $\mathbf{F}$. For an incompressible material, where the volume does not change during the deformation, we have

$$J = \det\mathbf{F} = 1. \tag{2.11}$$

The polar decomposition theorem, for example see Chadwick (1999), enables us to express an arbitrary invertible tensor $\mathbf{F}$ in the form

$$\mathbf{F} = \mathbf{R}\mathbf{U} = \mathbf{V}\mathbf{R}, \tag{2.12}$$

where $\mathbf{U}, \mathbf{V}$ are positive definite symmetric tensors, and $\mathbf{R}$ is an orthogonal tensor, $\mathbf{R}\mathbf{R}^T = \mathbf{R}^T\mathbf{R} = \mathbf{I}$, where $\mathbf{I}$ is the identity tensor and a superscript T denotes the transpose of a tensor. In addition, the right and left polar decompositions of $\mathbf{F}$ are unique. Since $\mathbf{U}$ and $\mathbf{V}$ are positive definite symmetric tensors, each of these tensors can be written in the spectral representations. For example, we have

$$\mathbf{U} = \sum_{r=1}^{3} \lambda_r (\mathbf{p}_r \otimes \mathbf{p}_r), \tag{2.13}$$

where λ_r are the eigenvalues of $\mathbf{U}$, or the principal stretches of $\mathbf{U}$, and $\mathbf{p}_r$ are the eigenvectors of $\mathbf{U}$. Note that the eigenvalues of $\mathbf{U}$ are the same as the eigenvalues of $\mathbf{V}$. The right and left Cauchy-Green deformation tensors are given by

$$\mathbf{C} = \mathbf{F}^T\mathbf{F} = \mathbf{U}^2, \quad \mathbf{B} = \mathbf{F}\mathbf{F}^T = \mathbf{V}^2, \tag{2.14}$$

respectively. Thus, we have

$$\mathbf{C} = \sum_{r=1}^{3} \lambda_r{}^2 (\mathbf{p}_r \otimes \mathbf{p}_r), \quad \mathbf{B} = \sum_{r=1}^{3} \lambda_r{}^2 (\mathbf{q}_r \otimes \mathbf{q}_r), \tag{2.15}$$

where $\mathbf{q}_r = \mathbf{R}\,\mathbf{p}_r$.

The velocity $\mathbf{v}$ of a material point $\mathbf{x}$ is given by

$$\mathbf{v} \equiv \frac{\partial \mathbf{x}}{\partial t} = \frac{\partial \chi(\mathbf{X}, t)}{\partial t}. \tag{2.16}$$

Therefore, the velocity gradient tensor $\mathbf{L}$ is defined by

$$\mathbf{L} = \mathrm{grad}\,\mathbf{v}. \tag{2.17}$$

Using the result $\mathrm{Grad}\mathbf{u} = (\mathrm{grad}\mathbf{u})\mathbf{F}$, we may write

$$\dot{\mathbf{F}} \equiv \frac{\partial}{\partial t}\mathbf{F} = \frac{\partial}{\partial t}\mathrm{Grad}\mathbf{x} = \mathrm{Grad}\mathbf{v}, \quad \mathbf{LF} = (\mathrm{grad}\,\mathbf{v})\mathbf{F} = \mathrm{Grad}\,\mathbf{v}, \tag{2.18}$$

which implies

$$\dot{\mathbf{F}} = \mathbf{LF}. \tag{2.19}$$

2.2.2　Balance laws and field equations

2.2.2.1　Conservation of mass

Let $\rho(\mathbf{x}, t)$ and $\rho_r(\mathbf{X})$ denote the mass densities in the current and reference configurations, respectively. Then the conservation of mass states that the total mass must not be destroyed or created under the deformation, i.e., the total mass remains constant.

Thus, we have

$$\rho\, dv = \rho_r\, dV. \tag{2.20}$$

Substituting (2.10) into (2.20), we get

$$\rho J = \rho_r, \quad \text{or} \quad \rho = J^{-1}\rho_r. \tag{2.21}$$

On differentiating $(2.21)_1$ with respect to t and using the result $\dot{J} = J \mathrm{div}\,\mathbf{v}$, we obtain

$$\dot{\rho} + \rho\, \mathrm{div}\,\mathbf{v} = 0, \tag{2.22}$$

where div is the divergence operator in $\mathcal{B}_t$. If the material is incompressible (i.e. $\det\mathbf{F} = 1$), then the density is constant $\rho = \rho_r$. Therefore, (2.22) reduces to $\mathrm{div}\,\mathbf{v} = 0$.

2.2.2.2   Principle of linear momentum

The principle of linear momentum, which may be viewed as a generalization of Newton's second law, states that the rate of change of the total linear momentum is equal to the resultant force. Let $\mathbf{b}$ denotes the body force acting on an arbitrary region in the current configuration R_t and $\mathbf{t}(\mathbf{x}, \mathbf{n})$ the tractions which act on the surface of the arbitrary region in the current configuration ∂R_t, where $\mathbf{n}$ is the outward unit vector normal to the surface of R_t. Then, we may write

$$\frac{d}{dt}\int_{R_t} \rho\mathbf{v}\, dv = \int_{R_t} \rho\mathbf{b}\, dv + \int_{\partial R_t} \mathbf{t}(\mathbf{x}, \mathbf{n})\, da. \tag{2.23}$$

Equations (2.10) and (2.21) can be used to convert the integral of the left hand side of (2.23) over R_t to their respective integral in the equivalent region in the reference configuration R_0 as follows

$$\frac{d}{dt}\int_{R_t} \rho\mathbf{v}\ dv = \frac{d}{dt}\int_{R_0} \rho\mathbf{v}J\ dV = \int_{R_0} \frac{d}{dt}\rho_r\mathbf{v}\ dV = \int_{R_t} \rho\dot{\mathbf{v}}\ dv. \tag{2.24}$$

Therefore, (2.23) can be written as

$$\int_{R_t} \rho(\dot{\mathbf{v}} - \mathbf{b})\ dv = \int_{\partial R_t} \mathbf{t}(\mathbf{x}, \mathbf{n})\ da. \tag{2.25}$$

2.2.2.3 Equations of motion

According to Cauchy's theorem (Ogden, 1997), if $\mathbf{t}(\mathbf{x}, \mathbf{n})$ is continuous in $\boldsymbol{x}$, then there exists a second-order tensor called the Cauchy stress tensor $\boldsymbol{\sigma}$, which is independent of $\mathbf{n}$, such that

$$\mathbf{t}(\mathbf{x}, \mathbf{n}) = \boldsymbol{\sigma}^T(\mathbf{x}, t)\mathbf{n}. \tag{2.26}$$

Consequently, (2.25) becomes

$$\int_{R_t} \rho(\dot{\mathbf{v}} - \mathbf{b})\ dv = \int_{\partial R_t} \boldsymbol{\sigma}^T(\mathbf{x}, t)\mathbf{n}\ da. \tag{2.27}$$

The divergence theorem allows us to transfer the surface integral in (2.27) into the volume integral as

$$\int_{\partial R_t} \boldsymbol{\sigma}^T(\mathbf{x}, t)\mathbf{n}\ da = \int_{R_t} \mathrm{div}\boldsymbol{\sigma}\ dv. \tag{2.28}$$

Thus, the equation of linear momentum (2.27) can be rewritten as

$$\int_{R_t} (\text{div}\boldsymbol{\sigma} + \rho\mathbf{b} - \rho\dot{\mathbf{v}})\, dv = 0, \quad \forall\, R_t. \qquad (2.29)$$

Since this is valid for every arbitrary region in the current configuration R_t, we derive the equations of motion

$$\text{div}\boldsymbol{\sigma} + \rho\,\mathbf{b} = \rho\,\dot{\mathbf{v}}. \qquad (2.30)$$

In a similar manner, we may use the principle of angular momentum to deduce the following

$$\boldsymbol{\sigma} = \boldsymbol{\sigma}^T. \qquad (2.31)$$

We shall introduce the nominal stress tensor $\mathbf{S}$ which will be used later. The nominal stress tensor $\mathbf{S}$ is connected to Cauchy stress tensor $\boldsymbol{\sigma}$ through

$$\mathbf{S} = J\mathbf{F}^{-1}\boldsymbol{\sigma}. \qquad (2.32)$$

In this case, the following equation holds,

$$\text{Div}\, \mathbf{S} + \rho_r\, \mathbf{b} = \rho_r\, \dot{\mathbf{v}}. \qquad (2.33)$$

In the absence of body force $\mathbf{b}$ and if the material is in equilibrium, i.e. $\dot{\mathbf{v}} = 0$, then the equations of motion (2.30) and (2.33) reduce to equilibrium equations

$$\text{div}\boldsymbol{\sigma} = 0, \qquad (2.34)$$

$$\text{Div } \mathbf{S} = 0. \tag{2.35}$$

2.2.3   Constitutive equations

The governing equations derived earlier are valid for any continuum. Thus, in order to derive the complete mathematical model, we need to introduce the constitutive equations, which are the mathematical descriptions of material response based upon their internal constitution. For our purpose, we need to specify these equations to the elastic materials. In the case of elasticity, we assume that the Cauchy stress depends only on the deformation gradient, no memory of past histories. Thus we have

$$\boldsymbol{\sigma} = g(\mathbf{F}), \tag{2.36}$$

where g is a symmetric tensor-valued function.

2.2.3.1   Principle of objectivity

The principle of objectivity, or material frame-indifference, states that the constitutive equations should be objective, i.e., material properties should be independent of observers. Thus, the symmetric tensor-valued function g satisfies

$$g(\mathbf{QF}) = \mathbf{Q}g(\mathbf{F})\mathbf{Q}^{T}, \tag{2.37}$$

for each deformation gradient $\mathbf{F}$ and all rotations $\mathbf{Q}$; see Ogden (1997) .

2.2.3.2   Isotropic materials

Physically, isotropy means that the properties of materials are direction independent. Therefore, the response function remains the same under any rotation $\mathbf{Q}$. So, we have

$$g(\mathbf{FQ}) = g(\mathbf{F}), \tag{2.38}$$

for every deformation gradient $\mathbf{F}$ and orthogonal tensor $\mathbf{Q}$. Replacing $\mathbf{F} = \mathbf{VR}$ and setting $\mathbf{Q} = \mathbf{R}^T$, we have

$$\boldsymbol{\sigma} = g(\mathbf{F}) = g(\mathbf{V}). \tag{2.39}$$

With the use of the definition of isotropy (2.38) together with material objectivity (2.37) and (2.39), we may then write

$$g(\mathbf{SFQ}) = g(\mathbf{SF}) = \mathbf{S}g(\mathbf{F})\mathbf{S}^T = \mathbf{S}g(\mathbf{V})\mathbf{S}^T, \tag{2.40}$$

where $\mathbf{S}$ is an arbitrary orthogonal tensor. Replacing $\mathbf{Q} = \mathbf{R}^T\mathbf{S}^T$ and $\mathbf{F} = \mathbf{VR}$ in equation (2.40), we get

$$g(\mathbf{SVS}^T) = \mathbf{S}g(\mathbf{V})\mathbf{S}^T, \tag{2.41}$$

for all orthogonal tensor $\mathbf{S}$. In this case, according to the representation theorem; see Ogden (1997), the Cauchy stress tensor can be written as

$$\boldsymbol{\sigma} = g(\mathbf{V}) = \phi_0\mathbf{I} + \phi_1\mathbf{V} + \phi_2\mathbf{V}^2, \tag{2.42}$$

where ϕ_0, ϕ_1, and ϕ_2 are scalar functions of the principal invariants of $\mathbf{V}$ defined by

$$i_1 = \text{tr } \mathbf{V}, \quad i_2 = \frac{1}{2}[\,(\text{tr } \mathbf{V})^2 - \text{tr}(\mathbf{V}^2)\,], \quad i_3 = \det\mathbf{V}. \tag{2.43}$$

These principal invariants i_1, i_2, i_3 can be written in terms of the principal stretches as

$$
\begin{aligned}
i_1(\mathbf{V}) &= \text{tr}\mathbf{V} = \lambda_1 + \lambda_2 + \lambda_3, \\
i_2(\mathbf{V}) &= \frac{1}{2}[\,(\text{tr } \mathbf{V})^2 - \text{tr}(\mathbf{V}^2)\,] = \lambda_2\lambda_3 + \lambda_3\lambda_1 + \lambda_1\lambda_2, \\
i_3(\mathbf{V}) &= \det\mathbf{V} = \lambda_1\lambda_2\lambda_3.
\end{aligned} \tag{2.44}
$$

Taking the expansion of (2.42), in terms of $\mathbf{B} = \mathbf{V}^2$, we get

$$\boldsymbol{\sigma} = \eta_0\mathbf{I} + \eta_1\mathbf{B} + \eta_2\mathbf{B}^2, \tag{2.45}$$

where η_0, η_1, and η_2 are scalar functions of the principal invariants of $\mathbf{B}$ (Ogden, 1997). In this case, the principal invariants of $\mathbf{B}$ can be written as

$$
\begin{aligned}
I_1(\mathbf{B}) &= \text{tr}\mathbf{B} = \lambda_1^2 + \lambda_2^2 + \lambda_3^2, \\
I_2(\mathbf{B}) &= \frac{1}{2}[\,(\text{tr } \mathbf{B})^2 - \text{tr}(\mathbf{B}^2)\,] = \lambda_2^2\lambda_3^2 + \lambda_3^2\lambda_1^2 + \lambda_1^2\lambda_2^2, \\
I_3(\mathbf{B}) &= \det\mathbf{B} = \lambda_1^2\lambda_2^2\lambda_3^2.
\end{aligned} \tag{2.46}
$$

2.2.4   Hyperelastic materials

The strain energy function $W(\mathbf{F})$ is a function which characterizes the stored elastic energy per unit volume in the reference configuration. A material is called hyperelastic if its mechanical properties are described by a strain energy function such that the following constitutive relation must hold

$$\frac{\partial}{\partial t} W(\mathbf{F}) = J \ \mathrm{tr}\left(\boldsymbol{\sigma}\mathbf{L}\right). \tag{2.47}$$

Now, if we take the partial derivative of W with respect to t and use (2.19) , we get

$$\frac{\partial}{\partial t} W(\mathbf{F}) = \frac{\partial W}{\partial F_{ij}}\frac{\partial F_{ij}}{\partial t} = \mathrm{tr}\left(\frac{\partial \mathrm{W}}{\partial \mathbf{F}}\dot{\mathbf{F}}\right) = \mathrm{tr}\left(\frac{\partial \mathrm{W}}{\partial \mathbf{F}}\mathbf{L}\mathbf{F}\right) = \mathrm{tr}\left(\mathbf{F}\frac{\partial \mathrm{W}}{\partial \mathbf{F}}\boldsymbol{L}\right), \tag{2.48}$$

where we have used the convention

$$\left(\frac{\partial W}{\partial F}\right)_{ji} = \frac{\partial W}{\partial F_{ij}}. \tag{2.49}$$

Therefore, a relation between the strain-energy function and the Cauchy stress can be obtained by comparing (2.47) and (2.48)

$$\boldsymbol{\sigma} = J^{-1}\mathbf{F}\frac{\partial W}{\partial \mathbf{F}}. \tag{2.50}$$

For incompressible materials, the above equation is replaced by

$$\boldsymbol{\sigma} = \mathbf{F}\frac{\partial W}{\partial \mathbf{F}} - p\mathbf{I}, \tag{2.51}$$

where p is a Lagrange multiplier arising from the incompressibility constraint; see Ogden (1997). Moreover, for an incompressible isotropic hyperelastic material, the strain-energy function depends on I_1 and I_2 only. Thus, the Cauchy stress can be written as

$$\boldsymbol{\sigma} = 2\frac{\partial W}{\partial I_1}\mathbf{B} + 2\frac{\partial W}{\partial I_2}(I_1\mathbf{B} - \mathbf{B}^2) - p\mathbf{I}. \tag{2.52}$$

It follows from (2.32) that the nominal stress is given by $\mathbf{S}$

$$\mathbf{S} = \frac{\partial W}{\partial \mathbf{F}}, \tag{2.53}$$

$$\mathbf{S} = \frac{\partial W}{\partial \mathbf{F}} - p\mathbf{F}^{-1}, \tag{2.54}$$

for compressible and incompressible materials, respectively.

Note that the strain-energy function W is either a function of three principal stretches, $W(\lambda_1, \lambda_2, \lambda_3)$, or the three principal invariants of $\mathbf{B}$ (also of $\mathbf{C}$), $W(I_1, I_2, I_3)$. In the case of isotropic elastic materials, the strain-energy function is a symmetric function of the three principal stretches, i.e.,

$$W(\lambda_1, \lambda_2, \lambda_3) = W(\lambda_2, \lambda_3, \lambda_1) = W(\lambda_3, \lambda_2, \lambda_1). \tag{2.55}$$

When the strain-energy function is a function of the three principal stretches, the three
Cauchy stresses are given by

$$\sigma_i = J^{-1}\lambda_i \frac{\partial W}{\partial \lambda_i}, \quad \text{no summation on } i, \quad i = 1, 2, 3, \tag{2.56}$$

for compressible materials, and by

$$\sigma_i = \lambda_i \frac{\partial W}{\partial \lambda_i} - p, \quad \text{no summation on } i, \tag{2.57}$$

for incompressible materials.

2.2.5   Strain energy functions

In the previous section, the existence of a strain energy function W is assumed for
hyperelastic materials. Here, we present some examples of strain energy functions
for isotropic, hyperelastic, incompressible materials which are commonly used in the
literature.

2.2.5.1   The neo-Hookean strain energy function

One of the most widely used strain energy functions is the neo-Hookean material
model. This model is obtained by taking the first term of the expansions of the strain
energy function in a power series of the first invariant I_1. The strain energy function

of neo-Hookean model, which involves one material constant only, is given by

$$W = \frac{1}{2}\mu(I_1 - 3) = \frac{1}{2}\mu(\lambda_1^2 + \lambda_2^2 + \lambda_3^2 - 3), \tag{2.58}$$

where μ denotes the shear modulus of the material. Although the neo-Hookean model gives good agreement with experimental results only for small strains (Gent, 2001), it is popular due to its simplicity.

2.2.5.2   The Mooney-Rivlin strain-energy function

The Mooney-Rivlin model is a generalization of the neo-Hookean model, which includes the second invariant I_2. The strain energy function is given by

$$W = \frac{\mu_1}{2}(I_1 - 3) + \frac{\mu_2}{2}(I_2 - 3), \tag{2.59}$$

where μ_1 and μ_2 are material constants. The Mooney-Rivlin model was proposed by Mooney (1940) and developed later by Rivlin (1948), so it is known as Mooney-Rivlin model. This model gives more accurate results than neo-Hookean model, and it may be the first choice in finite element analysis.

2.2.5.3   The Ogden material model

The previous models defined above are valid only for small deformations. Thus, an alternative model is needed to characterize the constitutive response of the material

subject to large deformation. Ogden (1972) introduced a strain energy function given in terms of the principal stretches in the form

$$W = \mu \sum_{n=1}^{3} \frac{\mu_n}{\alpha_n} (\lambda_1^{\alpha_n} + \lambda_2^{\alpha_n} + \lambda_3^{\alpha_n} - 3), \tag{2.60}$$

where μ is the shear modulus and μ_n and α_n are material constants such that

$$\mu_n \alpha_n > 0, \quad \text{and} \quad \sum_{n=1}^{3} \mu_n \alpha_n = 2\mu. \tag{2.61}$$

The values of the material constants were measured experimentally and given by

$$\alpha_1 = 1.3, \quad \alpha_2 = 5.0, \quad \alpha_3 = -2.0, \quad \mu_1^* = 1.491, \quad \mu_2^* = 0.003, \quad \mu_3^* = -0.023. \tag{2.62}$$

Note that the neo-Hookean and the Mooney-Rivlin models are special cases of Ogden model. This model is in good agreement with the experimental observations for stretches up to 7.

2.2.5.4   The Gent material model

In 1996, (Gent, 1996) proposed a simple constitutive model to characterise rubber materials, which is written in terms of the first principal invariant only as,

$$W = -\frac{1}{2}\mu J_m \ln\left(1 - \frac{I_1 - 3}{J_m}\right), \tag{2.63}$$

where μ denotes the shear modulus and J_m is a positive material constant representing the maximum extensibility. The Gent model reduces to the classic neo-Hookean model (2.58) on taking the limit as $J_m \to \infty$, and it may be sometimes called the generalized neo-Hookean model. Gent (1996) gives a value of $J_m = 97.2$, for rubber-like material while Horgan and Saccomandi (2003) give values of J_m between 0.422 and 3.93 for human arteries. When $J_m \leq 5$, the internal pressure against the volume does not have a maximum in uniform inflation; see Kanner and Horgan (2007). Although the Gent model involves just two material parameters, its theoretical predictions are in good agreement with experimental results for large strains. However, this model cannot accurately capture the experimental behaviour at moderate values of stretches. Thus, this model was later extended for the full range of deformations by Pucci and Saccomandi (2002). The modified model, which is known as the Gent-Gent model, is obtained by adding an extra term including a new material parameter C_2 and the second principal invariant I_2 as follows

$$W = -\frac{1}{2}\mu_0 J_m \ln\left(1 - \frac{I_1}{J_m}\right) + C_2 \ln\frac{I_2}{3}, \tag{2.64}$$

where μ_0 is a material constant. The Gent-Gent model gives much better results than the original Gent model when we compare the theoretical predictions with experimental results; see Zhou et al. (2018).

2.2.5.5   The Fung material model

The strain energy function proposed by Fung (1967) is one of the most widely used in the biomechanics literature. It has the exponential form

$$W = \frac{\mu}{2b} \left(e^{b(I_1 - 3)} - 1 \right), \tag{2.65}$$

where $b > 0$ is a material constant. The range of b for human arteries lies between 1.067 for a young thoracic artery and 5.547 for an older stiffer artery; see Horgan and Saccomandi (2003). The Fung model is reduced to the neo-Hookean by taking the limit $b \to 0$.

2.2.5.6   The Yeoh model

The Yeoh model was introduced by Yeoh (1990), where the strain energy function W is given by taking the expansions of W in a power series of the first principal invariant. The Yeoh strain energy function may be defined as

$$W = \sum_{i=1}^{3} C_i (I_1 - 3)^i, \tag{2.66}$$

where C_i are material constants. The Yeoh model is fitted to experimental data for all range of deformations. The neo-Hookean strain energy function can be viewed as a special case of the Yeoh material model model.

2.3   Incremental equations

The method of incremental deformations superposed on large deformations may be used to solve bifurcation problems. Here the governing equations of incremental deformations will be introduced. For more details of the derivation of incremental equations, we refer to Fu and Ogden (2001) and Destrade and Saccomandi (2007). Now let B be an elastic body which has an initial unstressed state B_0. This body is subject to large deformation $\boldsymbol{\chi}$ such that $\mathbf{x} = \boldsymbol{\chi}(\mathbf{X})$, where $\mathbf{X}$ is position vectors in B_0 and $\mathbf{x}$ is position vectors in the deformed configuration B_e. Then, we superimpose a small deformation, or an incremental deformation, on the deformed configuration B_e denoted by $\mathbf{x}' = \boldsymbol{\chi}'(\mathbf{X})$. Therefore, the incremental displacement can be written in the form

$$\hat{\mathbf{x}} = \mathbf{x}' - \mathbf{x} = \boldsymbol{\chi}'(\mathbf{X}) - \boldsymbol{\chi}(\mathbf{X}) \equiv \hat{\boldsymbol{\chi}}(\mathbf{X}), \tag{2.67}$$

and its gradient is

$$\mathrm{Grad}\hat{\boldsymbol{\chi}} = \mathrm{Grad}\boldsymbol{\chi}' - \mathrm{Grad}\boldsymbol{\chi} \equiv \hat{\mathbf{F}}. \tag{2.68}$$

Also, the nominal stress difference is given by

$$\hat{\mathbf{S}} = \mathbf{S}' - \mathbf{S} = \frac{\partial W}{\partial \mathbf{F}}(\mathbf{F}') - \frac{\partial W}{\partial \mathbf{F}}(\mathbf{F}), \tag{2.69}$$

for compressible materials. Note that equation (2.69) has the linear approximation in the form

$$\hat{\mathbf{S}} = \boldsymbol{\mathcal{A}}\hat{\mathbf{F}}, \tag{2.70}$$

where $\boldsymbol{\mathcal{A}}$ is the tensor of elastic moduli, with components

$$\mathcal{A}_{ijlk} = \frac{\partial^2 W}{\partial F_{ji} \partial F_{kl}}. \tag{2.71}$$

For incompressible materials we take the linearized incremental form of the the nominal stress (2.54) and the the incompressibility condition $\det\mathbf{F} = 1$ to get

$$\hat{\mathbf{S}} = \boldsymbol{\mathcal{A}}\hat{\mathbf{F}} - \hat{p}\mathbf{F}^{-1} + p\mathbf{F}^{-1}\hat{\mathbf{F}}\mathbf{F}^{-1}, \tag{2.72}$$

$$\mathrm{tr}(\hat{\mathbf{F}}\mathbf{F}^{-1}) = 0, \tag{2.73}$$

respectively, where $\hat{p}$ is the increment of p.

Similarly, the equilibrium equation (2.35) and the nominal stress difference (2.69) can be used to get

$$\mathrm{Div}\ \hat{\mathbf{S}} = 0. \tag{2.74}$$

All incremental quantities can be expressed as functions of the position vector $\mathbf{x}$ in the deformed configuration B_e instead of the position vector $\mathbf{X}$ in the reference configuration B_0. Thus, we have

$$\hat{\mathbf{x}} \equiv \mathbf{u}(\mathbf{x}) = \hat{\boldsymbol{\chi}}(\boldsymbol{\chi}^{-1}(\mathbf{x})), \quad \boldsymbol{\Gamma} = \hat{\mathbf{F}}\mathbf{F}^{-1}, \quad \hat{\mathbf{S}}_0 = J^{-1}\mathbf{F}\hat{\mathbf{S}}, \tag{2.75}$$

where $\mathbf{\Gamma} = \text{grad } \mathbf{u}$ is the gradient of incremental displacement u and $\hat{\mathbf{S}}_0$ is the push forward of $\hat{\mathbf{S}}$. Consequently, equations (2.72) and (2.73) may be rewritten as

$$\hat{\mathbf{S}}_0 = \boldsymbol{\mathcal{A}^1}\mathbf{\Gamma} + p\mathbf{\Gamma} - \hat{p}\mathbf{I}, \tag{2.76}$$

$$\text{tr}(\hat{\mathbf{F}}\mathbf{F}^{-1}) \equiv \text{tr}(\mathbf{\Gamma}) \equiv \text{div } \mathbf{u} = 0, \tag{2.77}$$

respectively, where

$$\mathcal{A}^1_{piqj} = J^{-1}F_{p\alpha}F_{q\beta}\mathcal{A}_{\alpha i\beta j}. \tag{2.78}$$

The updated incremental tensor $\hat{\mathbf{S}}_0$ has components

$$\hat{\mathbf{S}}_{0ji} = \mathcal{A}^1_{jilk}\Gamma_{kl} + p\Gamma_{ji} - \hat{p}\delta_{ji}. \tag{2.79}$$

Accordingly, the incremental equilibrium equation (2.74) becomes

$$\text{div } \hat{\mathbf{S}}_0 = 0. \tag{2.80}$$

2.4   Stroh formulation

The Stroh formulation was first introduced by Stroh (1958, 1962) for dealing with problems in general anisotropic elasticity. The applications of this formalism are extended later to other elasticity problems such as incremental deformation superimposed on large deformation. By using the Stroh formulation, the governing equations can be

reduced to a system of first-order ordinary differential equations. In this section the Stroh formulation will be outlined in cylindrical coordinates for incompressible materials.

We consider an incremental displacement field $\hat{\mathbf{x}}$ of the form

$$\hat{\mathbf{x}} = u(r,z)\mathbf{e}_r + v(r,z)\mathbf{e}_\theta + w(r,z)\mathbf{e}_z, \tag{2.81}$$

where $u(r,z), v(r,z)$ and $w(r,z)$ denote the incremental displacement in the r-, θ-, z-directions, respectively, and $\mathbf{e}_r, \mathbf{e}_\theta$ and $\mathbf{e}_z$ are the corresponding basis vectors. Here, it is assumed that the incremental displacement $\hat{\mathbf{x}}$ is independent of θ. We then assume that the solution takes the form

$$[u, v, w, \hat{p}] = [U(r), V(r), W(r), P(r)] \ \mathrm{e}^{\alpha z}, \tag{2.82}$$

where $U(r), V(r), W(r)$ and $P(r)$ are scalar functions of r only, and α is the axial spectral parameter. Similarly, the components of the incremental tensor $\hat{\mathbf{S}}_0$ can be rewritten in the following form

$$\left[\hat{S}_{0rr}, \hat{S}_{0r\theta}, \hat{S}_{0rz}\right] = [S_{0rr}(r), S_{0r\theta}(r), S_{0rz}(r)]\,\mathrm{e}^{\alpha z}. \tag{2.83}$$

With the use of equilibrium equations, $P(r)$ can be eliminated in terms of $U(r)$, $V(r)$, $W(r)$.

By introducing the displacement-traction vector $\boldsymbol{\eta}(r)$, as follows

$$\boldsymbol{\eta}(r) = \begin{bmatrix} \boldsymbol{U}(r) \\ \boldsymbol{S}(r) \end{bmatrix} \quad \text{with} \quad \begin{aligned} \boldsymbol{U}(r) &= [U(r), V(r), W(r)]^T \\ \boldsymbol{S}(r) &= [S_{0rr}(r), S_{0r\theta}(r), S_{0rz}(r)]^T \end{aligned}, \tag{2.84}$$

then we may rewrite the governing equations (2.80) as the following first-order differential system

$$\frac{d\boldsymbol{\eta}(r)}{dr} = \frac{1}{r}\mathbf{G}(r)\,\boldsymbol{\eta}(r), \tag{2.85}$$

where $\mathbf{G}(r)$ is the so-called Stroh matrix which has the following block representation

$$\mathbf{G} = \begin{pmatrix} \mathbf{G}_1 & \mathbf{G}_2 \\ \mathbf{G}_3 & \mathbf{G}_4 \end{pmatrix}, \tag{2.86}$$

where $\mathbf{G}_1, \mathbf{G}_2, \mathbf{G}_3$, and $\mathbf{G}_4$ are functions of r. We note that $\mathbf{G}_2$ and $\mathbf{G}_3$ are symmetric, and $\mathbf{G}_4 = -\mathbf{G}_1^T$.

2.5 The surface-impedance matrix method

The surface-impedance method is first presented by Biryukov (1985), and later developed by a number of authors; see Norris and Shuvalov (2010) and the references cited therein. Using this approach, we can rewrite the first-order differential equation (2.85) as a differential matrix Riccati equation.

Suppose that $\boldsymbol{\eta}_n (n = 1, \ldots, 6)$ are the independent solutions of the system (2.85) and

let the 6×6 matricant $\mathbf{M}(r, r_k)$ take the form

$$\mathbf{M}(r, r_k) = \begin{pmatrix} \mathbf{M}_1(r, r_k) & \mathbf{M}_2(r, r_k) \\ \mathbf{M}_3(r, r_k) & \mathbf{M}_4(r, r_k) \end{pmatrix} = \boldsymbol{\tau}(r)\boldsymbol{\tau}^{-1}(r_k), \tag{2.87}$$

where r_k is the point where the initial condition is assigned and

$$\boldsymbol{\tau}(r) = [\boldsymbol{\eta}_1, ..., \boldsymbol{\eta}_6]. \tag{2.88}$$

Then, $\mathbf{M}(r, r_k)$ is the solution of the initial value problem

$$\frac{d\mathbf{M}(r, r_k)}{dr} = \frac{1}{r}\mathbf{G}(r)\mathbf{M}(r, r_k), \qquad \text{with} \ \ \mathbf{M}(r_k, r_k) = I_{(6)}, \tag{2.89}$$

where $I_{(6)}$ is the 6×6 identity matrix. Accordingly, we may define the 3×3 conditional impedance matrix $\boldsymbol{z}$ as

$$\boldsymbol{S} = \boldsymbol{z}\boldsymbol{U}. \tag{2.90}$$

By substituting $(2.84)_1$ and (2.90) into (2.85), we get

$$\frac{d\boldsymbol{U}}{dr} = \frac{1}{r}\mathbf{G}_1\boldsymbol{U} + \frac{1}{r}\mathbf{G}_2\boldsymbol{z}\boldsymbol{U}, \tag{2.91}$$

$$\frac{d(\boldsymbol{z}\boldsymbol{U})}{dr} = \frac{1}{r}\mathbf{G}_3\boldsymbol{U} + \frac{1}{r}\mathbf{G}_4\boldsymbol{z}\boldsymbol{U}. \tag{2.92}$$

Therefore, the following differential matrix Riccati equation can be obtained by substituting (2.91) into (2.92), which gives,

$$\frac{d\boldsymbol{z}(r)}{dr} = \frac{1}{r}(\mathbf{G_3} - \boldsymbol{z}\mathbf{G_1} - \boldsymbol{z}\mathbf{G_2}\boldsymbol{z} + \mathbf{G_4}\boldsymbol{z}). \tag{2.93}$$

Once the boundary conditions are specified, equation (2.93) can be solved to fine non-trivial solutions.

Chapter 3

Localized bulging in cylinders and tubes under rotation

3.1 Introduction

In this chapter we consider a cylindrical, hyperelastic, isotropic, incompressible cylinder or tube subject to combined action of uniform inflation, axial extension and rotation. First, the problem is formulated and the expressions for the angular speed ω, the internal pressure P and the resultant axial force F associated with the primary shape-preserving deformation are summarized. We then derive the bifurcation condition, and conjecture and verify that the bifurcation condition in each case can be written simply in terms of the derivatives of ω, F and/or P with respect to the stretches. Next, the bifurcation condition is solved and numerical results are presented

when both the Gent and Ogden material models are used. Finally, a summary of our main results is presented. The results of this chapter have been published in Wang et al. (2017).

3.2   Primary deformation

We first write down the solution for the primary shape-preserving deformation associated with a circular cylindrical tube that is rotating about its axis of symmetry with angular velocity ω. The corresponding results for a solid cylinder will be obtained by taking $A = a = 0$. The tube is assumed to have inner radius A and outer radius B in the undeformed configuration, and these dimensions take the values a and b in the deformed configuration. The outer surface of the tube is traction-free, but its inner surface may in general be subjected to a hydrostatic pressure P or shrink-fitted to a rigid circular cylindrical spindle with a radius larger than A. It is also assumed that each plane end-face of the tube is subject to a resultant axial force F (e.g. $F = 0$ in which case the end faces are traction-free). In terms of cylindrical polar coordinates, the primary shape-preserving deformation is given by

$$r = \sqrt{\lambda_z^{-1}(R^2 - A^2) + a^2}, \quad \theta = \Theta + \omega t, \quad z = \lambda_z Z, \tag{3.1}$$

where (R, Θ, Z) and (r, θ, z) are the cylindrical polar coordinates in the undeformed and deformed configurations, respectively, t denotes time, and λ_z is a constant. The

associated principal stretches in the hoop, axial and radial directions are

$$\lambda_1 = \frac{r}{R} \equiv \lambda, \quad \lambda_2 = \lambda_z, \quad \lambda_3 = \frac{dr}{dR} = 1/(\lambda\lambda_z), \tag{3.2}$$

respectively. We assume that the constitutive behavior of the tube is described by a strain-energy function $W(\lambda_1, \lambda_2, \lambda_3)$. By integrating the only equilibrium equation in the r-direction, it can be shown that various quantities can be expressed in terms of the reduced strain-energy function w, and its derivatives w_1 and w_2, defined by

$$w(\lambda, \lambda_z) = W(\lambda, \lambda_z, \lambda^{-1}\lambda_z^{-1}), \quad w_1 = \partial w/\partial \lambda, \quad w_2 = \partial w/\partial \lambda_z; \tag{3.3}$$

see Haughton and Ogden (1980c). For instance, the radial stress on the inner surface is given by

$$\sigma_{33}(a) = \frac{1}{2}\rho\omega^2\lambda_z^{-1}(B^2 - A^2) - \int_{\lambda_b}^{\lambda_a} \frac{w_1}{\lambda^2\lambda_z - 1}d\lambda, \tag{3.4}$$

where ρ is the material density, the two limits λ_a and λ_b are defined by

$$\lambda_a = \frac{a}{A}, \quad \lambda_b = \frac{b}{B},$$

and are related to each other, through incompressibility, by

$$\lambda_a^2\lambda_z - 1 = \frac{B^2}{A^2}(\lambda_b^2\lambda_z - 1). \tag{3.5}$$

We observe that with λ_b eliminated using the above relation, the deformation is completely determined by the two stretches λ_a and λ_z.

The expression (3.4) suggests the introduction of a non-dimensional quantity Γ defined by

$$\Gamma = \rho\omega^2 B^2/\mu, \tag{3.6}$$

where μ denotes the ground-state shear modulus. For convenience we shall assume that the strain-energy function, stress components, and the pressure have all been scaled by μ, forces by μB^2, and the radii A, a, b by B. As a result of non-dimensionalization, equation (3.4) is now replaced by

$$\sigma_{33}(a) = \frac{1}{2}\Gamma\lambda_z^{-1}(1 - A^2) - \int_{\lambda_b}^{\lambda_a} \frac{w_1}{\lambda^2\lambda_z - 1}d\lambda, \tag{3.7}$$

and the resultant of σ_{22} at any cross section is given by

$$\tilde{F}_0(\lambda_a, \lambda_z, \Gamma) \equiv 2\pi\int_a^b \sigma_{22}rdr = \frac{1}{4}\pi\Gamma\lambda_z^{-2}(1 - A^2)^2 + \pi a^2\int_{\lambda_b}^{\lambda_a} \frac{w_1}{\lambda^2\lambda_z - 1}d\lambda$$

$$+ \pi A^2(\lambda_a^2\lambda_z - 1)\int_{\lambda_b}^{\lambda_a} \frac{2\lambda_z w_2 - \lambda w_1}{(\lambda^2\lambda_z - 1)^2}\lambda d\lambda, \tag{3.8}$$

where the first equation serves to define the function $\tilde{F}_0$. Finally, the radial stress component σ_{33} in the r-direction is given by

$$\sigma_{33}(r) = \frac{1}{2}\Gamma(b^2 - r^2) - \int_{\lambda_b}^{\lambda} \frac{w_1}{\lambda^2\lambda_z - 1}d\lambda. \tag{3.9}$$

This expression recovers (3.7) on evaluation at $r = a$ followed by the use of the identity $(b^2 - a^2)\lambda_z = B^2 - A^2$. We can now specialize the above formulae to three different loading and geometry conditions.

Firstly, consider a tube under the combined action of an internal pressure, rotation and an end thrust (referred to hereafter as the unconstrained case). Denoting the internal pressure by P, we have $\sigma_{33}(a) = -P$, and (3.7) then becomes

$$P = \tilde{P}(\lambda_a, \lambda_z) \equiv -\frac{1}{2}\Gamma\lambda_z^{-1}(1 - A^2) + \int_{\lambda_b}^{\lambda_a} \frac{w_1}{\lambda^2\lambda_z - 1}d\lambda, \qquad (3.10)$$

or equivalently,

$$\Gamma = \tilde{\Gamma}(\lambda_a, \lambda_z) \equiv \frac{2\lambda_z}{1 - A^2}\int_{\lambda_b}^{\lambda_a} \frac{w_1}{\lambda^2\lambda_z - 1}d\lambda - \frac{2\lambda_z P}{1 - A^2}, \qquad (3.11)$$

where the second expression in each equation defines the functions $\tilde{P}$ and $\tilde{\Gamma}$, respectively. To simplify notation, we have not shown explicitly the dependence of $\tilde{P}$ on Γ or $\tilde{\Gamma}$ on P.

The resultant axial force at any cross section, that is to be balanced by the net force F applied at each plane end-face, is given by

$$F = \tilde{F}(\lambda_a, \lambda_z) \equiv 2\pi\int_a^b \sigma_{22}r dr - \pi a^2 P$$

$$= \frac{1}{4}\pi\Gamma\lambda_z^{-1}(a^2 + b^2)(1 - A^2) + \pi A^2(\lambda_a^2\lambda_z - 1)\int_{\lambda_b}^{\lambda_a} \frac{2\lambda_z w_2 - \lambda w_1}{(\lambda^2\lambda_z - 1)^2}\lambda d\lambda, \qquad (3.12)$$

where the second equation defines the function $\tilde{F}$ which should be compared with the $\tilde{F}_0$ defined by (3.8). We note that the Γ in the expression for $\tilde{F}$ could be eliminated in favour of P with the use of (3.11). Thus, whenever $\tilde{F}$ is partially differentiated, it can be either Γ or P that is fixed. This will always be indicated explicitly.

Once the geometry of the tube is specified, either P or Γ can be assumed to take a dominant role together with F. If, for instance, P is specified and is assumed to take a passive role (by being sufficiently small), then Γ and F can be viewed as functions of the two stretches λ_a and λ_z, and we expect the following Jacobian to play a role in the characterization of localized bulging:

$$\Omega_u(\lambda_a, \lambda_z) \equiv J(\tilde{\Gamma}, \tilde{F}) = \frac{\partial \tilde{\Gamma}}{\partial \lambda_a} \frac{\partial \tilde{F}}{\partial \lambda_z} - \frac{\partial \tilde{\Gamma}}{\partial \lambda_z} \frac{\partial \tilde{F}}{\partial \lambda_a}, \tag{3.13}$$

where the first equation defines the function $\Omega_u(\lambda_a, \lambda_z)$ with the subscript u signifying "unconstrained". Physically, the condition is satisfied when the expressions for $\tilde{\Gamma}$ and $\tilde{F}$ can no longer be inverted to express λ_a and λ_z uniquely in terms of $\tilde{\Gamma}$ and $\tilde{F}$. Similarly, if Γ is assumed to take a passive role, then the Jacobian $J(\tilde{P}, \tilde{F})$ can be defined. However, it can be shown that this Jacobian is a non-zero multiple of $J(\tilde{\Gamma}, \tilde{F})$ when the connection (3.10) is used.

The case previously studied by Fu et al. (2016) can now be viewed as a special case, corresponding to $\Gamma \equiv 0$, of the current more general formulation. The observations made in the latter paper about $J(\tilde{P}, \tilde{F})$ can be extended to the case when Γ is non-zero but is held fixed. In particular, it can be shown that when F and Γ are both fixed, the

pressure will reach a maximum precisely when $J(\tilde{P}, \tilde{F}) = 0$. In a similar manner, we note that if both P and F are held fixed, $\tilde{\Gamma}$ is a function of λ_a only since $\tilde{F}(\lambda_a, \lambda_z) = F$ would define λ_z as a function of λ_a. In this case, $\tilde{\Gamma}$ reaches a maximum when

$$\frac{d\tilde{\Gamma}}{d\lambda_a} = \frac{\partial \tilde{\Gamma}}{\partial \lambda_a} + \frac{\partial \tilde{\Gamma}}{\partial \lambda_z}\frac{d\lambda_z}{d\lambda_a} = 0. \tag{3.14}$$

The ordinary derivative in the above expression can be eliminated by solving

$$\frac{\partial \tilde{F}}{\partial \lambda_a} + \frac{\partial \tilde{F}}{\partial \lambda_z}\frac{d\lambda_z}{d\lambda_a} = 0.$$

It follows that

$$\frac{\partial \tilde{\Gamma}}{\partial \lambda_a} - \frac{\partial \tilde{\Gamma}}{\partial \lambda_z}\frac{\partial \tilde{F}}{\partial \lambda_a}\left(\frac{\partial \tilde{F}}{\partial \lambda_z}\right)^{-1} = 0. \tag{3.15}$$

Thus, Γ reaches a maximum when the Jacobian $J(\tilde{\Gamma}, \tilde{F})$ vanishes. We emphasize that this correspondence is lost when, for instance, it is the λ_z that is held fixed in rotating the tube. Drawing upon the results of Fu et al. (2016), we may then further conjecture that when the inner surface is traction-free or subjected to a hydrostatic pressure P the bifurcation condition for localized bulging is simply $J(\tilde{\Gamma}, \tilde{F}) = 0$, whether it is the F or λ_z that is fixed in rotating the tube. We shall verify in the next section that this is indeed the case.

Next, consider the case when a tube is mounted on a rigid circular cylindrical spindle with a radius larger than A, which is the shrink-fit case discussed in Chadwick et al. (1977). We assume that the contact is smooth so that at the inner surface the stretch

λ_a is specified and the shear stress components are negligible. When such a tube is rotated, the expression (3.4) can be used to compute the contact pressure, and the resultant $\tilde{F}_0(\lambda_a, \lambda_z, \Gamma)$ of σ_{22} given by (3.8) is now a function of the only variable stretch λ_z. It will be shown in the next section that the bifurcation condition for localized bulging is simply

$$\Omega_c(\lambda_a, \lambda_z, \Gamma) \equiv \frac{\partial \tilde{F}_0}{\partial \lambda_z} = 0, \tag{3.16}$$

where the first equation defines the function $\Omega_c(\lambda_a, \lambda_z, \Gamma)$ with the subscript c signifying "constrained". Suppose that the equation $\tilde{F}_0(\lambda_a, \lambda_z, \Gamma) = F$, with $\tilde{F}_0$ given by (3.8), is solved for Γ and the result is denoted by $\Gamma = \tilde{\Gamma}_0(\lambda_a, \lambda_z, F)$. Then it can also be shown that the above bifurcation condition is equivalent to $\partial \tilde{\Gamma}_0 / \partial \lambda_z = 0$.

Finally, in the special case of a solid cylinder (A=a=0), the three principal stretches given by (3.2) reduce to

$$\lambda_1 = \lambda_z^{-1/2}, \quad \lambda_2 = \lambda_z, \quad \lambda_2 = \lambda_z^{-1/2}, \tag{3.17}$$

which are all independent of r. Then in terms of the reduced strain-energy function $\hat{w}$ defined by

$$\hat{w}(\lambda_z) = W(\lambda_z^{-1/2}, \lambda_z, \lambda_z^{-1/2}), \tag{3.18}$$

the principal stretch λ_z is determined by

$$\Gamma = 4\lambda_z^2 (\frac{F}{\pi} - \hat{w}'), \tag{3.19}$$

43

where the prime denotes differentiation with respect to the argument λ_z. If F is fixed, then setting $d\Gamma/\lambda_z = 0$ would yield, after F has been eliminated with the use of (3.19), the condition

$$\Omega_s(\lambda_z) \equiv 2\lambda_z^3 \hat{w}'' - \Gamma = 0, \tag{3.20}$$

where the first relation defines the function $\Omega_s(\lambda_z)$ with the subscript s signifying "solid". On the other hand, if Γ is fixed instead, then setting $dF/\lambda_z = 0$ would again yield the same condition (3.20). It will be shown in the next section that this is in fact the bifurcation condition for localized bulging.

3.3   Bifurcation conditions for localized bulging

To investigate the axisymmetric localized bulging of the finitely deformed configurations determined in the previous section, we consider an incremental displacement field $\dot{\boldsymbol{x}}$ given by

$$\dot{\boldsymbol{x}} = u(r, z)\boldsymbol{e}_r + v(r, z)\boldsymbol{e}_z, \tag{3.21}$$

where $u(r, z)$ and $v(r, z)$ are the incremental displacements in the r- and z-directions, respectively. The incremental equation of motion takes the form

$$\mathrm{div}\ \boldsymbol{\chi}^T = -\Gamma u \boldsymbol{e}_r, \tag{3.22}$$

where the incremental stress tensor $\boldsymbol{\chi}$ is defined by the following components relative to the orthonormal basis $\{\boldsymbol{e}_\theta, \boldsymbol{e}_z, \boldsymbol{e}_r\}$:

$$\chi_{ij} = \mathcal{B}_{jilk}\eta_{kl} + \bar{p}\eta_{ji} - p^*\delta_{ji}. \tag{3.23}$$

In the above expression, the $\mathcal{B}_{jilk}$'s are the incremental elastic moduli whose expression in terms of the principal stretches can be found in Haughton and Ogden (1979a), $\bar{p}$ and p^* are, respectively, the primary and incremental pressures associated with the constraint of incompressibility, δ is the Kronecker delta, and the gradient of incremental displacement $\boldsymbol{\eta}$ is given by

$$\boldsymbol{\eta} = \begin{bmatrix} u/r & 0 & 0 \\ 0 & v_z & v_r \\ 0 & u_z & u_r \end{bmatrix}, \quad \text{with } v_z \equiv \frac{\partial v}{\partial z}, \quad v_r \equiv \frac{\partial v}{\partial r} \text{ etc.} \tag{3.24}$$

The equation of motion is to be supplemented by the incompressibility condition

$$\operatorname{tr}\boldsymbol{\eta} = u_r + v_z + \frac{u}{r} = 0, \tag{3.25}$$

and is to be solved subject to appropriate boundary conditions on $r = a, b$. On the outer boundary $r = b$, we impose the traction-free boundary condition

$$\boldsymbol{\chi}\boldsymbol{n} = \boldsymbol{0} \quad \text{on } r = b \tag{3.26}$$

for all the three cases under consideration, where $\boldsymbol{n}$ denotes the unit normal to the surface. For a solid cylinder, this boundary condition is supplemented by the condition that the solution must be bounded at $r = 0$. For the case when a tube is subjected to an internal (hydrostatic) pressure P, the boundary condition on $r = a$ is given by

$$\boldsymbol{\chi}\boldsymbol{n} = P\boldsymbol{\eta}^T\boldsymbol{n} \quad \text{on } r = a. \tag{3.27}$$

Finally, for the shrink-fit case, the boundary conditions on $r = a$ are given by

$$\chi_{23} = 0, \quad u = 0 \quad \text{on } r = a. \tag{3.28}$$

As explained in Fu et al. (2016), the bifurcation condition can be derived by first looking for a solution of the form

$$u = f(r)\mathrm{e}^{\alpha z}, \quad v = g(r)\mathrm{e}^{\alpha z}, \quad p^* = h(r)\mathrm{e}^{\alpha z}, \tag{3.29}$$

where α is the axial spectral parameter. On substituting these expressions into the incremental equilibrium equations and then eliminating $g(r)$ and $h(r)$ in favor of $f(r)$, we find that $f(r)$ satisfies the single fourth-order ordinary differential equation

$$r^4 \left\{ r^{-1}[r^{-1}\mathcal{B}_{3232}(r^2 f'' + rf' - f)]' \right\}' + \alpha^2 r^2 \left\{ r[r(\mathcal{B}_{2222} + \mathcal{B}_{3333} - 2\mathcal{B}_{2233} - 2\mathcal{B}_{3223})f']' \right.$$

$$+ (r^2\sigma_{33}'' - r^2\mathcal{B}_{3232}'' + r\mathcal{B}_{2222}' + r\mathcal{B}_{1133}' - r\mathcal{B}_{1122}' - r\mathcal{B}_{2233}' - r\mathcal{B}_{3223}'$$

$$+2\mathcal{B}_{1122} + 2\mathcal{B}_{3223} - \mathcal{B}_{1111} - \mathcal{B}_{2222} + r^2\Gamma)f\} + \alpha^4 r^4 \mathcal{B}_{2323} f = 0. \qquad (3.30)$$

This corresponds to Haughton and Ogden (1980c)'s equation (49) with α replaced by $i\alpha$. In a similar manner, the two boundary conditions (3.26) and (3.27) yield

$$r^2 f'' + r f' - (\alpha^2 r^2 + 1)f = 0 \quad \text{on } r = a, b, \qquad (3.31)$$

and

$$r^2[r^{-1}\mathcal{B}_{3232}(r^2 f'' + r f' - f)]' + \alpha^2 r^3(\mathcal{B}_{2222} + \mathcal{B}_{3333} - 2\mathcal{B}_{2233} - 2\mathcal{B}_{3223} + \mathcal{B}_{3232})f'$$

$$-\alpha^2 r^2(r\sigma'_{33} - r\mathcal{B}'_{3232} + \mathcal{B}_{2222} + \mathcal{B}_{1133} - \mathcal{B}_{1122} - \mathcal{B}_{2233} - \mathcal{B}_{3223})f = 0 \quad \text{on } r = a, b. \quad (3.32)$$

The last boundary condition (3.32) on $r = a$ corresponds to (3.27) applied in the normal direction. For the shrink-fitting case, this is replaced by

$$f(a) = 0, \qquad (3.33)$$

and as a result the boundary condition (3.31), which corresponds to $\chi_{23} = 0$, reduces to

$$a f''(a) + f'(a) = 0. \qquad (3.34)$$

Because of the translational invariance in terms of z, $\alpha = 0$ is always an eigenvalue of the above eigenvalue problem. For sufficiently small values of Γ, P and F, none of the other eigenvalues can be pure imaginary since such eigenvalues give rise to

bifurcation modes that are sinusoidal in the z-direction, and we only expect such modes to appear for sufficiently large values of Γ, P and F. We note that Haughton and Ogden (1980a,b,c)'s analysis is concerned with the conditions under which such bifurcation modes would appear. Since our current analysis is concerned with a bifurcation mode that is localized in the axial direction, as a first attempt we may assume that the tube or solid cylinder is infinitely long so that boundary conditions at the two end faces need not be considered. This is essentially the perfect bifurcation case (i.e., bifurcation in the absence of any imperfections). Effects of finite length as well as material inhomogeneity and/or nonuniform wall thickness can all be considered as imperfections. Since localized bulging is in general a subcritical bifurcation, it is expected that in the presence of imperfections, the critical value of angular speed will be significantly lower than the value determined in the current study. For an illustration of the effect of imperfections, we refer to Fu and Xie (2012).

For the problem under consideration, we seek eigenvalues of α such that non-trivial solutions can be found. It can be shown that the distribution of eigenvalues is symmetric with respect to both axes in the complex α-plane. Suppose that the uniform inflation is characterized by λ_a. As λ_a increases from 1, it can be shown that there are five real eigenvalues of the form $\alpha = 0, \pm\alpha_1, \pm\alpha_2$; see Figure (3.1)(a). The two eigenvalues $\pm\alpha_1$ would move along the real axis towards the origin as λ_a is increased gradually. With increasing λ_a, zero becomes a triple eigenvalue which signals the initiation of a bifurcation into a localized solitary-wave type solution; see, e.g., Kirchgässner (1982) or Haragus and Iooss (2010). If we increase λ_a further, $\pm\alpha_1$ would move onto the
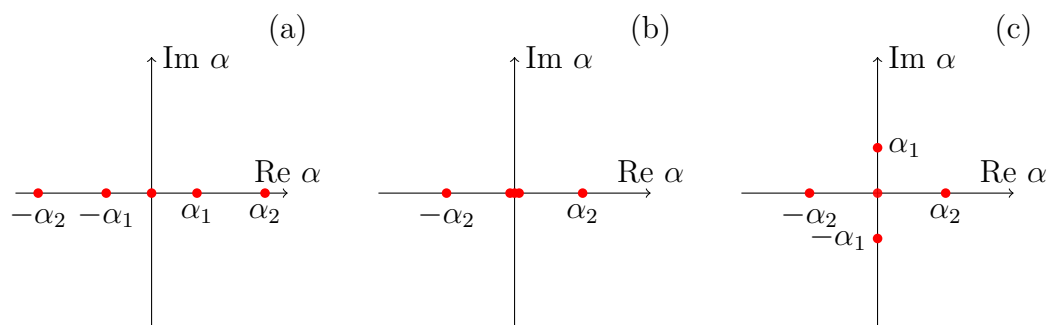
Figure 3.1: Movement of the eigenvalues as λ_a increases (Fu et al. (2016)).

imaginary axis, and the exponential $\mathrm{e}^{\alpha z}$ then becomes sinusoidal. Therefore, a necessary condition for a localized bulging bifurcation to take place is when α_1 vanishes, making zero a triple eigenvalue. Thus, localized bulging must necessarily occur before any bifurcation into periodic patterns. This necessary condition will be derived for the three different cases defined earlier.

3.3.1 Solid cylinder

For the case of a solid cylinder, all the elastic moduli are constants and the reduced eigenvalue problem can be solved analytically. Adapting Haughton and Ogden (1980a)'s results slightly, we obtain the following equation satisfied by all the eigenvalues of α:

$$K_1 - K_2 = 0, \tag{3.35}$$

where K_1 and K_2 are defined by

$$\nu_\mu(\nu_\mu^2+1)I_1(\nu_\mu\alpha b)K_\mu = \alpha b(\nu_\mu^2\mathcal{B}_{1212}+\mathcal{B}_{2121})I_0(\nu_\mu\alpha b)-\nu_\mu(2\mathcal{B}_{1313}+\Gamma b^2)I_1(\nu_\mu\alpha b), \quad (3.36)$$

where I_0 and I_1 are the modified Bessel functions of the first kind and ν_1, ν_2 denoting the two positive roots of the bi-quadratic equation

$$\nu^4\mathcal{B}_{1212} - \nu^2(\mathcal{B}_{1111} + \mathcal{B}_{2222} - 2\mathcal{B}_{1122} - 2\mathcal{B}_{1221}) + \mathcal{B}_{2121} = 0. \quad (3.37)$$

The condition for zero to become a triple eigenvalue can be obtained by expanding (3.35) in terms of α and then setting the leading term to zero. The result is

$$(2\mathcal{B}_{1313} - 2\mathcal{B}_{1212} + \Gamma a^2)\nu_1^2\nu_2^2 - 2\mathcal{B}_{2121}(\nu_1^2 + \nu_2^2) - 2\mathcal{B}_{2121} = 0,$$

which, on using (3.37), can be reduced to

$$\Gamma a^2 - 2\mathcal{B}_{1111} + 4\mathcal{B}_{1122} - 4\mathcal{B}_{1212} + 4\mathcal{B}_{1221} + 2\mathcal{B}_{1313} - 2\mathcal{B}_{2222} = 0. \quad (3.38)$$

With the use of the expressions for the elastic moduli given by Haughton and Ogden (1979a), we have verified that (3.38) can be reduced to (3.20). Thus, we conclude that for a rotating solid cylinder, a localized bulge will initiate when the rotation speed ω or the axial force given by (3.19) reaches a maximum.

3.3.2   Unconstrained tube

We next consider the case of an unconstrained tube that is subjected to the combined action of rotation, internal inflation and an axial force. An inspection of the associated eigenvalue problem governed by (3.30), (3.31) and (3.32) shows that it can be obtained from the case with $\Gamma = 0$ by the simple substitution

$$\mathcal{B}_{1111} \to \mathcal{B}_{1111} - \Gamma r^2. \tag{3.39}$$

As a result, the exact bifurcation condition can be derived following the same procedure as in Fu et al. (2016). Guided by the results in the latter paper, we may further conjecture that with the above substitution, the new bifurcation condition should be equivalent to $\Omega_u(\lambda_a, \lambda_z) = 0$, where $\Omega_u(\lambda_a, \lambda_z)$ is defined by (3.13). We have checked to verify that this is indeed the case. Furthermore, in the thin-wall limit, with the aid of an expansion procedure adapted from Fu et al. (2016), we find that the exact bifurcation condition to leading order reduces to

$$\lambda_m(w_1 - \lambda_z w_{12})^2 + \lambda_z^2 w_{22}(w_1 - \lambda_1 w_{11}) + \lambda_m^3 \Gamma^2 + 2\lambda_m^2(\lambda_z w_{12} - w_1)\Gamma = 0, \tag{3.40}$$

where λ_m denotes the circumferential stretch in the mid-surface, and all the partial derivatives are now evaluated at $\lambda = \lambda_m$. The associated leading-order expressions for Γ and F take the form

$$\Gamma = w_1/\lambda_m - \lambda_z P_0, \quad F = \pi(2w_2 - P_0\lambda_m^2), \tag{3.41}$$

where $P_0 = P/\epsilon$, ϵ being the wall thickness scaled by the averaged radius. If $(3.41)_1$ is used to eliminate Γ in (3.40), we obtain the alternative bifurcation condition

$$\lambda_m(w_{11}w_{22} - w_{12}^2) - w_1 w_{22} + P_0 \lambda_m^2 (2w_{12} - \lambda_m P_0) = 0, \qquad (3.42)$$

which is valid if P_0 is held fixed in rotating the tube. As a useful check, this leading-order bifurcation condition can also be obtained from $J(\Gamma, F) = 0$ when the leading-order expressions (3.41) are used.

As expected, when $\Gamma = 0$, (3.40) reduces to its counterpart for the pure inflation case given in Fu et al. (2008), and it is known that this reduced bifurcation condition has a solution that defines λ_z as a function of λ_m for most of the commonly used strain-energy functions. In contrast, if we set $P_0 = 0$ in (3.42), the existence of solution of the reduced bifurcation condition depends very much on the material model used: it again has a solution when the Ogden material model is used, but it does not have a solution when the Gent material model is used. This difference carries over even when finite wall thickness is considered, which will be discussed further in the next section. We also observe that equation (3.42) with $P_0 = 0$ is the same as Haughton and Ogden (1980b)'s equation (63) which emerged as the limit of the condition of bifurcation into axially symmetric periodic modes in an infinitely long tube. This equation reappeared as equation (71) in the same paper where it was observed as characterizing the turning point of ω when the axial force F is held fixed.

3.3.3   The shrink-fit case

Finally, we consider the shrink-fit case for which the applicable boundary conditions at $r = a, b$ are (3.33) and (3.34), and (3.31) and (3.32), respectively. Again, the bifurcation condition is the condition under which zero becomes a triple eigenvalue. To derive this condition, we expand the stretches as

$$\lambda_a = \lambda_a^{(0)} + \alpha^2 \lambda_a^{(1)} + \cdots , \quad \lambda_z = \lambda_z^{(0)} + \alpha^2 \lambda_z^{(1)} + \cdots , \tag{3.43}$$

and look for a regular perturbation solution of the form

$$f(r) = f^{(0)}(r) + \alpha^2 f^{(1)}(r) + \cdots , \tag{3.44}$$

where the constants $\lambda_a^{(i)}$ and $\lambda_z^{(i)}$ $(i = 0, 1, \cdots)$ and functions $f^{(i)}(r)$ $(i = 0, 1, \cdots)$ are to be determined. The boundary conditions can similarly be expanded. We are basically assuming that there is a small real eigenvalue α and then determining the required values of the stretches that support such a small eigenvalue. If such a non-trivial solution can be found, then the leading order values $\lambda_a^{(0)}$ and $\lambda_z^{(0)}$ are the stretch values at which zero becomes a triple eigenvalue.

On substituting (3.44) into (3.30) and equating the coefficients of α^0 and α^2, we obtain a homogeneous equation for $f^{(0)}(r)$ and an inhomogeneous equation for $f^{(1)}(r)$. These equations are the same as their counterparts derived in Fu et al. (2016) except for the

substitution (3.39). We thus have

$$f^{(0)}(r) = c_1 r + c_2 \frac{1}{r} + c_3 \kappa_1(r) + c_4 \kappa_2(r), \tag{3.45}$$

where c_1, c_2, c_3, c_4 are constants and

$$\kappa_1(r) = \frac{1}{r} \int_a^r t \int_a^t \frac{s}{\zeta(s)} ds \, dt, \quad \kappa_2(r) = \frac{1}{r} \int_a^r t \int_a^t \frac{1}{s\zeta(s)} ds \, dt, \tag{3.46}$$

with the function $\zeta(r) = \mathcal{B}_{3232}$. Substituting equation (3.45) into the leading-order boundary condition, we find that $c_3 = c_4 = 0$. At the next order, we get

$$f^{(1)}(r) = d_1 r + d_2 \frac{1}{r} + d_3 \kappa_1(r) + d_4 \kappa_2(r) + c_1 \kappa_3(r) + c_2 \kappa_4(r), \tag{3.47}$$

where d_1, d_2, d_3, d_4 are constants and

$$\kappa_3(r) = \frac{1}{r} \int_a^r y \int_a^y \frac{1}{x\zeta(x)} \int_a^x t \int_a^t \omega_1(s) ds \, dt \, dx \, dy, \tag{3.48}$$

$$\kappa_4(r) = \frac{1}{r} \int_a^r y \int_a^y \frac{1}{x\zeta(x)} \int_a^x t \int_a^t \omega_2(s) ds \, dt \, dx \, dy, \tag{3.49}$$

with

$$\omega_1(r) = \mathcal{B}'_{1122} - \mathcal{B}'_{1133} + 3\mathcal{B}'_{2233} - 2\mathcal{B}'_{2222} - \mathcal{B}'_{3333} + 3\mathcal{B}'_{3223} + r(\mathcal{B}''_{3223} + \bar{p}'')$$

$$+ \frac{1}{r}(\mathcal{B}_{1111} - \Gamma r^2 - 2\mathcal{B}_{1122} + 2\mathcal{B}_{2233} - \mathcal{B}_{3333}),$$

$$\omega_2(r) = \frac{1}{r}(\mathcal{B}''_{3223} + \bar{p}'') + \frac{1}{r^2}(\mathcal{B}'_{1122} - \mathcal{B}'_{1133} - \mathcal{B}'_{2233} - \mathcal{B}'_{3333} - \mathcal{B}'_{3223})$$

$$+\frac{1}{r^3}(\mathcal{B}_{1111} - \Gamma r^2 - 2\mathcal{B}_{1122} + 2\mathcal{B}_{2233} - \mathcal{B}_{3333}).$$

We observe that the last two terms in (3.47) are simply particular integrals. On substituting (3.45) together with (3.47) into the leading- and second-order boundary conditions, we find that $c_2 = -a^2 c_1$, $d_2 = -a^2 d_1$, and that the three constants c_1, d_3, d_4 satisfy three homogeneous linear equations. For a non-trivial solution, we set the determinant of its coefficient matrix to zero, thus obtaining the condition

$$\Omega(\lambda_a^{(0)}, \lambda_z^{(0)}) = 0, \tag{3.50}$$

where

$$\Omega(\lambda_a, \lambda_z) = (a^2 b^2 - b^4)F_1 + (a^2 b^4 - a^4 b^2)F_2 + 2b^2 F_3 - 2a^2 b^2 F_4 + (a^4 - b^4)\sigma_3(b)$$

$$+b^4(\mathcal{B}_{1122}(b) - \mathcal{B}_{1133}(b) - 2\mathcal{B}_{2222}(b) + 3\mathcal{B}_{2233}(b) + 2\mathcal{B}_{3223}(b) - 2\mathcal{B}_{3232}(b) - \mathcal{B}_{3333}(b))$$

$$+a^2 b^2(2\mathcal{B}_{1133}(b) + 2\mathcal{B}_{2222}(b) + 2\mathcal{B}_{3232}(b) - 2\mathcal{B}_{1122}(b) - 2\mathcal{B}_{2233}(b) - 2\mathcal{B}_{3223}(b))$$

$$+b(a^2 - b^2)^2(\mathcal{B}'_{3223}(b) + \bar{p}'(b)) + a^4(\mathcal{B}_{1122}(b) - \mathcal{B}_{1133}(b) - \mathcal{B}_{2233}(b) + \mathcal{B}_{3333}(b)).$$

In the last expression, the constants $F_1, \ldots, F_4$ are given by

$$F_1 = \int_a^b \omega_1(t)dt, \quad F_3 = \int_a^b t\left(\int_a^t \omega_1(s)ds\right)dt,$$

$$F_2 = \int_a^b \omega_2(t)dt, \quad F_4 = \int_a^b t\left(\int_a^t \omega_2(s)ds\right)dt.$$

We may conjecture that the bifurcation condition (3.50) is equivalent to (3.16). This is verified numerically to be indeed the case.

3.4 Numerical results

We present some representative numerical results by considering two commonly used material models for rubber-like materials, the Ogden and Gent material models. The associated strain-energy function is given by (2.60) and (2.63), respectively. We adopt $J_m = 97.2$ which is typical value for rubbers following Gent (1996). All our numerical computations were carried out using Mathematica (Wolfram, 1991).

3.4.1 Solid cylinder

When the axial force F is specified, we find the value of Γ at which localized bulging may take place. In Figure (3.2), we have shown the relation between Γ and F when the bifurcation condition (3.20) is satisfied. The relation is obtained by varying λ_z continuously from 0.2 to 1.2 and computing the associated Γ and F using (3.19) and (3.35). It is seen that both curves contain a cusp point, corresponding to the fact that the Γ given by $\Gamma = 2\lambda_z^3 \hat{w}''$, defined by the bifurcation condition (3.20), attains a minimum at $\lambda_z = 0.39$ for the Gent material, and $\lambda_z = 0.20$ for the Ogden material; see Figure(3.3), left. In Figure (3.3), right, is shown the dependence of F on λ_z

(a) Gent material   (b) Ogden material
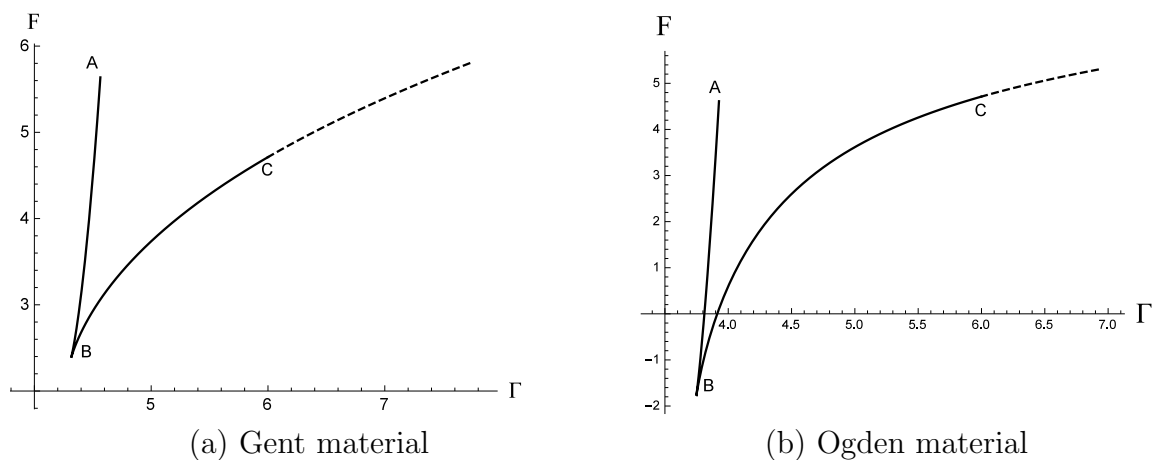
Figure 3.2: Relation between Γ and F when localized bulging takes place. The solid and dashed parts on each curve corresponds to $\lambda_z < 1$ and $\lambda_z > 1$, respectively.

(a)   (b)
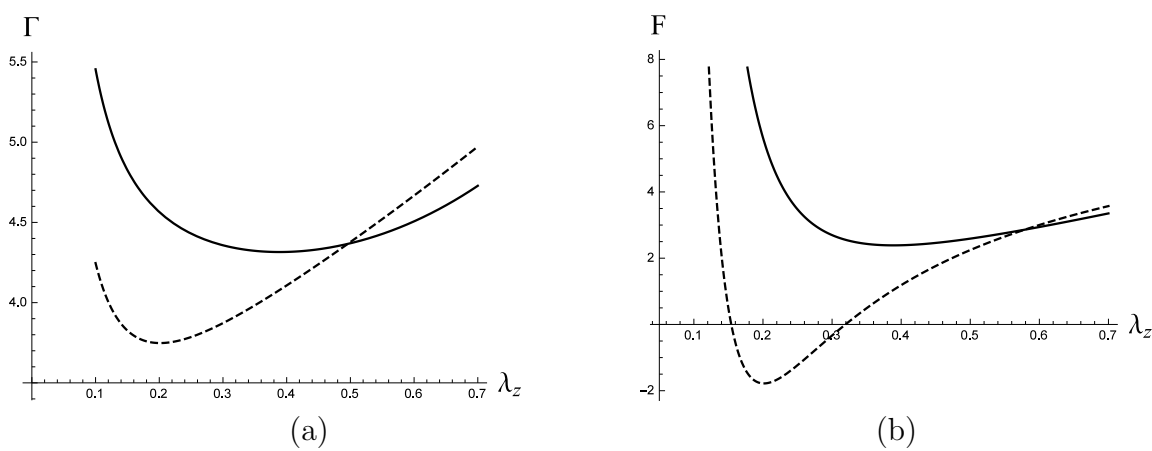
Figure 3.3: Dependence of Γ and F on λ_z when localized bulging takes place. Solid and dashed lines correspond to the Gent and Ogden material models, respectively.

57
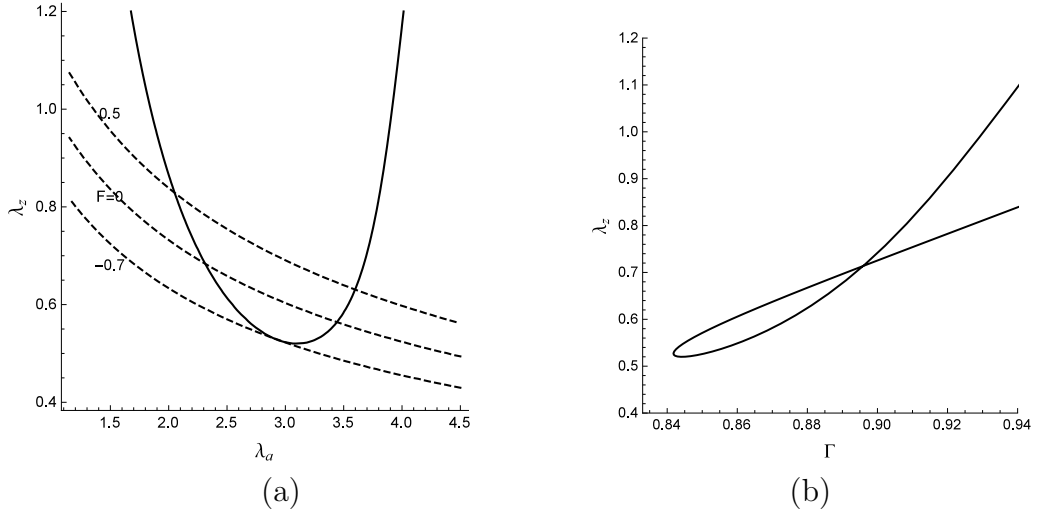
Figure 3.4: Solution of the bifurcation condition $\Omega_u(\lambda_a, \lambda_z) = 0$, when the Ogden material is used, for a rotating tube with $A = 0.8$ and $P = 0$ in terms of (λ_a, λ_z) (left figure) and (Γ, λ_z) (right figure), respectively. The dashed lines represent the loading paths with $F = 0, 0.5, -0.7$, respectively.

when localized bulging occurs. It is seen that there is a major difference between the predictions between the two material models: whereas the Ogden model predicts that localized bulging may take place when $F = 0$ and the associated critical value of $\Gamma = 3.81$ is attained at $\lambda_z = 0.15$, the Gent material model predicts that localized bulging can never take place when $F = 0$.

3.4.2 Unconstrained tube

We first consider the simplest case when $P = 0$, and we determine the critical value of Γ at which localized bulging may occur. We have in mind two possible types of

end conditions: either F or λ_z is fixed when Γ is increased. We note, however, that

the solution of the bifurcation condition $\Omega_u(\lambda_a, \lambda_z) = 0$ is independent of the end

conditions. It is found that when the Gent material model is used, this bifurcation

condition does not have a solution, and so localized bulging can never occur however

large the rotation speed is. This fact was already noted in the previous section in the

thin-wall limit. In contrast, when the Ogden material model is used, $\Omega_u(\lambda_a, \lambda_z) = 0$

has a solution giving λ_z as a function of λ_a; see the solid line in Figure (3.4)(a) where

we have also shown a typical loading curve defined by $\tilde{F}(\lambda_a, \lambda_z) = 0$. As Γ is increased

gradually from zero, loading starts from the point where $(\lambda_a, \lambda_z) = (1, 1)$ and traces

down the loading curve $\tilde{F}(\lambda_a, \lambda_z) = 0$. Localized bulging would occur when this curve

intersects the bifurcation curve $\Omega_u(\lambda_a, \lambda_z) = 0$ at

$$(\lambda_a, \lambda_z) = (2.313, 0.683),$$

with the associated value of Γ equal to 0.885.

As a comparison, we have also shown in Figure (3.4)(a) the loading paths associated

with $F = 0.5$ and -0.7. It is seen that as F is increased from zero, the loading path

is shifted upwards, whereas as F is decreased from zero, the loading paths is shifted

downwards, eventually losing the intersections with the bifurcation curve when F is

approximately equal to -0.7. This means that when $P = 0$, localized bulging is always

possible when a stretching force is applied axially in addition to the rotation, but

becomes impossible when a compressive force exceeding 0.7 in magnitude is applied.

(a) Gent material   (b) Ogden material
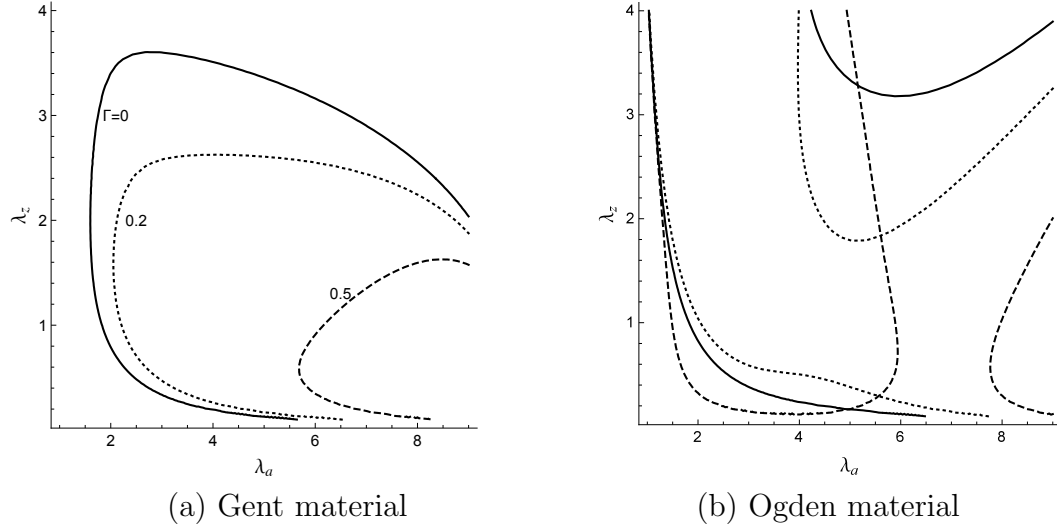
Figure 3.5: Solution of the bifurcation condition $J(\tilde{P}, \tilde{F}) = 0$ for the different values of Γ indicated. The solid, dotted and dashed lines correspond to $\Gamma = 0, 0.2$ and 0.5, respectively.

To offer a different perspective on the bifurcation, we have shown in Figure (3.4)(b) the critical value of λ_z as a function of Γ. This curve is obtained as follows. For each value of λ_z, the bifurcation condition $\Omega_u(\lambda_a, \lambda_z) = 0$ is solved to find the corresponding value of λ_a, and hence the value of Γ. This alterative plot of the bifurcation condition is particularly useful when it is the axial stretch that is fixed as the rotation speed is increased gradually. For each such axial stretch, λ_{z0} say, the corresponding critical value of Γ can simply be obtained from the intersection of the horizontal line $\lambda_z = \lambda_{z0}$ in this plot with the bifurcation curve. For instance, when λ_z is fixed at unity so that the tube is not allowed to contract axially as the rotation speed is increased, the associated critical value of Γ is equal to 0.997. It is seen that the critical value of Γ is an increasing function of λ_z.

60

We have also carried out calculations to find out how the results in Figure (3.4) depend on A. It is found that as A decreases (so that the wall thickness increases), the curve corresponding to $F = 0$ would shift downwards relative to the curve of $\Omega_u(\lambda_a, \lambda_z) = 0$. When A reaches 0.428 approximately, the two curves would no longer intersect, implying that localized bulging becomes impossible below this threshold value. In Table (3.1), we have listed the critical values of Γ for a selection of values of A. Since the wall thickness is a decreasing function of A/B, it can be seen that the larger the wall thickness, the larger the critical value of Γ. The numbers in brackets in the last row are the corresponding results based on the thin-wall approximation (3.41) and (3.42), and is seen to provide a good approximation, with a relative error of less than 5%, for values of A as small as 0.5.

A/B	0.43	0.5	0.6	0.7	0.8	0.9	0.99
λ_a	3.4779	2.9635	2.6486	2.4518	2.3128	2.2085	2.1346
λ_z	0.6291	0.6591	0.6729	0.6797	0.6834	0.6851	0.6956
Γ	1.4446	1.2984	1.1304	0.9958	0.8855	0.7935	0.7230
$\Gamma \approx$	(1.3641)	(1.2397)	(1.0896)	(0.9907)	(0.8837)	(0.7931)	(0.7230)

Table 3.1: Critical values of ω in free rotation ($F = 0$).

We next consider the effect of allowing for a non-zero internal pressure. There are now two subcases. The first subcase is when the unconstrained tube is mainly subjected to the action of internal inflation and an axial force, with rotation being small and

playing a minor role. This subcase covers the case of zero rotation which has previously been investigated Fu et al. (2016). In Figure (3.5) we have shown the solution of the bifurcation condition $\Omega_u(\lambda_a, \lambda_z) = 0$ for three representative values of Γ and the common value of $A = 0.8$. We note that when Γ is non-zero, the solution again has two branches when the Ogden material model is used. We shall focus our discussion on the parameter regime near $\lambda_a = \lambda_z = 1$. It is seen that adding a rotation to the tube delays the onset of localized bulging when the Gent material is used, but when the Ogden material is used the rotation has a delaying effect when the rotation speed is small, but has an opposite effect when the rotation speed is large enough.

Finally, we assume that the internal pressure P is zero or small, and it is the rotation and axial force F that play a dominant role. In Figure (3.6) we have shown the solution of $\Omega_u(\lambda_a, \lambda_z) = 0$ for three representative values of P. There is a big difference between the predictions of the two material models. For Gent material model, the bifurcation condition $\Omega_u(\lambda_a, \lambda_z) = 0$ disappears when $P = 0$, as mentioned previously. Localized bulging first becomes possible when P is increased to the value of 0.051. In contrast, according to the Ogden material model, localized bulging is possible even if P is zero. The dotted line in each figure represents the loading path, the solution of $\tilde{F}(\lambda_a, \lambda_z) = 0$, when $P = 0.06$.

(a) Gent material   (b) Ogden material
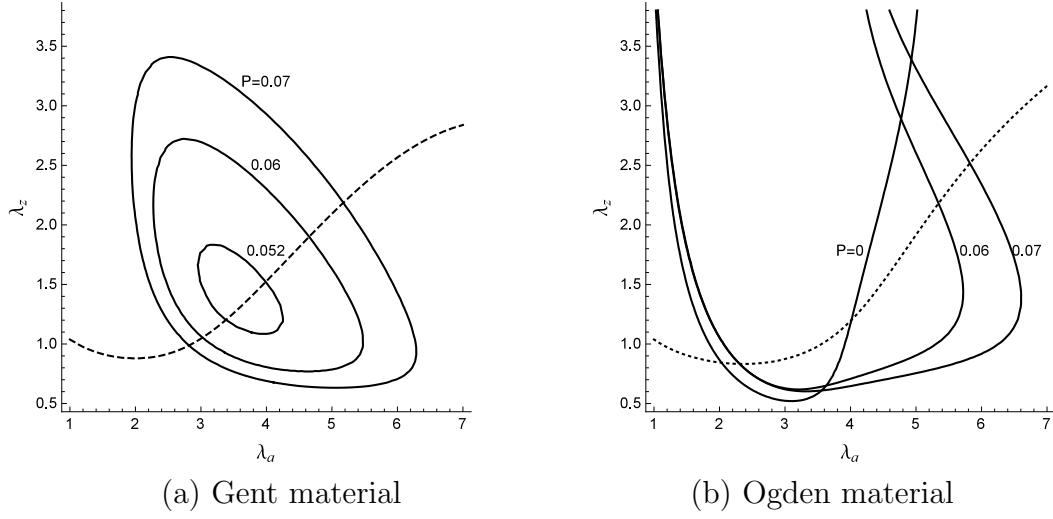
Figure 3.6: Solution of the bifurcation condition $\Omega_u(\lambda_a, \lambda_z) = 0$ for the three different values of P indicated. The dashed line corresponds to the solution of $\tilde{F}(\lambda_a, \lambda_z) = 0$ when $P = 0.06$, and is the loading path when there is no net axial force applied at the plane end-faces. Its intersection with the solid curve associated with $P = 0.06$ gives the values of the two stretches when localized bulging takes place.

3.4.3 The shrink-fit case

In this case the stretches must satisfy $\tilde{F}_0(\lambda_a, \lambda_z, \Gamma) = F$. This equation may also be solved to express Γ in terms of F. The bifurcation condition (3.16) then depends on F as well as λ_a and λ_z. For each specified F, this condition defines a curve in the $\lambda_a\lambda_z$-plane. A typical solution with $F = 2$ is shown in Figure (3.7), where the solution of $\sigma_{33}(a) = 0$ is also shown in a dashed line. It is seen that although localized bulging is possible, the contact force at $r = a$ must necessarily be tensile. This means that no matter how tight the initial fitting is, localized bulging will not occur before the tube

(a) Gent material

(b) Ogden material
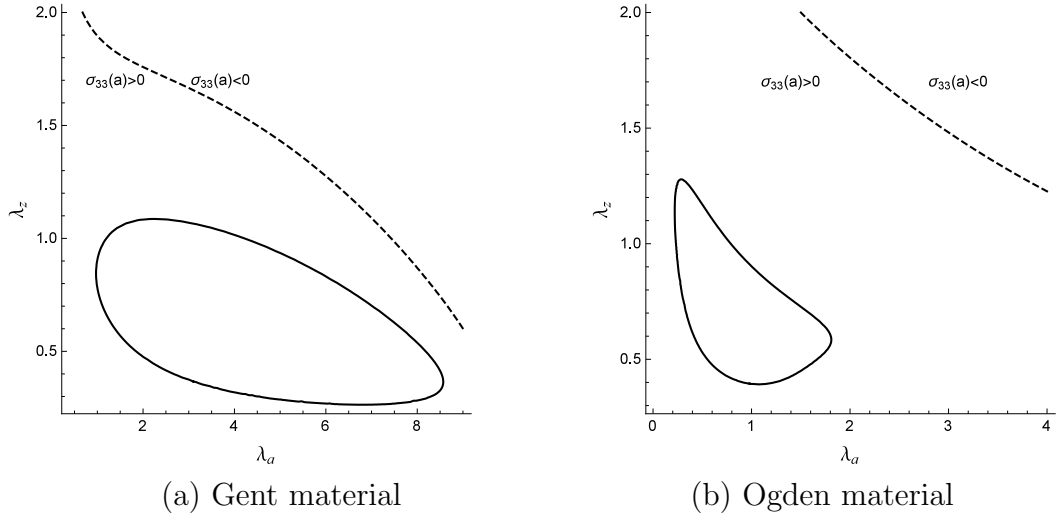
Figure 3.7: Solution of the bifurcation condition (3.16). The result corresponds to $F = 2$ and is shown in solid line. The dashed line in each plot represents the solution of $\sigma_{33}(a) = 0$.

loses contact with the rigid spindle. It is also found that as F is gradually reduced, the closed curve shrinks in size and eventually disappear at $F = 1.29$ when the Gent material model is used and at $F = 1.66$ when the Ogden material model is used. Thus, in particular, when the plane ends of the tube is traction-free, localized bulging will not occur no matter how large λ_a or Γ is.

3.5 Conclusion

In this Chapter we have studied the bifurcation condition for localized bulging of a circular solid cylinder or cylindrical tube which is rotated about its axis of symmetry.

Additional external forces may include a non-zero net axial force and/or internal pressure. In each case, the bifurcation condition is derived with the aid of the dynamical systems theory and found to have simple interpretations in terms of physical quantities such as the rotation speed, axial force and internal pressure. For instance, when the axial force and internal pressure are both fixed, the bifurcation condition simply corresponds to the angular velocity reaching a maximum when viewed as a function of λ_a for a tube or λ_z for a solid cylinder. However, this correspondence is lost when for instance it is the axial stretch λ_z that is fixed in rotating the tube.

The simplest case is perhaps the case of free rotation when both F and P are zero. Our illustrative calculations show that the Ogden material model would predict that localized bulging may occur but the Gent material model would predict that localized bulging can never occur. According to the Gent material model, localized bulging could occur only if a sufficiently large internal pressure is added. Also, according to both models, localized bulging will not occur in the shrink-fit case if $F = 0$. An experimental study is needed to compare the theoretical predictions for these two models with experimental results.

Chapter 4

Prevention of localized bulging in an inflated hyperelastic tube

4.1 Introduction

This chapter studies the bifurcation behavior in an inflated bilayer tube of arbitrary thickness under inflation and axial extension. It is assumed that both layers are composed of the Gent material with each layer having its own J_m, where J_m is a material parameter in the Gent model that signifies the maximum extensibility. First, we determine several critical parametrical regions where localized bulging disappears for a single-layer tube. Then we investigate localized bulging in an inflated bilayer

tube, where one layer (layer I) of the tube cannot bulge whereas the other part (layer II) can. The cases of fixed axial force and fixed axial stretch are both studied, and the critical geometrical parameters marking the transition between bulging and no bulging are determined. In Chapter 5, we will study the effects of shear modulus and constitutive models on the initiation of localized bulging in bilayer tubes. The results of this chapter have been published in Liu et al. (2019).

4.2   Bulging in a single-layer tube

We first consider a single-layer hyperelastic tube with inner radius A, outer radius B and length L. It is assumed that the tube is composed of an incompressible Gent material with the strain energy function given by (2.63). The tube is subject to the combined action of axial extension and an internal pressure P. Then we start from two previous papers (Haughton and Ogden, 1979a; Fu et al., 2016) and summarize some necessary results from them. After deformation, the inner and outer radii become a and b, respectively. Denoting the coordinates of the deformed and undeformed configurations by (θ, z, r) and (Θ, Z, R), respectively, we obtain the deformation in terms of cylindrical polar coordinates as follows:

$$r = \sqrt{\lambda_z^{-1}(R^2 - A^2) + a^2}, \quad \theta = \Theta, \quad z = \lambda_z Z, \tag{4.1}$$

where λ_z is the principal stretch in the axial direction.

By use of the incompressibility condition, the principal stretches are given by

$$\lambda_1 = \frac{r}{R} \equiv \lambda, \quad \lambda_2 = \lambda_z, \quad \lambda_3 = 1/(\lambda\lambda_z), \tag{4.2}$$

and the strain energy function can be rewritten as $w(\lambda, \lambda_z)$. Note that the indices $1, 2, 3$ correspond to θ-, z-, r-directions, respectively. Then the pressure P and resultant axial force F are expressed as

$$P(\lambda_a, \lambda_z) = \int_{\lambda_b}^{\lambda_a} \frac{w_{,1}}{\lambda^2 \lambda_z - 1} d\lambda, \tag{4.3}$$

$$F(\lambda_a, \lambda_z) = \pi A^2 (\lambda_a^2 \lambda_z - 1) \int_{\lambda_b}^{\lambda_a} \frac{2\lambda_z w_{,2} - \lambda w_{,1}}{(1 - \lambda^2 \lambda_z)^2} \lambda d\lambda, \tag{4.4}$$

where $\lambda_a = a/A$ and $\lambda_b = b/B$ are the circumferential stretches, and a comma behind a function represents the derivative with respect to the corresponding variable, i.e., $w_{,1} = dw/d\lambda$ and $w_{,2} = dw/d\lambda_z$. The relation between λ_a and λ_b can be obtained from equation (4.1) and is given by

$$\lambda_b = \sqrt{\frac{B^2 - A^2 + A^2 \lambda_a^2 \lambda_z}{B^2 \lambda_z}}. \tag{4.5}$$

In an inflated tube, localized bulging may occur if the internal pressure attains a critical value. In some literature or experiments, either the resultant axial force F or the axial stretch λ_z can be fixed, and the two loading approaches will also be investigated in

this chapter. For convenience, we label them as case I (fixed axial force) and case II (fixed axial stretch), respectively. In both cases, the outer surface is traction free. For case I, the tube is subject to both internal pressure and a fixed axial load F_0. For case II, the tube is first subjected to a uniform pre-stretch λ_{z0} and then the total length is fixed. However, the resultant force F can change during the inflation process under the length restriction. We mention that, for an inflated tube of arbitrary thickness, the bifurcation condition for localized bulging has been derived by Fu et al. (2016), which possesses the following form

$$J(P,F) = \frac{\partial P}{\partial \lambda_a}\frac{\partial F}{\partial \lambda_z} - \frac{\partial P}{\partial \lambda_z}\frac{\partial F}{\partial \lambda_a} = 0. \tag{4.6}$$

Generally speaking, for fixed axial force F, the curve for P against λ_a has an N shape where the local maximum corresponds to the pressure triggering localized bulging. However, the corresponding relation of P and λ_a might be monotonic for fixed axial stretch. We refer to Fu et al. (2018) for other possible forms of this bifurcation condition.

By utilizing the bifurcation condition (4.6), the first bifurcation point for cases I and II can be obtained by solving the following equations

$$\text{fixed axial force:} \quad J(P,F) = 0, \quad F(\lambda_a, \lambda_z) = F_0, \tag{4.7}$$

$$\text{fixed axial stretch:} \quad J(P,F) = 0, \quad \lambda_z = \lambda_{z0}. \tag{4.8}$$

Since all functions are related to two variables λ_a and λ_z, the above equations actually

provide the values of λ_a and λ_z at which localized bulging emerges. The critical pressure can then be obtained from equation (4.3).

From now on, we specify the shear modulus $\mu = 1$ and the outer radius $B = 1$ without loss of generality. Indeed, this is equivalent to normalizing the pressure P by μ and the quantities of length dimension by B, respectively. We aim to examine the effects of J_m and λ_{z0} on eliminating bulging in an inflated tube. In practice, the range of J_m varies for different materials. It was suggested in Gent (1996) that $J_m = 97.2$ or 114 for rubber. On the other hand, the corresponding range for human arteries is between 0.422 and 3.93 (Horgan and Saccomandi, 2003).

It is worth mentioning that, Pearce (2012) found that there exist critical values of J_m and λ_{z0} at which the bifurcation point vanishes for a membrane tube. Here we extend the corresponding results to a tube of arbitrary thickness. For definiteness, the inner radius is specified as $A = 0.8$, and we let $F_0 = 0$ in case I and $\lambda_{z0} = 1.5$ in case II.

According to equations (4.7) we plot Figures (4.1) and (4.2) where the first intersection between $J(P, F)-$curve and $F-$curve triggers localized bulging. An exhaustive explanation of the curves in these figures can be found in Fu et al. (2016). Figure (4.1) adopts a commonly used parameter $J_m = 97.2$ whereas Figure (4.2) uses a smaller $J_m = 17$. It can be seen that the tube can bulge in Figure (4.1) whereas there is no bulging in Figure (4.2). Furthermore, the curves for $J(P, F) = 0$ are always convex and will shrink towards the λ_a-axis if J_m reduces; see Figure (4.3).
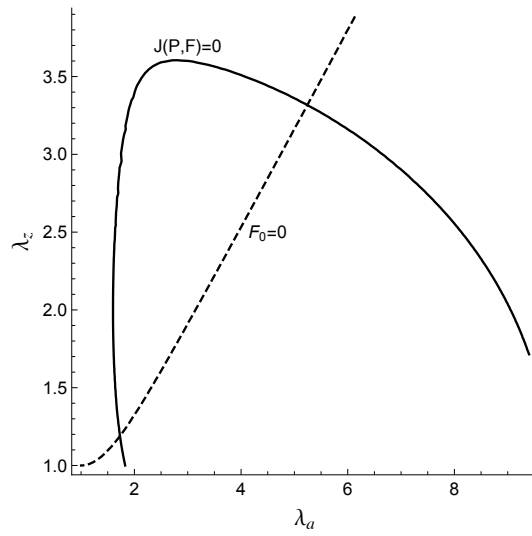
Figure 4.1: Results for the Gent model when $J_m = 97.2$. The left intersection of $J(P, F) = 0$ and $F_0 = 0$ corresponds to localized bulging.
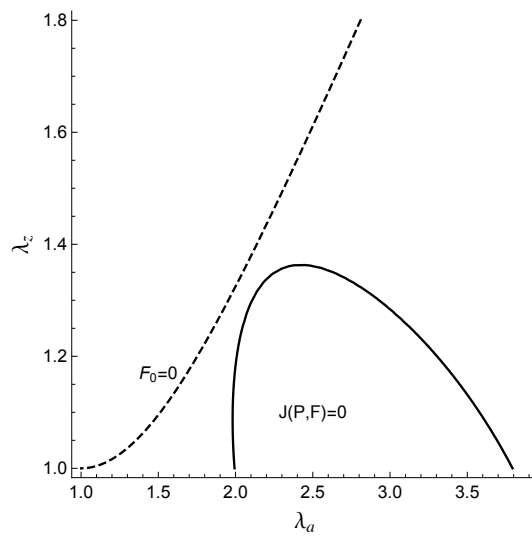
Figure 4.2: Results for the Gent model when $J_m = 17$ and $F_0 = 0$.

Using equation (4.8), we plot Figures (4.4) and (4.5) where the first intersection be-tween $J(P, F)-$curve and λ_z-line corresponds to localized bulging. It can be seen
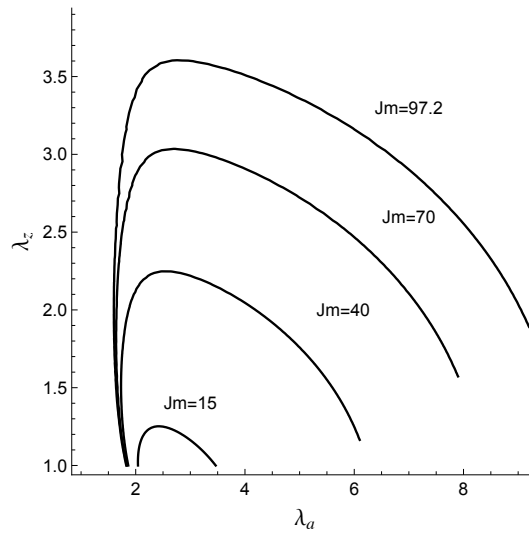
Figure 4.3: Plot of $J(P,F) = 0$ for four representative values of J_m.
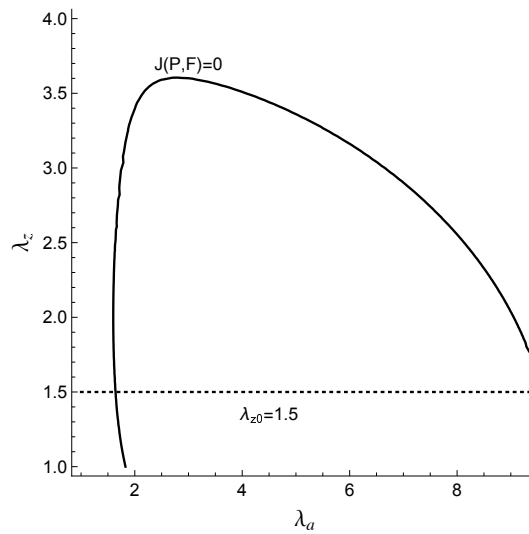
Figure 4.4: Results for the Gent model when $J_m = 97.2$. The left intersection of $J(P,F) = 0$ and $\lambda_{z0} = 1.5$ corresponds to localized bulging.

that localized bulging takes place in Figure (4.4) whereas there is no bulging in Figure (4.5).
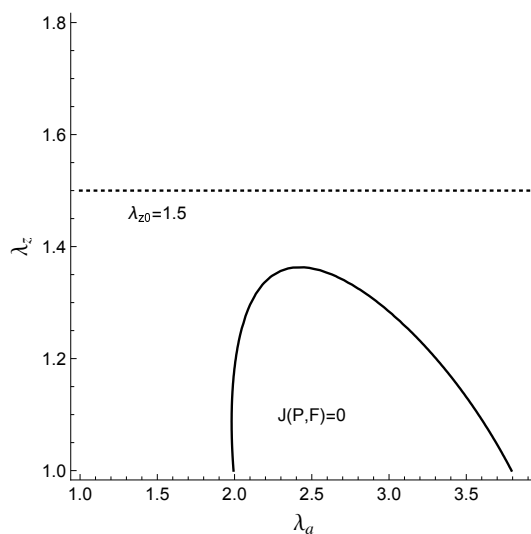
Figure 4.5: Results for the Gent model when $J_m = 17$ and $\lambda_{z0} = 1.5$.

Therefore, for case I, there may exist a critical value of J_m, say J_m^c, at which the tube never bulges if $J_m < J_m^c$. For case II, if λ_{z0} exceeds the maximum value of $J(P, F)-$curve, localized bulging is also eliminated. This implies that either a small J_m or a large pre-stretch λ_{z0} could preclude bulging in a rubber tube. Since J_m represents the extension limit, to reduce J_m is somehow equivalent to imposing a pre-stretch since the final effect diminishes the incremental stretching ability. Therefore, we say that the above-mentioned approaches to prevent bulging are actually equivalent.

It has been fully understood that in case I, localized bulging occurs when the pressure reaches its local maximum, and this kind of instability is the so-called limit-point instability (Alexander, 1971; Kanner and Horgan, 2007; Wang et al., 2018). In contrary, if the pressure-stretch (or volume) curve is monotonic, bulging formation never emerges. For completeness, we show the pressure-stretch curves for $J_m = 97.2$ and $J_m = 17$ in
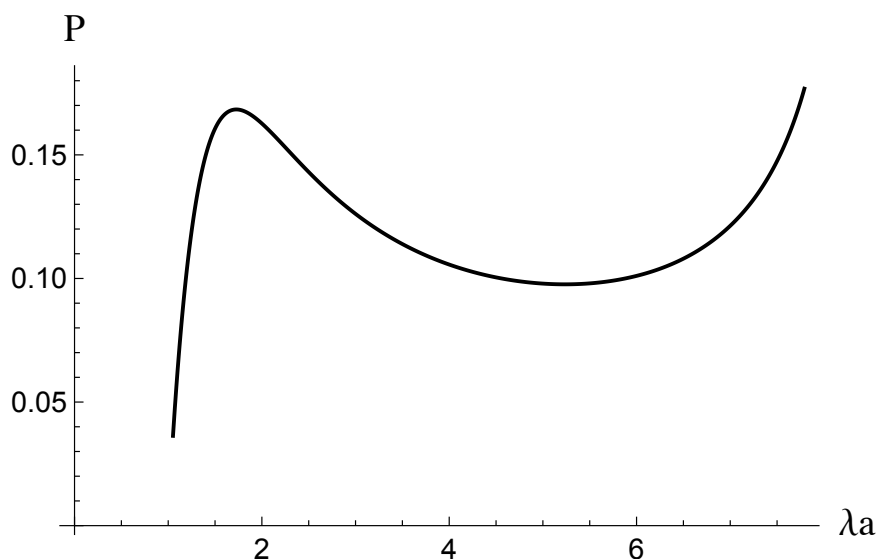
Figure 4.6: The pressure-stretch curve has a local maximum when $J_m = 97.2$.

Figures (4.6) and (4.7). In accordance with the expectation, the curve for $J_m = 97.2$ has an N shape, whereas the curve for $J_m = 17$ is monotonic. Since the objective of our study is to investigate how to remove bulging formation in a bilayer tube, we first should characterize the above critical parametric domains where localized bulging disappears. For case I, we need to determine J_m^c.

Before proceeding further, we note that the curve for $F(\lambda_a, \lambda_z) = 0$ is the lower bound for $F(\lambda_a, \lambda_z) = F_0$ when $F_0 \geq 0$, and this has been shown in Fu et al. (2016). Consequently, that there is no intersection between $F(\lambda_a, \lambda_z) = 0$ and $J(P, F) = 0$ provides a sufficient condition for avoiding localized bulging. As mentioned earlier, it is known that the pressure-stretch curve becomes monotonic when J_m becomes less than J_m^c. Thus, an inflection ceases to exist at the critical value J_m^c and we could
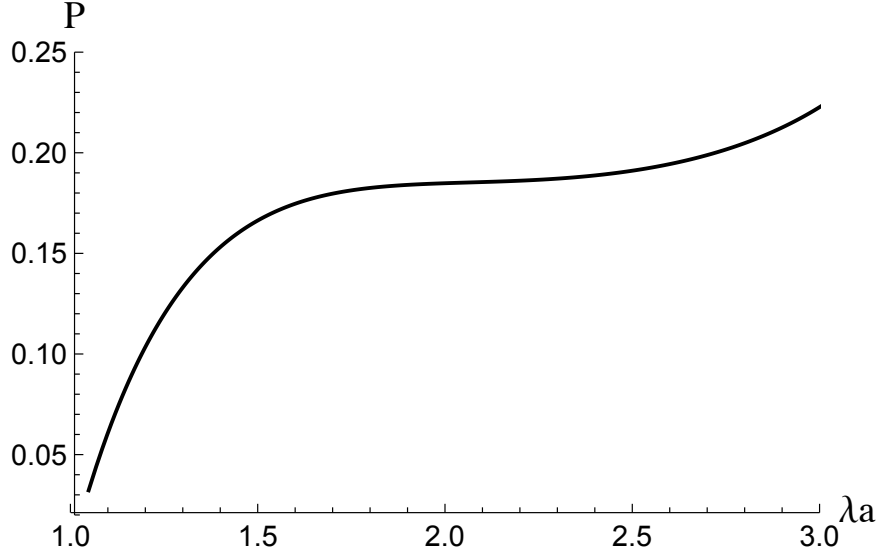
Figure 4.7: The pressure-stretch curve is monotonic when $J_m = 17$.

determine J_m^c by solving the equations (Mangan and Destrade, 2015)

$$\frac{dP}{d\lambda_a} = P_{,1} + P_{,2}\frac{d\lambda_z}{d\lambda_a} = 0, \tag{4.9}$$

$$\frac{d^2P}{d\lambda_a^2} = P_{,11} + \left(2P_{,12} + P_{,22}\frac{d\lambda_z}{d\lambda_a}\right)\frac{d\lambda_z}{d\lambda_a} + P_{,2}\frac{d^2\lambda_z}{d\lambda_a^2} = 0, \tag{4.10}$$

$$F(\lambda_a, \lambda_z) = 0, \tag{4.11}$$

where

$$\frac{d\lambda_z}{d\lambda_a} = -\frac{F_{,1}}{F_{,2}}, \tag{4.12}$$

$$\frac{d^2\lambda_z}{d\lambda_a^2} = \frac{F_{,1}\left(F_{,21} + F_{,22}\frac{d\lambda_z}{d\lambda_a}\right) - F_{,2}\left(F_{,11} + F_{,12}\frac{d\lambda_z}{d\lambda_a}\right)}{(F_{,2})^2}, \tag{4.13}$$

are from implicit differentiation $F(\lambda_a, \lambda_z) = 0$. However, the situation in case II is
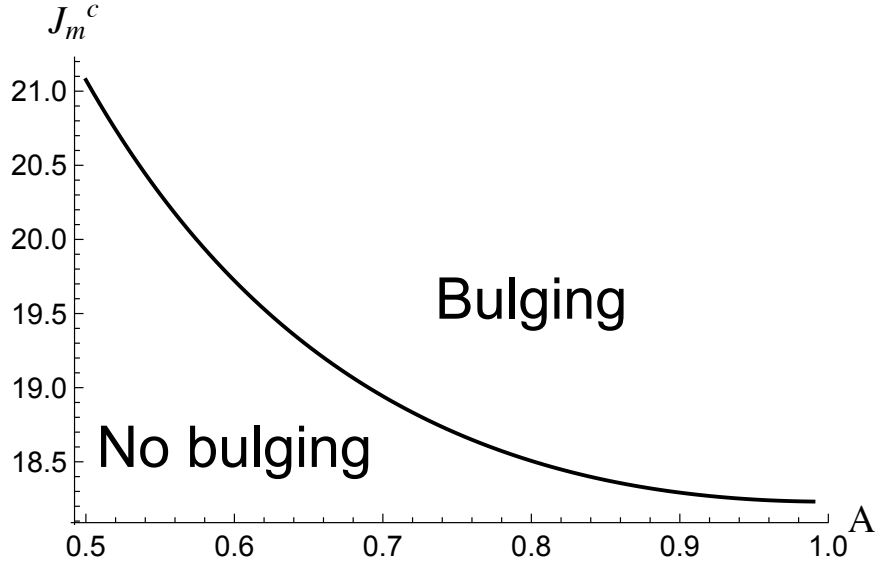
Figure 4.8: Critical curve where a transition of bulging behavior occurs in the case of fixed axial force $F_0 = 0$.

different because the pressure-stretch curve is always monotonic for Gent model. Then we refer to Figure (4.5) and observe that when the pre-stretch λ_{z0} increases from 1 to 1.5 the $\lambda_{z0}-$line varies from the secant line of $J-$curve to the tangent line and finally departs from it. Therefore, the critical parameter λ_z^c corresponds to the tangent case, and we could determine λ_z^c by solving the equations

$$\frac{d\lambda_z}{d\lambda_a} = -\frac{\Omega_{,1}}{\Omega_{,2}}, \tag{4.14}$$

$$\Omega(\lambda_a, \lambda_z) = 0, \tag{4.15}$$

where we have represented the bifurcation condition as $\Omega(\lambda_a, \lambda_z) = J(P, F) = 0$.

By using equations (4.9)-(4.11) and (4.14), (4.15), we may determine J_m^c with varying
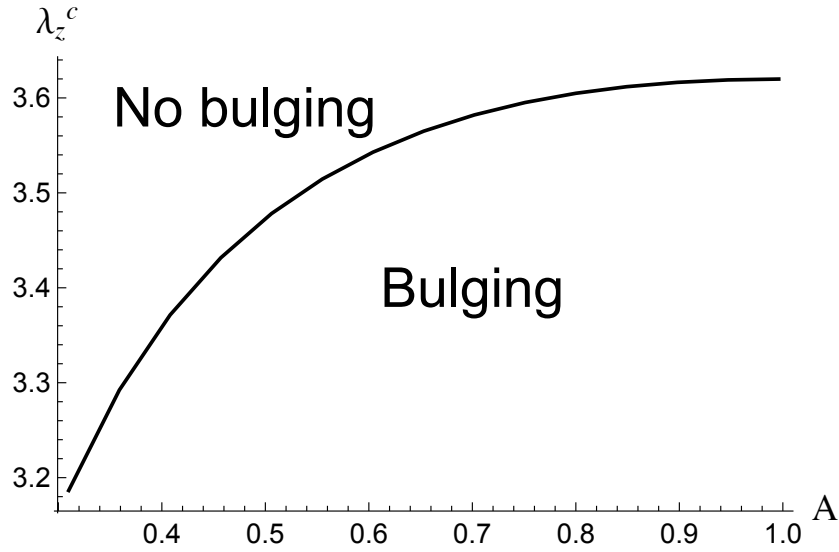
Figure 4.9: Critical curve where a transition of bulging behavior occurs in the case of fixed axial stretch when $J_m = 97.2$.

tube thickness and λ_z^c with different J_m and tube thickness, respectively (the outer radius has been set to $B = 1$). The corresponding results are displayed in Figures (4.8)-(4.10), and the regions where localized bulging cannot emerge are shown. It can be see that J_m^c is a decreasing function of A while λ_z^c is an increasing function of both A and J_m. For a membrane tube, it was found in (Pearce, 2012; Mangan and Destrade, 2015) that $J_m^c \simeq 18.231$ or $J_m^c \simeq 17.638$ respectively, which is very close to the value based on the exact theory when A goes to 1. Meanwhile, a similar curve of λ_z^c with varying J_m was also shown in Pearce (2012).

Now localized bulging in an inflated tube of composed of Gent material has been discussed, and some critical values for removing bulging are characterized. Indeed, we are interested in what happens when a bilayer tube is inflated when one layer
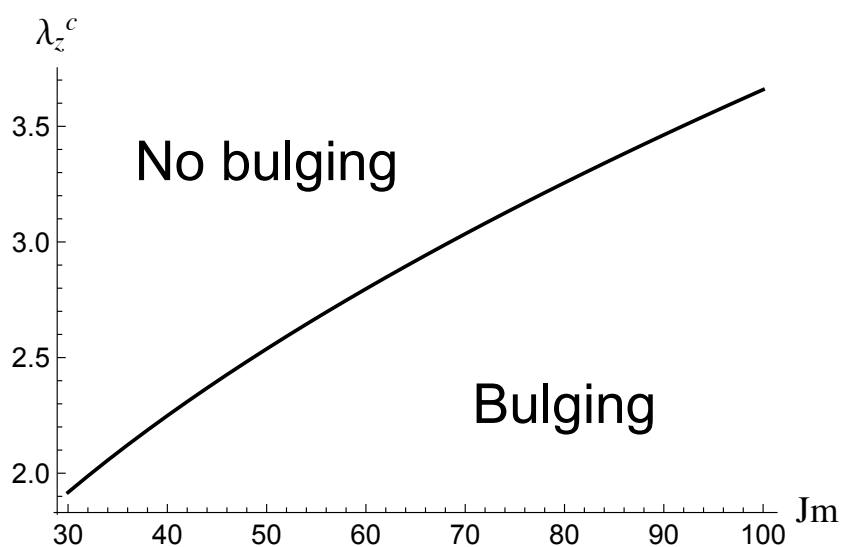
Figure 4.10: Critical curve where a transition of bulging behavior occurs in the case of fixed axial stretch when $A = 0.8$.

cannot bulge. Intuitively, one may think that if a tube is unable to bulge, a bilayer tube formed by covering another tube inside or outside this tube cannot bulge as well. However, the following analyses reveal an unexpected result.

4.3   A bilayer tube under inflation and axial loads

The aim of this section is to study the bulging possibility of the whole tube when one layer can bulge and the other layer cannot. In this section, we consider a bilayer tube with inner radius A and outer radius B under combined internal inflation P and axial load F. The geometry is given in Figures (4.11). In our setup, the bilayer tube

Figure 4.11: A bilayer tube with inner radius A and outer radius B under internal pressure P and axial load F.

has a finite length L. The interface is located at $R = D$. Accordingly, the deformed radii become a, b and d, respectively. Each layer is composed of the Gent material with the same shear modulus μ whereas the other parameter J_m is different. In the sequel, we adopt the convention that a bar on a quantity belongs to the inner layer, otherwise it represents a quantity for the outer layer; for instance, $\bar{\mu}$ and μ denote the shear moduli for the inner and outer layers, respectively. Furthermore, we focus on the effect of the proportion of each layer on bulging formation, so we set $\bar{\mu} = \mu = 1$ hereafter. The loading condition and boundary conditions are the same as that in the previous section. During inflation, we assume that the interface remains perfect bonded, i.e., the displacement and traction are continuous on the interface. In the following analysis, only the derivations for the outer layer will be shown for simplicity, and the results for the inner layer can be obtained by proper variable substitutions.

It is convenient to adopt cylindrical polar coordinates for the current problem. We use (θ, z, r) and (Θ, Z, R) to represent the coordinates of a representative material point in the deformed state and undeformed state, respectively. Note that the deformed state

is axisymmetric, the deformation gradient tensor F for the outer layer is given by

$$F = \begin{pmatrix} \dfrac{r}{R} & 0 & 0 \\ 0 & \lambda_z & 0 \\ 0 & 0 & \dfrac{\mathrm{d}r}{\mathrm{d}R} \end{pmatrix}. \tag{4.16}$$

By use of the incompressibility condition, we find

$$r^2 = \lambda_z^{-1}(R^2 - A^2) + a^2, \quad \theta = \Theta, \quad z = \lambda_z Z, \quad a \leq r \leq d, \tag{4.17}$$

$$r^2 = \lambda_z^{-1}(R^2 - D^2) + d^2, \quad \theta = \Theta, \quad z = \lambda_z Z, \quad d \leq r \leq b. \tag{4.18}$$

The only equation that is not satisfied automatically for the outer layer reads

$$\frac{\mathrm{d}\sigma_{33}}{\mathrm{d}r} + \frac{\sigma_{33} - \sigma_{11}}{r} = 0, \tag{4.19}$$

where σ_{ij} is the Cauchy stress tensor. Denoting the principal stretches as $\lambda_1, \lambda_2, \lambda_3$, we write the strain energy function as $W(\lambda_1, \lambda_2, \lambda_3)$. Here the indices 1, 2, 3 correspond to $\theta-$, $z-$, and $r-$ directions, respectively. Therefore, the principal Cauchy stresses are given by

$$\sigma_{ii} = \lambda_i W_{,i} - p, \quad \text{no summation}, \tag{4.20}$$

where p is the Lagrange multiplier, and the comma depicts the derivative with respect to the corresponding variable, for instance, $W_{,1} = \partial W / \partial \lambda_1$.

Utilizing the incompressibility condition, we denote the principal stretches as

$$\lambda = \lambda_1 = \frac{r}{R}, \ \lambda_2 = \lambda_z, \ \lambda_3 = \frac{1}{\lambda_1 \lambda_2}. \tag{4.21}$$

Then we use a reduced strain energy function $w(\lambda, \lambda_z) = W(\lambda, \lambda_z, 1/(\lambda_z \lambda_z))$ and obtain

$$
\begin{aligned}
w_{,1} &= W_{,1} - \frac{1}{\lambda^2 \lambda_z} W_{,3}, \\
w_{,2} &= W_{,2} - \frac{1}{\lambda \lambda_z^2} W_{,3}.
\end{aligned}
\tag{4.22}
$$

Finally, substituting equation (4.20) into the governing equation (4.19) yields

$$\sigma_{rr} = \int_{r_0}^{r} \frac{\lambda_1 w_{,1}}{r} \mathrm{d}r, \tag{4.23}$$

where r_0 is a constant to be determined. Then we apply a variable exchange $\lambda = r/R$ to furnish

$$\frac{\mathrm{d}\lambda}{\mathrm{d}r} = \frac{\lambda(1 - \lambda^2 \lambda_z)}{r}, \tag{4.24}$$

and by use of which the Cauchy stress σ_{rr} is rewritten as

$$\sigma_{rr} = \int_{\lambda_0}^{\lambda} \frac{w_{,1}}{1 - \lambda^2 \lambda_z} \mathrm{d}\lambda, \tag{4.25}$$

where λ_0 is an undetermined constant. Accordingly, we introduce the principal stretches in the circumferential direction at the inner surface, outer surface, and interface as follows

$$\lambda_a = \frac{a}{A}, \ \lambda_b = \frac{b}{B}, \ \lambda_d = \frac{d}{D}. \tag{4.26}$$

From equation (4.17) and (4.18), their relations are given by

$$\lambda_b = \sqrt{\frac{B^2 - A^2 + A^2\lambda_a^2\lambda_z}{B^2\lambda_z}}, \quad \lambda_d = \sqrt{\frac{D^2 - A^2 + A^2\lambda_a^2\lambda_z}{D^2\lambda_z}}. \tag{4.27}$$

It is assumed that the outer surface of the bilayer tube is traction-free and the inner surface is inflated by a pressure P. Furthermore, the interface between the two layers keeps perfectly bonded during the deformation. Therefore, the displacement and traction are continuous at the interface. Then we obtain

$$\sigma_{rr}|_{\lambda=\lambda_b} = 0, \quad (\bar{\sigma}_{rr} - \sigma_{rr})|_{\lambda=\lambda_d} = 0, \quad \bar{\sigma}_{rr}|_{\lambda=\lambda_a} = -P. \tag{4.28}$$

From equation $(4.28)_1$, the integration constant for the outer layer reads $\lambda_0 = \lambda_b$. Moreover, employing the traction continuity condition $(4.28)_2$ and the traction condition at the inner surface $(4.28)_3$, we have

$$P(\lambda_a, \lambda_z) = \int_{\lambda_d}^{\lambda_b} \frac{w_{,1}}{1 - \lambda^2\lambda_z}\mathrm{d}\lambda + \int_{\lambda_a}^{\lambda_d} \frac{\bar{w}_{,1}}{1 - \lambda^2\lambda_z}\mathrm{d}\lambda. \tag{4.29}$$

On the other hand, the resultant axial force in any cross section possesses the form

$$\begin{aligned}
F =& 2\pi\left(\int_a^d \bar{\sigma}_{zz}r\mathrm{d}r + \int_d^b \sigma_{zz}r\mathrm{d}r\right) - P\pi a^2 \\
=& \pi\left(\int_a^d (2\lambda_z\bar{w}_{,2} - \lambda\hat{w}_{,1})r\mathrm{d}r + \int_d^b (2\lambda_z w_{,2} - \lambda w_{,1})r\mathrm{d}r\right).
\end{aligned} \tag{4.30}$$

By use of the variable substitution $\lambda = r/R$ again and combining equations (4.17) and (4.18), we obtain the simplified form of resultant axial force

$$
\begin{aligned}
F(\lambda_a, \lambda_z) =& \pi A^2 (\lambda_a^2 \lambda_z - 1) \int_{\lambda_d}^{\lambda_a} \frac{2\lambda_z \bar{w}_{,2} - \lambda \bar{w}_{,1}}{(\lambda^2 \lambda_z - 1)^2} \lambda \mathrm{d}\lambda \\
&+ \pi D^2 (\lambda_d^2 \lambda_z - 1) \int_{\lambda_b}^{\lambda_d} \frac{2\lambda_z w_{,2} - \lambda w_{,1}}{(\lambda^2 \lambda_z - 1)^2} \lambda \mathrm{d}\lambda.
\end{aligned}
\tag{4.31}
$$

Once the formulas of P and F are expressed, we could utilize the bifurcation condition (4.6) to determine the critical stretch triggering bulging formation. Although this condition is derived for a single-layer tube, Wang and Fu (2018) have applied it to double-fiber reinforced tubes to investigate the effect of fiber angle on localized bulging.

4.4   Results and discussions

In this section, we concentrate on a bilayer tube whose inner or outer layer cannot bulge and depict the parametrical domains where localized bulging vanishes. Without loss of generality, the outer radius is also set to $B = 1$. For case I, referring to Figure (4.8), we specify $J_m = 15$ that is less than the critical value of J_m^c . For case II, we assume that the bilayer tube is uniformly stretched by $\lambda_{z0} = 2.5$ before inflation and then the length is fixed.

4.4.1   Case I: fixed axial force

By considering case I, we are interested in how to remove bulging formation in a bilayer tube. First of all, a tube of $J_m = 97.2$ bulges when the internal pressure attains a critical value, and we now wish to prevent bulging by coating this tube with another tube with $J_m = 15$. Thus a bilayer tube with $\bar{J}_m = 15$ and $J_m = 97.2$ is studied. Since the remaining free parameters are the inner radius and interfacial radius, respectively, we could specify either the whole thickness of the tube or the thickness of the outer layer to reveal the influence of the other parameter on the inflation behavior.

When the whole tube thickness is specified, we apply equations (4.9)-(4.11) again to determine the critical value of D, say D_c, where the inflection point becomes a turning point in the pressure-stretch curve. On the other hand, the same approach is applied to find an analogue value A_c if the thickness of the outer layer is fixed. Similarly, we only need to consider $F = 0$ to obtain a sufficient condition that a bilayer tube never bulges under inflation, and the corresponding results are shown in Figure (4.12). We mention that the dashed lines in Figure (4.12) (see also Figures (4.13), (4.14), (4.15)) are $A = D$, which indicates the lower bound of D for a given A or the upper bound of A for a given D. In other words, in Figure (4.12)(a), for example, the area under bulging zone is in the forbidden region since D must be greater than A. Figure (4.12)(a) illustrates the critical curve for D_c, and the corresponding curve for A_c is shown in Figure (4.12)(b).

For convenience, we also highlight the region where bulging can or cannot occur.

(a) Critical D_c if A is specified.

(b) Critical A_c if D is specified.
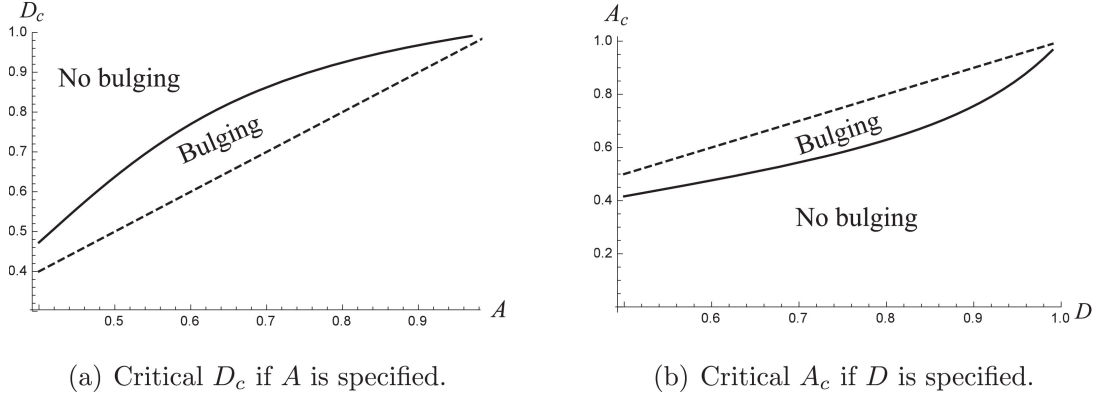
Figure 4.12: The inner layer cannot bulge whereas the outer layer can ($\bar{J}_m = 15$ and $J_m = 97.2$). The dashed line depicts the maximum or minimum value of the vertical-axis parameter. Figure (a) illustrates the critical curve of D, say D_c, where a transition of bulging behavior occurs. We also indicate the corresponding region. Figure (b) shows the corresponding curve of A_c.

Actually, the critical curves D_c and A_c denote the corresponding transitions. It can be seen that, if A is specified, the tube still bulges under sufficient internal pressure with a small D. However, with increasing D, the tube cannot bulge when $D > D_c$. In other words, the inner layer occupies a small part of the whole tube if D is small. Therefore, the deformed configuration for a bilayer tube is governed by the major part, i.e., the outer layer, and localized bulging occurs at a critical pressure. When $D > D_c$, the dominant part becomes the inner layer, thus the tube loses the ability to bulging. Meanwhile, we obtain the same property for fixed D. Thus, to prevent bulging from appearing in a tube, we could attach a tube that is unable to bulge with a small specified thickness at the inner surface of the original one.

(a) Critical D_c if A is specified.

(b) Critical A_c if D is specified.
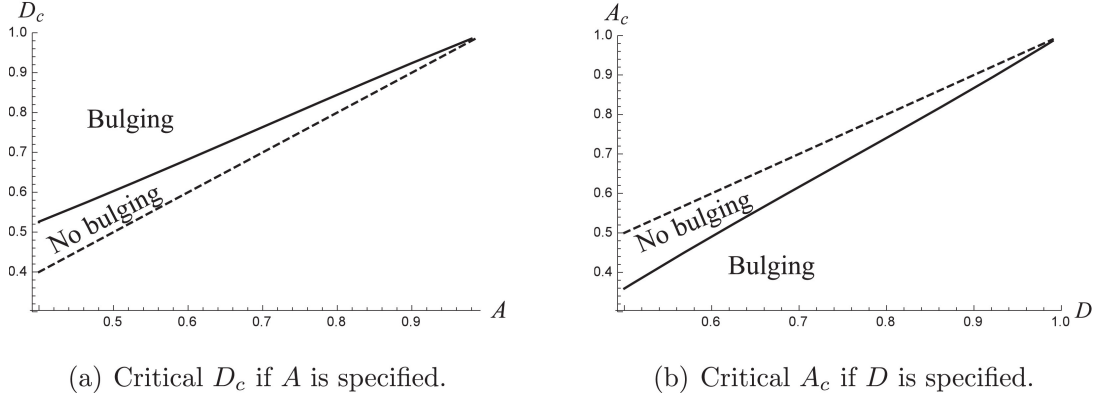
Figure 4.13: The outer layer cannot bulge whereas the inner layer can ($\bar{J}_m = 97.2$ and $J_m = 15$). The dashed line depicts the maximum or minimum value of the vertical-axis parameter. Figure (a) illustrates the critical curve of D_c, and figure (b) shows the corresponding curve of A_c.

Conversely, we further study the case where the outer layer can not bulge by only exchanging the value of the parameter J_m. Similarly, whether bulging formation occurs or not in the bilayer tube depends on the proportion of the outer layer. We also consider two different situations, i.e., either the thickness of the tube or the thickness of the outer layer is fixed. The corresponding results are shown in Figure (4.13). Figure (4.13)(a) illustrates the dependence of D_c on the inner radius A. This also corresponds to the situation of fixed total thickness of the tube. Figure (4.13)(b) plots the curve of A_c with varying D. Likewise, we also highlight the region where localized bulging disappears. It can be seen that the critical curves for both A_c and D_c are almost straight. Furthermore, the no bulging area is small compared with the bulging area. Combining the results in Figures (4.12) and (4.13), we conclude that the inner layer likes to dominate the deformation, namely, the final deformed configuration is

(a) Critical D_c if A is given.

(b) Critical A_c if D is given.
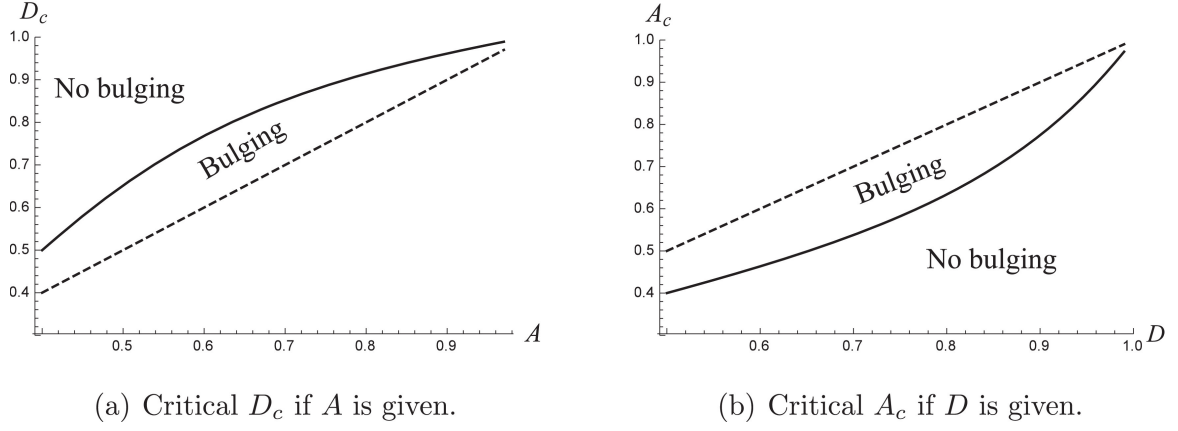
Figure 4.14: The inner layer cannot bulge ($\bar{J}_m = 40$ and $J_m = 97.2$), and the axial length is fixed $\lambda_z = 2.5$.

mainly governed by the inner layer. We mention that the approach in Bucchi and Hearn (2013) to prevent bulging formation is to attach some inextensible fibers at the outside of the tube. Although this is valid, yet the current analysis suggests that covering the tube with fibers at the inner surface of the tube might be more efficient.

4.4.2   Case II: fixed axial stretch

Next, we assume that a bilayer tube is uniformly stretched in the axial direction by $\lambda_{z0} = 2.5$ and then the axial length is fixed. The bilayer tube is also composed of two parts. One layer cannot bulge (layer I) while the other layer (layer II) can under the pre-stretch $\lambda_{z0} = 2.5$. For that purpose, we specify $J_m = 40$ for layer I and $J_m = 97.2$ for layer II, respectively, according to the result in Figure (4.10).

(a) Critical D_c if A is given.

(b) Critical A_c if D is given.
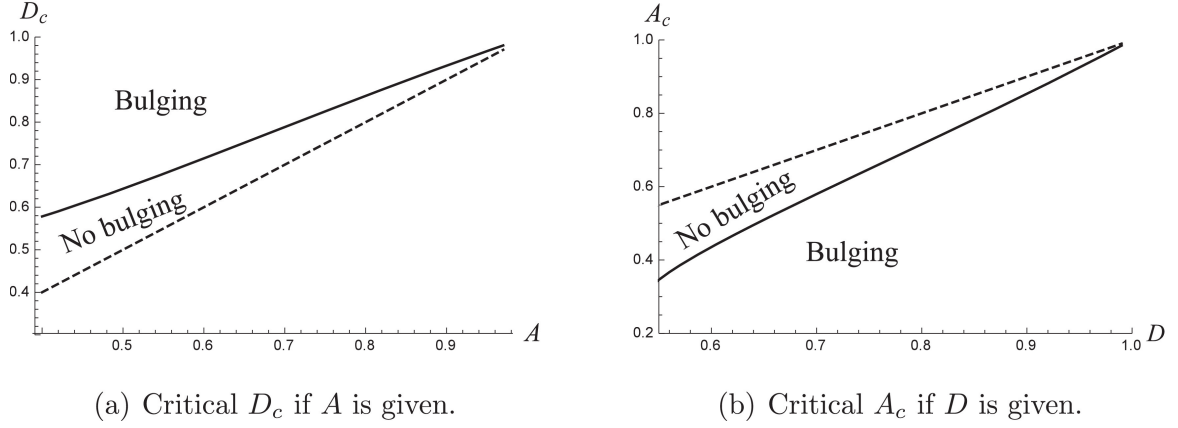
Figure 4.15: The outer layer cannot bulge ($\bar{J}_m = 97.2$ and $J_m = 40$), and the axial length is fixed $\lambda_z = 2.5$.

We first consider similarly the situation that the inner layer is unable to bulge and then study the converse case. The corresponding results are shown in Figures (4.14) and (4.15), respectively. It can be seen that the features are quite similar to case I. This is not surprising since we have mentioned before that J_m is a parameter describing the maximum extensibility of a tube. If one regards the stretched tube as a new one without pre-stretch, the new J_m actually reduces. On the other hand, the no bulging area is dependent on the location of layer I. If the inner layer is unable to bulge, the no bulging area is higher, or otherwise, the no bulging area is lower. In other words, the inner layer has a significant effect on the final deformed configuration of the bilayer tube.

4.5 Conclusion

In the framework of nonlinear elasticity and by use of the Gent model, we investigate the effects of J_m and pre-stretch λ_{z0} on localized bulging in an inflated single-layer tube and determine several parametric domains where localized bulging vanishes. The critical parameters are denoted by J_m^c and λ_z^c respectively. Bulging formation never occurs if $J_m < J_m^c$ for fixed axial force or the pre-stretch $\lambda_{z0} > \lambda_z^c$ for fixed axial length.

Then we apply the results to a bilayer tube composed of the Gent material. In addition, both layers share the same shear modulus but the other parameter J_m can be varied. This tube is special because one layer (layer I) never bulges and the other layer (layer II) may bulge under sufficient pressure. We find that whether localized bulging occurs or not in this composite tube is dependent on the competition between two layers. Localized bulging never occurs if the proportion of layer I increases to a critical value, no matter whether layer I occupies the inner side or the outer side, also regardless of whether the thickness of whole tube or the thickness of the outer layer is specified. In particular, a better choice for bulging prevention is to locate layer I on the inner side since a relatively thin thickness is enough to preclude bulging formation.

Finally, we note that bulging bifurcation is usually subcritical (Fu and Xie, 2012; Wang et al., 2019) associated with the so-called snap-through phenomenon. Indeed, this research is a primary study of localized bulging in inflated layered tubes, and we do not address the stability of the bulging solution. The underlying assumption is that

bulging instability is also subcritical in a bilayer tube. Other topics concerning effect of shear modulus and constitutive models will be investigated in the next chapter.

Chapter 5

Effects of the stiffness ratio on localized bulging in a bilayer tube

5.1   Introduction

In this Chapter we consider a bilayer tube subject to an internal pressure and axial force to study the effects of s, the interfacial radius D, and different constitutive models on the bulge initiation, where s is the ratio of the shear modulus of the outer layer to that of the inner layer. By use of the internal volume ratio v as the bifurcation parameter, a parametric study of bulge initiation is carried out. The two typical cases

of fixed axial force and fixed axial length are considered using the Gent and Ogden material models. The results of this chapter have been published in Ye et al. (2019).

5.2   Problem formulation

We consider a bilayer tube composed of incompressible hyperelastic materials with inner radius A, outer radius B, interfacial radius D, and initial length L, as shown in Figure 4.11. Under inflation and axial extension, the tube is first dilated, but the cross-section maintains a circular geometry. We call this deformed state the basic state (or uniform inflation), and the corresponding radii become a, b, and d, respectively. Then a further increase of the pressure may trigger localized bulging. Note that the basic solution for a single-layer tube has been provided in Haughton and Ogden (1979b) and Fu et al. (2016). Here we simply extend the corresponding results to a bilayer tube. The deductions for the basic solution of the uniform inflation are shown in Chapter 4. Therefore, in the following, we use the expressions of the internal pressure $P(\lambda_a, \lambda_z)$ (4.29) and resultant axial force $F(\lambda_a, \lambda_z)$ (4.31) as shown in the previous chapter.

With the aid of dynamical systems theory, Fu et al. (2016) has provided an explicit bifurcation condition for localized bulging in an inflated single-layer tube of arbitrary thickness in a very concise form

$$J(P, F) = \frac{\partial P}{\partial \lambda_a} \frac{\partial F}{\partial \lambda_z} - \frac{\partial P}{\partial \lambda_z} \frac{\partial F}{\partial \lambda_a} = 0. \tag{5.1}$$

Indeed, the above equation means that the Jacobian of P and F in terms of variables λ_a and λ_z vanishes if localized bulging occurs. Furthermore, it was also shown by Fu et al. (2016) that the pressure triggering bulging formation is just the maximum pressure in uniform inflation when F is fixed. Recently, this bifurcation condition was applied to fiber-reinforced tubes (Wang and Fu, 2018).

In an inflated tube, localized bulging may occur if the internal pressure attains a critical value. As mentioned earlier, there are two loading types. The first case is to fix the resultant axial force F and the other case has a fixed axial stretch (or fixed axial length). In this chapter, we also consider these two loading types. For convenience, we label them as case I (fixed axial force) and case II (fixed axial stretch), respectively, and both cases share the same boundary conditions and continuity conditions. Case I corresponds to the situation that one end of the tube is free to inflate and the other end is subject to a dead weight. We refer to the experiment by Kyriakides and Chang (1990, 1991); Guo et al. (2016); Wang et al. (2019) for such a kind of setup. Case II can be achieved by first uniformly stretching the tube and then fixing the total length. This kind of setup was adopted in the experiment by Pamplona et al. (2006); Gonçalves et al. (2008); Wang et al. (2019).

By utilizing the bifurcation condition (5.1), the first bifurcation point for cases I and II can be obtained by solving the following equations

$$\text{fixed axial force:} \quad J(P,F) = 0, \quad F(\lambda_a, \lambda_z) = F_0, \tag{5.2}$$

$$\text{fixed axial stretch:} \quad J(P,F) = 0, \quad \lambda_z = \lambda_{z0}, \tag{5.3}$$

where F_0 and λ_{z0} are constants. Since all functions are related to variables λ_a and λ_z, the above equations actually provide the values of λ_a and λ_z at which localized bulging emerges. Accordingly, the critical pressure can be obtained from equation (4.29).

In our illustrative calculations, the incompressible Gent model (Gent, 1996) and Ogden model (Ogden, 1972) are employed, with the strain energy functions given by (2.63) and (2.60), respectively. In the following analysis, we will consider that both layers are composed of the Gent material or Ogden material, respectively. In particular, we adopt $J_m = 97.2$ which is typical value for rubbers for both layers (Gent, 1996) when the Gent model is employed.

Before proceeding further, we set the outer radius to $B = 1$ (this is equivalent to scaling all quantities of length dimension by B) and introduce a parameter $s = \mu/\bar{\mu}$ denoting the shear modulus ratio of the outer and inner layers. In Chapter 4, by use of the Gent model, the situation that the two layers share the same modulus but different J_m has been studied. In this chapter, however, we focus on the effect of stiffness ratio s and constitutive model on bulge initiation.

On scaling the pressure P by $\bar{\mu}$ and the axial force F by $\bar{\mu}B^2$ (for convenience, we still keep the original symbols), the bifurcation condition (5.1) is dependent on three parameters s, A, and D. In order to carry out a bifurcation analysis, a proper bifurcation parameter shall be selected. Actually, three loading parameters including mass, pressure and volume can be controlled in experiments. Mass control can be achieved by inflating a rubber tube by an air pump (Pamplona et al., 2006; Gonçalves et al.,

2008; Guo et al., 2016; Wang et al., 2019). Pressure control is difficult to perform and must involve a large enough water tank with a fixed height. Furthermore, bulging solutions under pressure control are unstable (Fu and Xie, 2010).

In the case of volume control, one usually pumps water into the tube. Since water may be treated as incompressible, it is the injected volume that can be controlled (Kyriakides and Chang, 1990, 1991). For inflation problems, Varatharajan and Das-Gupta (2017) considered a single-layer membrane tube surrounded by soft tissues and adopted the circumferential stretch as the bifurcation parameter. In this study, we directly employ the volume ratio $v = V_1/V_0$ as our controlled bifurcation parameter, where V_0 and V_1 denote the internal volume for the bilayer tube in the initial and basic states, respectively. After simple calculations, it is found that

$$v = \lambda_a^2 \lambda_z. \tag{5.4}$$

In the sequel, we investigate the effects of modulus ratio and different proportion of each layer on the bulge initiation and maximum radius of the bulge that a tube can attain. Once the critical volume ratio v_{cr} is known, the corresponding pressure can be obtained by use of equation (4.29). In the next section, we study both of the fixed axial force and fixed axial stretch. Since we adopt v as the bifurcation parameter, a criterion in this study reads that a larger v_{cr} corresponds to a more stable structure. Indeed, for a volume control problem, this criterion is suitable since it is the volume pumped into the tube that is controlled. However, for other kinds of control problems,

the current study also provides useful insights into the bulging behavior in inflated bilayer tubes.

5.3   Parametric studies of bulge initiation

In this section, we investigate the bulge initiation by use of equations (5.2) and (5.3). In the initial state, the volume ratio is $v = 1$. When inflating a bilayer tube, the volume ratio v increases and reaches a critical value v_{cr} at which a bifurcation leading to bulge formation occurs. Next, we study case I and case II separately.

5.3.1   Case I: fixed axial force

In this case, the axial resultant force $F = F_0$ is fixed. For convenience, we consider $F_0 = 0$ in the subsequent analysis. By use of equation (5.2), the stretches λ_a^{cr} and λ_z^{cr} where localized bulging emerges can be determined. Then we can find the bifurcation threshold v_{cr} from (5.4). Next, without loss of generality, we specify the inner radius by $A = 0.6$ and investigate the relations between v_{cr} and the modulus ratio s with different D, and the corresponding results are shown in Figure (5.1) for the Gent model. It can be seen that, for a given D, the critical volume ratio v_{cr} is an increasing function of s. Therefore, a stiffer outer part creates a more stable structure, which is consistent with the results in Varatharajan and DasGupta (2017) where the enclosed substrate can delay the onset of bulging with increased stiffness. However, when s
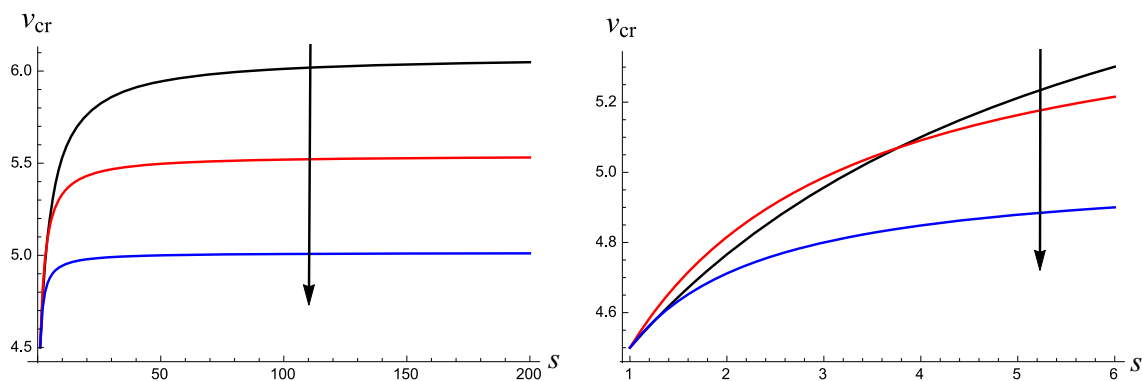
Figure 5.1: Relations between v_{cr} and s when $D = 0.9$, 0.8, 0.7, respectively, for the Gent model. The inner and outer radii are given by $A = 0.6$ and $B = 1$. The arrow indicates the decrease of D. The right plot displays an enlarged part of the left one.

is roughly larger than 100, the improvement of v_{cr} becomes marginal. On the other hand, when s is small, it is found from the right figure in Figure (5.1) that v_{cr} is non-monotonic with varied D. Furthermore, bifurcation curves for the Ogden model are illustrated in Figure (5.2), and a similar feature is observed.

From the analysis, we can deduce that a stiffer outer layer generates a larger v_{cr} when all other parameters are prescribed. However, the critical volume ratio v_{cr} is a non-monotonic function of D if the thickness of bilayer tube and the modulus ratio s are specified. Since layered tubes can be used to model human arteries (Gasser et al., 2005) and a thinner tube is easier to bifurcate (Fu et al., 2016), we then focus on a composite tube with a given thickness (or inner radius). We aim at providing new insights into the role of the mechanical property of different layers in bulge initiation.
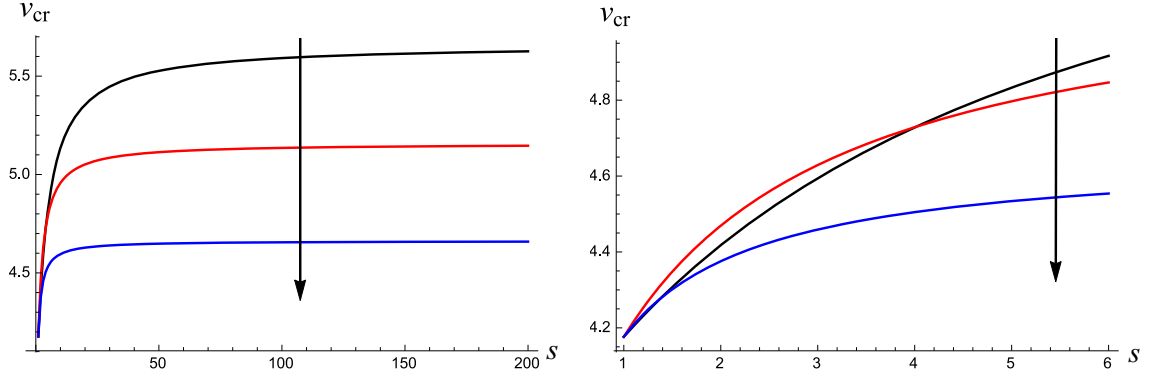
Figure 5.2: Relations between v_{cr} and s when $D = 0.9$, 0.8, 0.7, respectively, for the Ogden model. The inner and outer radii are given by $A = 0.6$ and $B = 1$. The arrow indicates the decrease of D. The right plot displays an enlarged part of the left one.

From now on we study how v_{cr} depends on D. From equation (5.4), both λ_a and λ_z contribute to v_{cr}. Therefore, we first seek the source of non-monotonicity of v_{cr} with respect to D and plot λ_a^{cr} and λ_z^{cr} in Figure (5.3) for the Gent model. It can be seen that both λ_a^{cr} and λ_z^{cr} have a maximum when the outer layer is stiffer. However, as shown in Figure (5.3(b)), λ_z^{cr} varies in a very small range such that the behavior of v_{cr} in terms of D is mainly dominated by λ_a^{cr}. Therefore, we may speculate that v_{cr} also has a maximum when $s > 1$.

Next, the curves of v_{cr} in terms of D for six values of s are depicted for the Gent model and Ogden model in Figures (5.4) and (5.5), respectively. In consistency with the previous results, when D is given, a larger s produces a higher v_{cr}. Moreover, the curve has a maximum if $s > 1$ but a minimum if $s < 1$. When the inner layer is stiffer, the composite tube is less stable. Since further enhancement of stability when $s > 100$

is negligible, we then only show the results for $s \leqslant 100$. In addition, if the inner layer is stiffer, we consider $s \geqslant 0.01$.
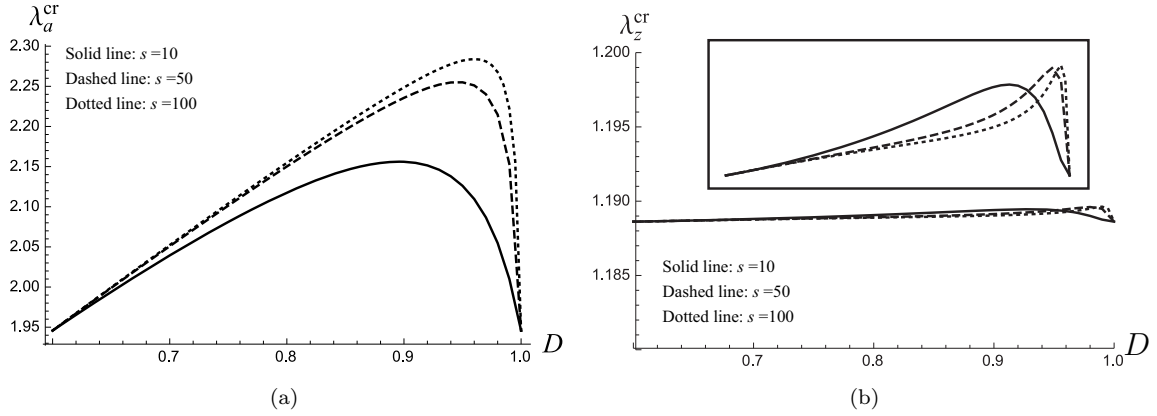
Figure 5.3: Dependence of λ_a^{cr} and λ_z^{cr} on D when $A = 0.6$ and $B = 1$. The figure in the rectangular of (b) indicates the curve of λ_z^{cr} when a large scale of the vertical axis is adopted.
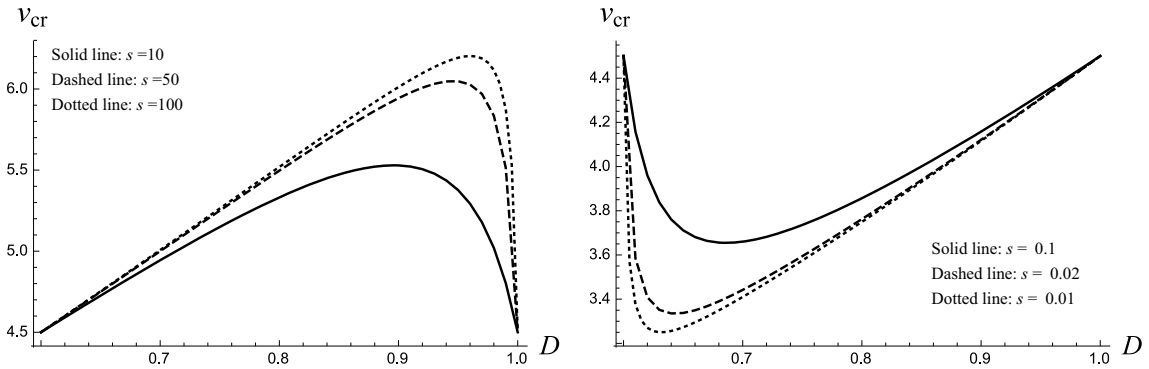
Figure 5.4: Dependence of v_{cr} on D when $A = 0.6$ and $B = 1$ for the Gent model. Three values of s are shown in each figure.

Now, it is known that v_{cr} is always a monotonically increasing function of s but can have a maximum or minimum in terms of D. We may determine the maximum or
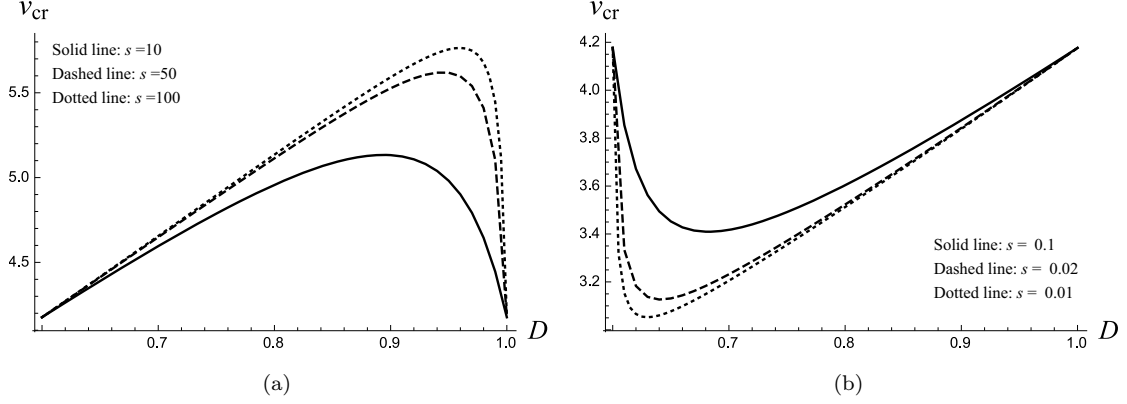
Figure 5.5: Dependence of v_{cr} on D when $A = 0.6$ and $B = 1$ for the Ogden model. Three values of s are shown in each figure.

minimum of v_{cr} by simply differentiating v_{cr} with respect to D and solve the following equations

$$\frac{\mathrm{d}v_{cr}}{\mathrm{d}D} = \frac{\tilde{F}_{,3}\Omega_{,2} - \tilde{F}_{,2}\Omega_{,3}}{\tilde{F}_{,1}\Omega_{,2} - \tilde{F}_{,2}\Omega_{,1}} = 0, \tag{5.5}$$

$$\Omega(v, \lambda_z, D) = 0, \tag{5.6}$$

$$\tilde{F}(v, \lambda_z, D) = 0, \tag{5.7}$$

where the first equation is obtained from implicit differentiations of $\Omega(v, \lambda_z, D) = 0$ and $\tilde{F}(v, \lambda_z, D) = 0$, the bifurcation condition is rewritten as $\Omega(v, \lambda_z, D) = J(P, F)$, and the resultant axial force is replaced by $\tilde{F}(v, \lambda_z, D) = F(\lambda_a, \lambda_z)$.

In fact, equations (5.5)-(5.7) determine the maximum or minimum critical volume ratio, the corresponding interfacial radius, and the axial stretch in terms of the inner radius A and ratio of modulus s. Obviously, a two dimensional picture is more clear.

(a) Gent model.

(b) Ogden model.
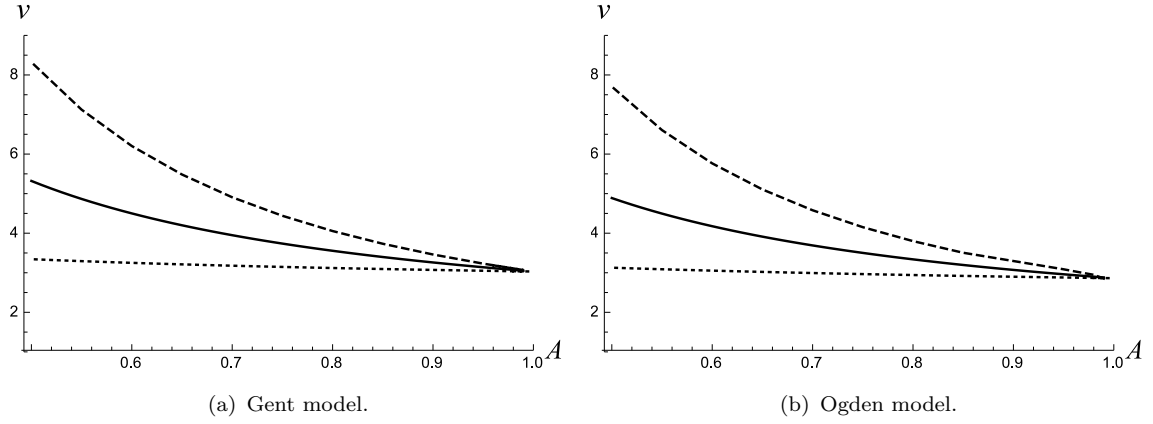
Figure 5.6: The maximum and minimum volumes when $0.01 \leqslant s \leqslant 100$. The solid line is a single-layer tube. The dashed line and dotted line correspond to $s = 100$ and $s = 0.01$, respectively.

Next, we consider that the ratio of modulus s belongs to the interval $0.01 \leqslant s \leqslant 100$. Since a higher s generates a larger v_{cr}, the lower and upper bounds of v_{cr} when $0.01 \leqslant s \leqslant 100$ just equate to $v_{cr}\mid_{s=0.01}$ and $v_{cr}\mid_{s=100}$, respectively. On the other hand, since we fix $B = 1$, varying the inner radius A is equivalent to considering the effect of thickness. The results for both the Gent model and Ogden model are plotted in Figure (5.6). The solid curve denoting the critical volume ratio for a single-layer tube is also shown for comparison. It can be seen that, for the same geometry, the critical volume ratio v_{cr} for a bilayer tube varies in a large range compared to a single-layer tube. Therefore, in some situations where localized bulging is preferred or undesired, a composite tube with specified ratio of modulus but the same geometry might offer a potential way to control the bulge initiation.

Furthermore, we deal with the situation with specified A and varied s. In order to be

101

(a) $s > 1$.   (b) $s < 1$.
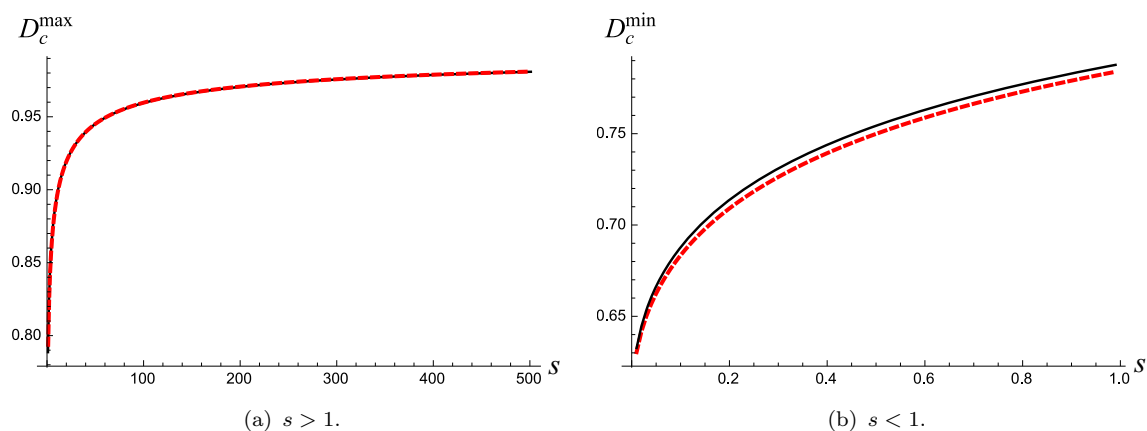
Figure 5.7: Dependence of $D_c^{\max}$ and $D_c^{\min}$ on s. The geometrical parameters are given by $A = 0.6$ and $B = 1$. The solid lines correspond to the Gent Model and the dashed lines represent the Ogden model.

consistent with the previous analysis, the inner radius is also set to $A = 0.6$. As the $v_{cr} - D$ curve has a maximum when $s > 1$ but a minimum otherwise, we use ($D_c^{\max}$, $v_{cr}^{\max}$) to represent the turning point if $s > 1$. The counterpart when $s < 1$ is denoted by ($D_c^{\min}$, $v_{cr}^{\min}$). Accordingly, the relations between $D_c^{\max}$ and s or $D_c^{\min}$ and s for the Gent and Ogden models are displayed in Figure (5.7). It is observed that the critical interfacial radius $D_c^{\max}$ or $D_c^{\min}$ increases monotonically. In particular, it turns out that the difference between the results based on the two models is very small.

By combining both analyses in this subsection, we may summarize that, at least for fixed axial force, the effect of modulus ratio on bulge initiation v_{cr} in an inflated bilayer tube is a kind of intrinsic property. Different choice of the constitutive models might affect the value of v_{cr}. However, the qualitative property remains the same. In the next subsection, we shall study the other loading type, i.e., fixed axial stretch.
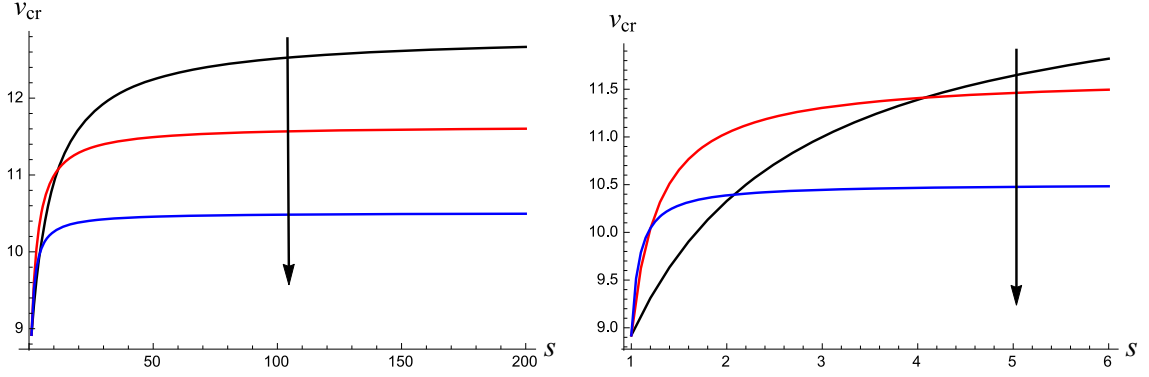
Figure 5.8: Relations between v_{cr} and s when $D = 0.95$, 0.85, 0.75, respectively, for the Gent model. The inner and outer radii are given by $A = 0.6$ and $B = 1$. The arrow indicates the decrease of D. The right plot shows the details of the left one when s is around 1.

5.3.2   Case II: fixed axial stretch

In this case, it is the axial length that is fixed. Note that this kind of setup has been used in the experiments by Pamplona et al. (2006); Gonçalves et al. (2008); Wang et al. (2019). As shown by Gonçalves et al. (2008), if the pre-stretch λ_{z0} is not large enough, the tube may suffer Euler-type buckling. Consequently, we impose a pre-stretch $\lambda_{z0} = 2.5$ without loss of generality on the bilayer tube and then fix the axial length. In addition, the human arteries also undergo a pre-stretch λ_{z0} *in situ* and λ_{z0} decreases with increased age (Hornỳ et al., 2014). Since the pressure-stretch (or volume) curve may be monotonic, we need to find the bifurcation threshold by utilizing equation (5.3). Referring to case I, we also anticipate that the critical volume ratio v_{cr} is an increasing function of s but may have maximum or minimum with varied D.

Thus, we first plot the dependence of v_{cr} on s for three values of D in Figure (5.8) for the Gent model. As we expected, the tendency of the $v_{cr} - s$ curve is quite similar to the corresponding results in case I, and the gradient of v_{vr} changes fast with increasing s. In other words, a bilayer tube becomes more stable with a higher s. However, when s is large enough, further improvement of v_{cr} is negligible. Also, for a given s which is less than 6, the relation between v_{cr} and D is non-monotonic. For the sake of simplicity, the counterpart for the Ogden model is not shown.

Furthermore, we also display the curves of v_{cr} with varying D if all other parameters are specified in Figure (5.9) for the Gent model and Figure (5.10) for the Ogden model. It can be seen that the critical volume ratio v_{cr} has a maximum if $s > 1$ and a minimum if $s < 1$, and this is consistent with the results in case I. Nevertheless, unlike case I (cf. Figures (5.4) and (5.5)), the magnitude of v_{cr} for the Gent model is larger than that for the Ogden model. In addition, we can determine the maxima and minima in Figures (5.9) and (5.10) by directly differentiating v_{cr} with respect to D. Because the axial stretch λ_z is known, we need to solve the following equations

$$\frac{\mathrm{d}v_{cr}}{\mathrm{d}D} = \frac{\Phi_{,2}}{\Phi_{,1}} = 0, \tag{5.8}$$

$$\Phi(v, D) \equiv J(P, F) = 0. \tag{5.9}$$

In the second equation, the bifurcation condition is rewritten as a function of v and D. The above two equations provide the turning point $(D_c^{\max}, v_{cr}^{\max})$ or $(D_c^{\min}, v_{cr}^{\min})$ when the inner radius A and ratio of modulus s are specified. Here, $D_c^{\max}$ corresponds
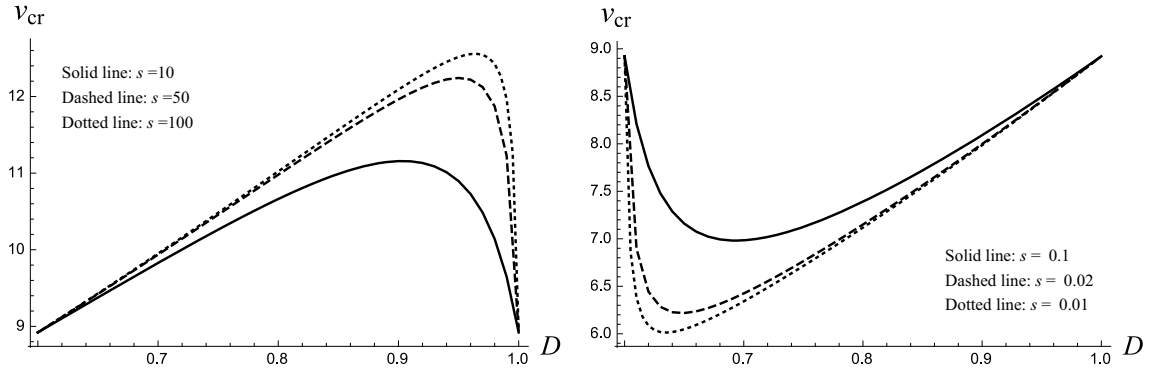
Figure 5.9: Dependence of v_{cr} on D when $A = 0.6$ and $B = 1$ for the Gent model. Three values of s are shown in each figure.
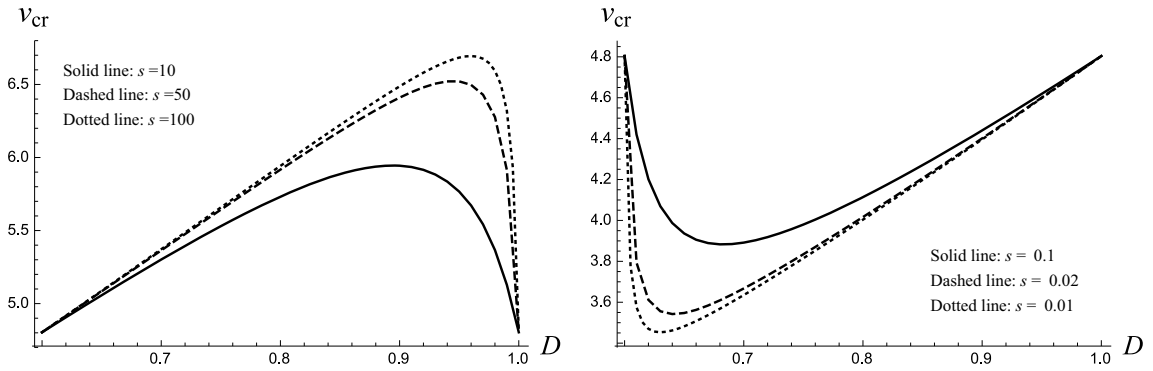
Figure 5.10: Dependence of v_{cr} on D when $A = 0.6$ and $B = 1$ for the Ogden model. Three values of s are shown in each figure.

to the case where $v_{cr} - D$ curve is convex, and $D_c^{\min}$ is the counterpart when $v_{cr} - D$ curve is concave, which are in accordance with the notations in case I.

Next, we plot the interval of v_{cr} when $0.01 \leqslant s \leqslant 100$ with varied A in Figure (5.11) for the Gent model and Ogden model. The solid curves correspond to a single-layer tube. In the case of fixed axial length, a composite tube can also be easier or harder

(a) Gent model.

(b) Ogden model.
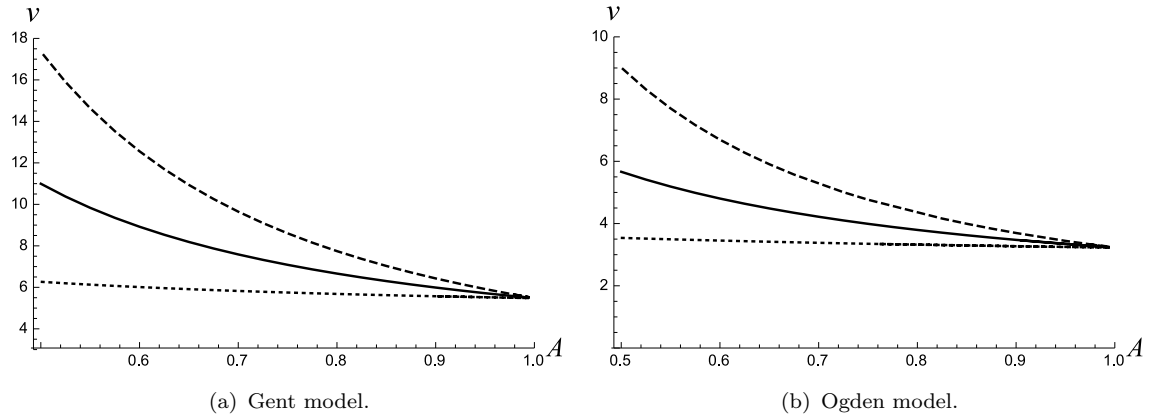
Figure 5.11: The maximum and minimum volumes when $0.01 \leqslant s \leqslant 100$. The solid line is a single-layer tube. The dashed line and dotted line correspond to $s = 100$ and $s = 0.01$, respectively.
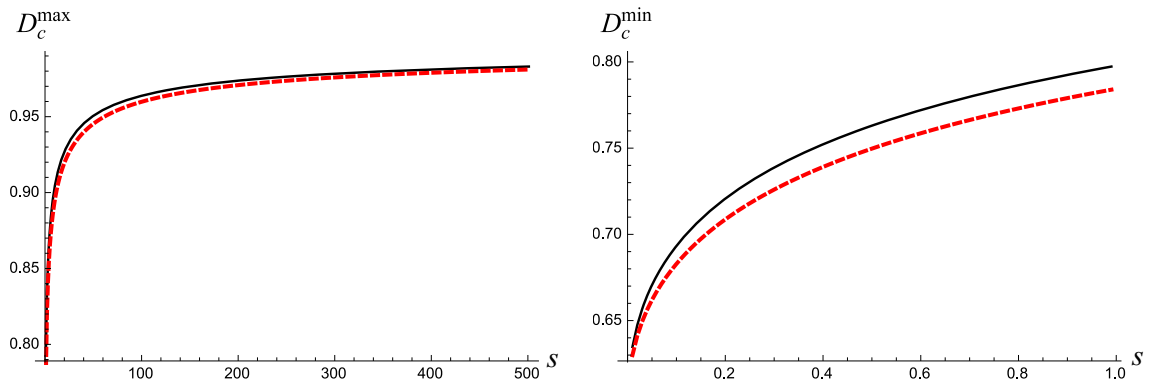
Figure 5.12: Dependence of the turning point on s. The geometrical parameters are given by $A = 0.6$ and $B = 1$. The solid lines correspond to the Gent Model and the dashed lines represent the Ogden model.

to bifurcate than a single-layer tube with the same geometry, according to the value of s. Finally, we fix the inner radius by $A = 0.6$ and show the dependence of $D_c^{\max}$ or $D_c^{\min}$ on the ratio of modulus s in Figure (5.12) for the Gent model and Ogden model.

106

We observe that in case II both models also generate very similar properties. Also, the difference of the critical interfacial radius corresponding to maximum or minimum critical volume ratio between two models is marginal, which also manifests the fact that the effect of the modulus ratio is an intrinsic property.

5.4   Conclusion

In this chapter, we have studied localized bulging in an inflated bilayer tube of arbitrary thickness. We focus on the situation that each layer has its own shear modulus, and the influence of constitutive models are examined as well. The current study improves the understanding of localized bulging in a hyperelastic tubes of arbitrary thickness. Since layered structures are often observed in biological tissues, our results could also provide deep insight into aneurysm formation and furnish a potential way to delay bulge initiation.

By introducing the ratio of modulus s and regarding the volume ratio v as the bifurcation parameter, we establish a criterion that a higher v_{cr} corresponds to a more stable structure, where v_{cr} refers to the bifurcation threshold. When all geometrical parameters are specified, we find that v_{cr} is an increasing function of s. However, if s is large enough, say $s \geqslant 100$, the increment of v_{cr} becomes negligible with increased s.

When the thickness of the whole tube is given, the dependence of v_{cr} on the interfacial radius D is non-monotonic. In particular, a composite tube is always more stable than a single-layer tube if $s > 1$ or less stable if $s < 1$. Furthermore, the critical volume

ratio v_{cr} has a maximum when $s > 1$ but a minimum otherwise, and the corresponding critical radii $D_c^{\max}$ and $D_c^{\min}$ are also determined. In addition, all results for the Gent model and Ogden model are qualitatively similar, which implies that the bifurcation behavior of an inflated bilayer tube is insensitive to the applied constitutive model.

Chapter 6

Localized bulging of hyperelastic tubes under inflation and torsion

6.1 Introduction

In this chapter localized bulging of a cylindrical, incompressible, isotropic tube that is subject to combined action of internal pressure, torsion and axial extension is investigated. The expressions for the twisting moment M, the internal pressure P and the resultant axial force F associated with the deformation are first given for the Mooney-Rivlin material model. With the use of dynamical systems theory, we derive the bifurcation condition for localized bulging when the twisting moment M is fixed.
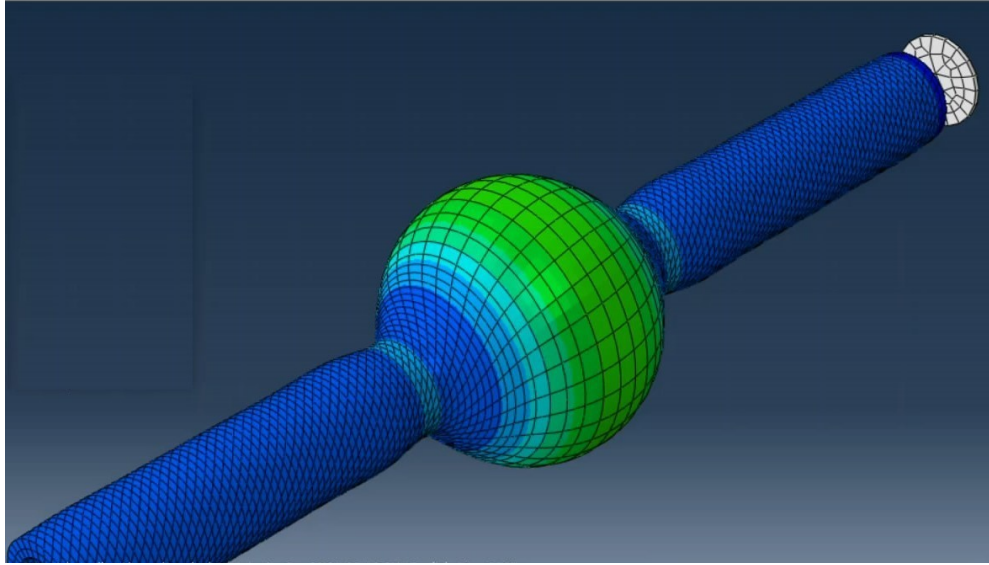
Figure 6.1: Localized bulging under inflation and torsion.

We then determine several critical regimes where localized bulging disappears. Finally, we study the wrinkled solution to ensure that the tube will not wrinkle before localized bulging takes place.

6.2   Problem formulation

First we consider a hyperelastic cylindrical tube with inner radius A and outer radius B, which can be described by

$$A \leq R \leq B, \quad 0 \leq \Theta \leq 2\pi, \quad 0 \leq Z \leq L, \tag{6.1}$$

in the undeformed configuration, where (R, Θ, Z) are cylindrical polar coordinates, and L is the length of the tube. The tube is subject to torsion together with an axial extension and an internal pressure; see Figure (6.1). After the deformation, the inner and outer radii take the values a and b, respectively.

Assuming that the material is incompressible, the deformation can be defined by

$$r = r(R) = \sqrt{\lambda_z^{-1}(R^2 - A^2) + a^2}, \quad \theta = \Theta + \gamma\lambda_z Z, \quad z = \lambda_z Z, \tag{6.2}$$

where (r, θ, z) are cylindrical polar coordinates after the deformation, λ_z is the axial stretch, and γ is the amount of twist per unit axial length in the deformed configuration. Accordingly, the deformation gradient tensor $\mathbf{F}$ can be written in matrix form as

$$\mathbf{F} = \begin{pmatrix} \frac{\partial r}{\partial R} & 0 & 0 \\ 0 & \frac{r}{R} & \lambda_z\gamma r \\ 0 & 0 & \lambda_z \end{pmatrix}. \tag{6.3}$$

Then, the left Cauchy-Green strain tensor $\mathbf{B} = \mathbf{F}\mathbf{F}^{\mathrm{T}}$ takes the form

$$\mathbf{B} = \begin{pmatrix} \left(\frac{\partial r}{\partial R}\right)^2 & 0 & 0 \\ 0 & \left(\frac{r}{R}\right)^2 + (\lambda_z\gamma r)^2 & \lambda_z^2\gamma r \\ 0 & \lambda_z^2\gamma r & \lambda_z^2 \end{pmatrix}, \tag{6.4}$$

where the superscript T denotes the transpose of a tensor.

We shall use the Mooney-Rivlin strain-energy function, which is given by (2.59), to

characterize the constitutive response of the material. Hence, according to equation (2.52), the Cauchy stress tensor $\boldsymbol{\sigma}$ can be written as

$$\boldsymbol{\sigma} = \mu_1 \mathbf{B} + \mu_2(I_1 \mathbf{B} - \mathbf{B}^2) - p\mathbf{I}. \tag{6.5}$$

So, the non-zero components of Cauchy stress are given by

$$
\begin{aligned}
\sigma_{rr}(r) &= \frac{\mu_1(r^2 - h)}{r^2 \lambda_z} + \mu_2 \left(\frac{1}{\lambda_z^2} + \frac{(r^2 - h)(1 + r^2\gamma^2)\lambda_z)}{r^2} \right) - p, \\
\sigma_{\theta\theta}(r) &= \frac{(\gamma^2 h \lambda_z^3 - \gamma^2 r^2 \lambda_z^3 - 1) \left(\mu_2 \left(h - r^2 \lambda_z^3 - r^2 \right) - \mu_1 r^2 \lambda_z \right)}{(r^2 - h)\lambda_z^2} - p, \\
\sigma_{zz}(r) &= \lambda_z \left(\mu_2 + \mu_1 \lambda_z - \frac{h\mu_2}{r^2} + \mu_2 r^2 \left(\frac{1}{r^2 - h} + \gamma^2 \lambda_z^3 \right) \right) - p, \\
\sigma_{\theta z}(r) &= \gamma r \lambda_z^2 \left(\mu_1 - \gamma \mu_2 r \lambda_z^2 \right),
\end{aligned}
\tag{6.6}
$$

where $h = a^2 - A^2/\lambda_z$. The equilibrium equation which is not satisfied automatically is given by

$$\frac{d\sigma_{rr}}{dr} = -\frac{\sigma_{rr} - \sigma_{\theta\theta}}{r}. \tag{6.7}$$

It is assumed that the internal surface of the tube is subjected to the internal pressure P while its external surface is traction-free, so the boundary conditions are

$$\sigma_{rr}(a) = -P, \quad \sigma_{rr}(b) = 0. \tag{6.8}$$

By integrating equation (6.7) subject to the boundary conditions (6.8), the internal pressure P is given by

$$P = \int_a^b \frac{\sigma_{\theta\theta} - \sigma_{rr}}{r} dr. \tag{6.9}$$

The Lagrange multiplier p can then be obtained from equation (6.7) with the use of equations (6.8)$_1$ and (6.6)$_1$. It takes the form

$$p = \frac{\mu_1(r^2 - h)}{r^2\lambda_z} + \mu_2\left(\frac{1}{\lambda_z^2} + \frac{(r^2 - h)(1 + r^2\gamma^2)\lambda_z}{r^2}\right) + P + \int_a^r \frac{\sigma_{rr} - \sigma_{\theta\theta}}{r}dr. \quad (6.10)$$

It follows that the twisting moment M on any cross section of the tube and the axial stress resultant N are expressed as

$$\begin{aligned}
M &= \int_a^b \int_0^{2\pi} \sigma_{\theta z} r^2 dr d\theta = 2\pi \int_a^b \sigma_{\theta z} r^2 dr, \\
N &= \int_a^b \int_0^{2\pi} \sigma_{zz} r dr d\theta = 2\pi \int_a^b \sigma_{zz} r dr.
\end{aligned} \quad (6.11)$$

Assuming that one end is closed and is subject to the action of an additional force F (e.g. a dead weight), then

$$F = N - \pi\ a^2\ P. \quad (6.12)$$

The corresponding equations for a neo-Hookean model can be obtained by setting $\mu_1 = \mu$ and $\mu_2 = 0$.

We shall assume that the twisting moment M is fixed, say M_0, throughout this research. As a result, the torsional twist γ may be written, by using equation (6.11)$_1$, in the following way

$$\gamma = \frac{20M_0}{5\pi\mu_1\left(b^4 - a^4\right)\lambda_z^2 + \sqrt{5\pi}\sqrt{\lambda_z^4\left(32\mu_2\tau\left(a^5 - b^5\right) + 5\pi\mu_1^2\left(a^4 - b^4\right)^2\right)}}. \quad (6.13)$$

By introducing the circumferential stretches $\lambda_a = a/A$ and $\lambda_b = b/B$, the internal

pressure P and the resultant axial force F are viewed as functions of λ_z and λ_a only where λ_b has been eliminated using (6.2) as follows

$$\lambda_b = \sqrt{\frac{B^2 - A^2 + A^2 \lambda_a^2 \lambda_z}{B^2 \lambda_z}}.$$ (6.14)

The special case when the torsional twist $\gamma = 0$, or equivalently $M = 0$, was studied by Fu et al. (2016). It was shown in the latter paper that a necessary condition for localized bulging to take place is given by the following expression

$$J(P, F) = \frac{\partial P}{\partial \lambda_a} \frac{\partial F}{\partial \lambda_z} - \frac{\partial P}{\partial \lambda_z} \frac{\partial F}{\partial \lambda_a} = 0.$$ (6.15)

We may then question if this correspondence can be extended to the case of twisted tubes. We shall verify that $J(P, F) = 0$ is the bifurcation condition for localized bulging in inflated tubes when the twisting moment M is fixed. We highlight that the torsion γ may be changed during the inflation. In the inflation of a tube, there are two different loading conditions, either the resultant axial force F or axial length that can be fixed, which shall be considered here.

6.3   Incremental equations

To investigate the axi-symmetric bifurcation of the deformation determined earlier, we consider an incremental displacement field $\dot{\boldsymbol{r}}$ of the form

$$\dot{\boldsymbol{r}} = u(r,z)\boldsymbol{e}_r + v(r,z)\boldsymbol{e}_\theta + w(r,z)\boldsymbol{e}_z,$$

where $u(r,z), v(r,z)$ and $w(r,z)$ denote the incremental displacement in the r-, θ-, z-directions, respectively, and $\boldsymbol{e}_r, \boldsymbol{e}_\theta$ and $\boldsymbol{e}_z$ are the corresponding basis vectors. Accordingly, the gradient of incremental displacement has the form

$$\boldsymbol{\Gamma} = \begin{bmatrix} u_r & \frac{-1}{r}v & u_z \\ v_r & \frac{1}{r}u & v_z \\ w_r & 0 & w_z \end{bmatrix}, \qquad u_r \equiv \frac{\partial u}{\partial r}, \qquad v_r \equiv \frac{\partial v}{\partial r} \text{ etc.} \tag{6.16}$$

According to the analysis developed in Chapter 2, the associated incremental stress tensor $\hat{S}_0$ is defined by

$$\hat{S}_0 = \mathcal{B}\,\boldsymbol{\Gamma} + p\,\boldsymbol{\Gamma} - p^*\delta, \tag{6.17}$$

where p^* is the incremental of p, δ is the Kronecker delta, and $\mathcal{B}$ are the incremental elastic moduli given by (2.78) with $J = 1$. Then, the three incremental equilibrium

equations are

$$\frac{\partial \hat{S}_{0rr}}{\partial r} + \frac{\partial \hat{S}_{0zr}}{\partial z} + \frac{\hat{S}_{0rr} - \hat{S}_{0\theta\theta}}{r} = 0,$$

$$\frac{\partial \hat{S}_{0r\theta}}{\partial r} + \frac{\partial \hat{S}_{0z\theta}}{\partial z} + \frac{\hat{S}_{0\theta r} + \hat{S}_{0r\theta}}{r} = 0, \qquad (6.18)$$

$$\frac{\partial \hat{S}_{0rz}}{\partial r} + \frac{\partial \hat{S}_{0zz}}{\partial z} + \frac{\hat{S}_{0rz}}{r} = 0.$$

Furthermore, the incremental incompressibility condition takes the form

$$\operatorname{tr} \boldsymbol{\Gamma} = u_r + \frac{u}{r} + w_z = 0. \qquad (6.19)$$

Taking the increment of boundary conditions (6.8), we find

$$\hat{S}_0^T \, \boldsymbol{n} = P \, \Gamma^T \boldsymbol{n}, \quad \text{on} \quad r = a, \qquad \hat{S}_0^T \, \boldsymbol{n} = 0, \quad \text{on} \quad r = b. \qquad (6.20)$$

The incremental equilibrium equations (6.18) and the incremental incompressibility condition (6.19) will be solved numerically subject to the incremental boundary conditions (6.20) in the next two sections.

6.4   Stroh formulation

Several methods can be used to solve the incremental eigenvalue problem derived above. Here, we introduce the Stroh formulation which enables us to rewrite the governing equations (6.18) and (6.19) as a first-order differential system, as illustrated in

Chapter 2. We present the results for the neo-Hookean model only, and the associated results for the Mooney-Rivlin model are not presented for the sake of brevity. Balbi and Ciarletta (2015) investigate the helical buckling of pre-stressed tubes subject to a torsion, and the attention is mainly focused on sinusoidal patterns. In the present analysis, we only focus on the bifurcation having zero mode number.

For our purpose, we seek a solution of the form

$$[u, v, w, p^*] = [U(r), -V(r), -W(r), P(r)] \ \mathrm{e}^{\alpha z}, \tag{6.21}$$

where $U(r), V(r), W(r)$ and $P(r)$ are scalar functions of r, and α the is axial spectral parameter. Similarly, the components of the incremental nominal stress tensor can be rewritten in the following form

$$\left[\hat{S}_{0rr}, \hat{S}_{0r\theta}, \hat{S}_{0rz} \right] = \left[\frac{1}{r} S_{0rr}(r), \frac{1}{r} S_{0r\theta}(r), \frac{1}{r} S_{0rz}(r) \right] \mathrm{e}^{\alpha z}. \tag{6.22}$$

Note that $P(r)$ is eliminated by substituting equation (6.17) into (6.22).

We now introduce the displacement-traction vector $\boldsymbol{\eta}(r)$, as follows

$$\boldsymbol{\eta}(r) = \begin{bmatrix} \boldsymbol{U}(r) \\ \boldsymbol{S}(r) \end{bmatrix} \quad \text{with} \quad \begin{aligned} \boldsymbol{U}(r) &= [U(r), V(r), W(r)]^T \\ \boldsymbol{S}(r) &= [S_{0rr}(r), S_{0r\theta}(r), S_{0rz}(r)]^T \end{aligned}. \tag{6.23}$$

Using the incremental incompressibility condition (6.19) together with equations (6.17), (6.21), and (6.22), we may rewrite the differential equations (6.18) as the following

first-order differential system

$$\frac{d\boldsymbol{\eta}(r)}{dr} = \frac{1}{r}\mathbf{G}(r)\,\boldsymbol{\eta}(r), \tag{6.24}$$

where $\mathbf{G}(r)$ is the so-called Stroh matrix which has the following block representation

$$\mathbf{G} = \begin{pmatrix} \mathbf{G}_1 & \mathbf{G}_2 \\ \mathbf{G}_3 & \mathbf{G}_4 \end{pmatrix}, \tag{6.25}$$

where

$$\mathbf{G_1} = \begin{pmatrix} -1 & 0 & \alpha r \\ 0 & \phi & 0 \\ \alpha r\phi & 0 & 0 \end{pmatrix}, \quad \mathbf{G_2} = \begin{pmatrix} 0 & 0 & 0 \\ 0 & -1/\mathcal{B}_{r\theta r\theta} & 0 \\ 0 & 0 & -1/\mathcal{B}_{r\theta r\theta} \end{pmatrix}, \tag{6.26}$$

$$\mathbf{G_3} = \begin{pmatrix} \tau_{11} & \tau_{12} & \tau_{13} \\ \tau_{12} & \tau_{22} & 0 \\ \tau_{13} & 0 & \tau_{33} \end{pmatrix}, \quad \mathbf{G_4} = -\mathbf{G_1}^{\mathrm{T}}, \tag{6.27}$$

with

$$\tau_{11} = \alpha^2 r^2(-\mathcal{B}_{zrzr} + \mathcal{B}_{r\theta r\theta}\phi^2) + \mathcal{B}_{rrrr} + \mathcal{B}_{\theta\theta\theta\theta} + 2p,$$

$$\tau_{12} = -2\alpha r\mathcal{B}_{\theta\theta z\theta},$$

$$\tau_{13} = -\alpha r(\mathcal{B}_{rrrr} + p),$$

$$\tau_{22} = \alpha^2 r^2 \mathcal{B}_{z\theta z\theta} - \mathcal{B}_{\theta r\theta r} + \phi^2 \mathcal{B}_{r\theta r\theta},$$

$$\tau_{33} = \alpha^2 r^2 (\mathcal{B}_{rrrr} - \mathcal{B}_{zzzz} + 2p + 2\mathcal{B}_{z\theta z\theta}),$$

$$\phi = p/\mathcal{B}_{r\theta r\theta}.$$

Note that the superscript T denotes the transpose and G_2 and G_3 are symmetric. After writing the system of governing equations as a system of first order ordinary differential equations, we solve equation (6.24) by using the impedance matrix method in the following.

6.5   Numerical solution of the bifurcation condition

In this section, we present the the numerical results of the above problem using impedance matrix method. As explained in Chapter 2, we assume that $\boldsymbol{\eta}_n$ are the independent solutions of the system (6.24) and then the 6×6 matricant $\mathbf{M}(r, r_k)$ is introduced, such that

$$\mathbf{M}(r, r_k) = \begin{pmatrix} \mathbf{M}_1(r, r_k) & \mathbf{M}_2(r, r_k) \\ \mathbf{M}_3(r, r_k) & \mathbf{M}_4(r, r_k) \end{pmatrix} = \boldsymbol{\tau}(r)\boldsymbol{\tau}^{-1}(r_k), \tag{6.28}$$

where $r_k = a, b$ and

$$\boldsymbol{\tau}(r) = [\boldsymbol{\eta}_1, ..., \boldsymbol{\eta}_6]. \tag{6.29}$$

Therefore, $\mathbf{M}(r, r_k)$ is the solution of the initial value problem

$$\frac{d\mathbf{M}(r, r_k)}{dr} = \frac{1}{r}\mathrm{G}(r)\mathbf{M}(r, r_k), \qquad \text{with} \ \ \mathbf{M}(r_k, r_k) = I_{(6)}. \tag{6.30}$$

Thus, we may define the 3×3 conditional impedance matrix $\boldsymbol{z}$ in the following form

$$\boldsymbol{S} = \boldsymbol{z}\boldsymbol{U}. \tag{6.31}$$

As a results, equation (6.28) can rewritten as

$$\boldsymbol{\eta}(r) = \mathbf{M}(r, r_k)\boldsymbol{\eta}(r_k), \tag{6.32}$$

which gives

$$\boldsymbol{U}(r) = \mathbf{M}_1(r, r_k)\boldsymbol{U}(r_k) + \mathbf{M}_2(r, r_k)\boldsymbol{S}(r_k), \tag{6.33}$$

$$\boldsymbol{S}(r) = \mathbf{M}_3(r, r_k)\boldsymbol{U}(r_k) + \mathbf{M}_4(r, r_k)\boldsymbol{S}(r_k). \tag{6.34}$$

By substituting $(6.23)_1$ and (6.31) into (6.24), we get

$$\frac{d\boldsymbol{U}}{dr} = \frac{1}{r}\mathbf{G}_1\boldsymbol{U} + \frac{1}{r}\mathbf{G}_2\boldsymbol{z}\boldsymbol{U}, \tag{6.35}$$

$$\frac{d(\boldsymbol{z}\boldsymbol{U})}{dr} = \frac{1}{r}\mathbf{G}_3\boldsymbol{U} + \frac{1}{r}\mathbf{G}_4\boldsymbol{z}\boldsymbol{U}. \tag{6.36}$$

Therefore, the following differential matrix Riccati equation can be obtained by substituting (6.35) into (6.36), which gives,

$$\frac{d\boldsymbol{z}(r)}{dr} = \frac{1}{r}(\mathbf{G_3} - \boldsymbol{z}\mathbf{G_1} - \boldsymbol{z}\mathbf{G_2}\boldsymbol{z} + \mathbf{G_4}\boldsymbol{z}). \tag{6.37}$$

So far, the equation (6.24) is rewritten as the differential matrix Riccati equation (6.37) and the corresponding boundary conditions can be obtained as the following. The boundary condition (6.20) on $r = b$ requires

$$\boldsymbol{S}(b) = 0. \tag{6.38}$$

Substituting equation (6.38) and (6.31) into equation (6.34) gives

$$\mathbf{M}_3(b, r_k)\boldsymbol{U}(r_k) + \mathbf{M}_4(b, r_k)\boldsymbol{z}(r_k)\boldsymbol{U}(r_k) = 0. \tag{6.39}$$

Taking $r_k = b$ in equation (6.39), we have

$$\mathbf{M}_3(b, b) + \mathbf{M}_4(b, b)\boldsymbol{z}(b) = 0. \tag{6.40}$$

According to equation $(6.30)_2$, $\mathbf{M}_3(b, b) = 0$ and $\mathbf{M}_4(b, b) = I_{3\times3}$. Therefore, the boundary condition of the differential matrix Riccati equation on $r = b$ becomes

$$\boldsymbol{z}(b) = 0. \tag{6.41}$$

Now, using (6.22) and (6.16), the boundary condition (6.20) on $r = a$ becomes

$$\frac{1}{a} \begin{bmatrix} S_{0rr} \\ S_{0r\theta} \\ S_{0rz} \end{bmatrix} = P \begin{bmatrix} U' \\ \frac{1}{a}V \\ \alpha\, U \end{bmatrix},$$

(6.42)

which can be rewritten by the use of (6.24) as

$$\boldsymbol{S} = P \begin{bmatrix} G_1^{(11)} & G_1^{(12)} & G_1^{(13)} \\ 0 & 1 & 0 \\ a\,\alpha & 0 & 0 \end{bmatrix} \boldsymbol{U},$$

(6.43)

where $G_1^{(11)}, G_1^{(12)}$ and $G_1^{(13)}$ are the first, second and third elements in the first row of $\mathbf{G}_1$, respectively. More precisely expressed as,

$$G_1^{(11)} = -1, \quad G_1^{(12)} = 0, \quad G_1^{(13)} = \alpha\, a.$$

(6.44)

Substituting (6.43) into (6.31), we get

$$\det \left[\boldsymbol{z}(a) - P \begin{pmatrix} -1 & 0 & \alpha\, a \\ 0 & 1 & 0 \\ a\,\alpha & 0 & 0 \end{pmatrix} \right] = 0.$$

(6.45)

The eigenvalue problem derived above has two non-zero real eigenvalues, say $\pm\alpha_1$. Increasing the amount of M and/or F will move these two eigenvalues towards the

(a) $\lambda_z = 1.07$.

(b) $\lambda_z = 1.15$.

(c) $\lambda_z = 1.165$.
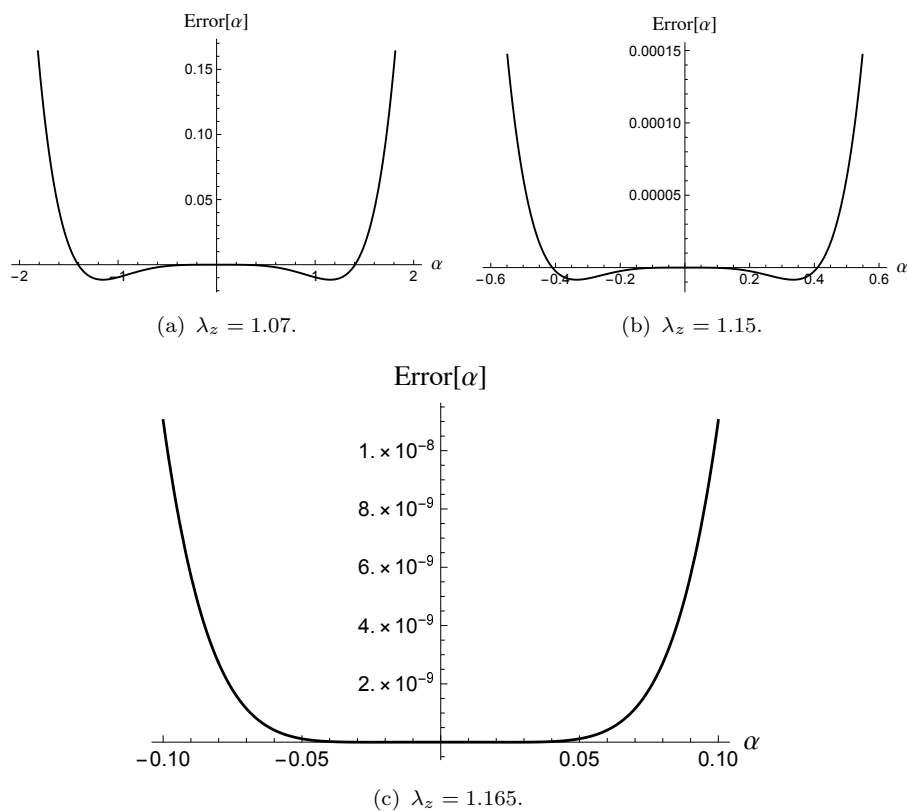
Figure 6.2: The error function against α when $B = \mu = 1, F = 0, \gamma = 0.2$, and $A = 0.8$. Localized bulging takes place in (c).

origin. Based on the dynamical systems theory, a condition of the existence of localized bulging is when α_1 vanishes, see Kirchgässner (1982) and Haragus and Iooss (2010). Figure (6.2) shows the movement of three real eigenvalues as λ_z increases. Localized bulging may occur when $\alpha_1 = 0$, making zero a triple eigenvalue. Thus, the bifurcation condition is reduced to the condition when the two eigenvalues $\pm \alpha_1$ equal to zero.

Now, we present the numerical results of the eigenvalue problem by solving the differential matrix Riccati equation (6.37) subject to the boundary conditions (6.41) and
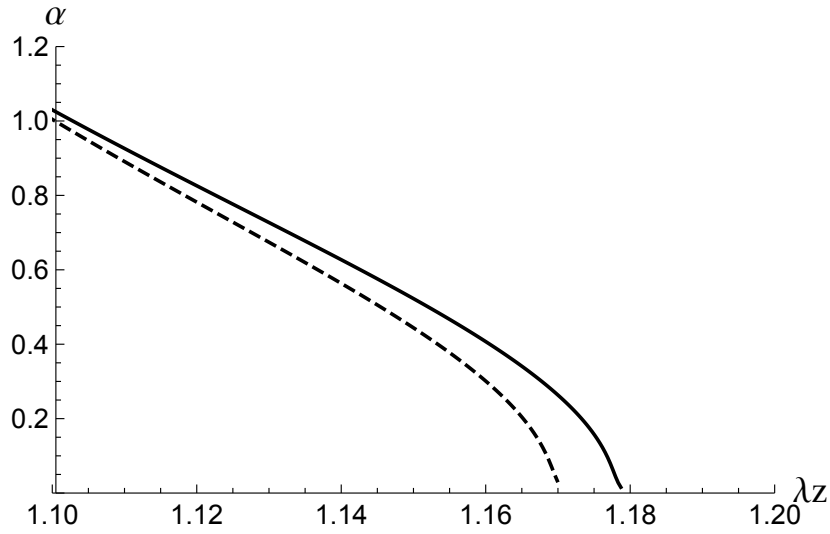
Figure 6.3: The relation between α and λ_z when $A = 0.8$ and $F = 0$. Solid and dashed lines correspond to $M_0 = 0, 0.4$ repectively.

(6.45). Without loss of generality, we set the shear modulus $\mu = 1$ and the outer radius $B = 1$. By fixing λ_z, we integrate numerically the differential Riccati equation (6.37) subject to the boundary condition (6.41) and α is iterated until the boundary condition (6.45) is satisfied. Therefore, the connection between α and λ_z can be obtained numerically. Figure 6.3 displays our numerical results for the variation of α against λ_z for different M_0 when the inner radius $A = 0.8$ and the resultant axial force $F = 0$. Note that $F = 0$ is solved to define λ_a as a function of λ_z. It is seen that when M is specified by $0, 0.4$ then the corresponding values of λ_z at which $\alpha = 0$ are 1.1783, 1.1699, respectively. If $M = 0.4$, we have verified that the pressure attains its maximum when $\lambda_z = 1.1699$. Thus, determination of the initiation pressure for localized bulging is the condition under which zero becomes a triple eigenvalue. The

relation between negative α and λ_z can be obtained in similar manner. Also, the relation between $\pm\alpha$ and λ_a can be obtained similarly in the case of fixed axial stretch λ_z.

6.6   Bifurcation condition

In this section we further derive a bifurcation condition for small α using the neo-Hookean material model. Therefore, the incremental equilibrium equations (6.18) together with the incremental incompressibility condition (6.19) will be solved analytically. Now, we look for a solution of the form

$$[u, v, w, p^*] = [U(r), V(r), W(r), P(r)] \ \mathrm{e}^{\alpha \, z}. \tag{6.46}$$

On substituting equation (6.46) into the incremental equilibrium equations (6.18) and the incremental incompressibility condition (6.19), and then eliminating $W(r)$ and $P(r)$ in favor of $U(r)$ and $V(r)$, we obtain

$$\begin{aligned}
&\mathcal{B}_{r\theta r\theta} \, U^{(4)} + \psi_1 \, U^{(3)} + \left(-3\mathcal{B}_{r\theta r\theta}/r^2 + \alpha^2\psi_2\right) U'' + \left(\psi_3 + \alpha^2\psi_4\right) U' \\
&+ \left(\psi_5 + \alpha^2\psi_6 + \alpha^4\lambda_z^2 \, \right) U = -2\gamma\lambda_z^2\alpha^2 V^*, \\
&\mathcal{B}_{r\theta r\theta}V^{*''} + \psi_7 \, V^{*'} + \left(\psi_8 + \alpha^2\lambda_z^2\right) V^* = 2\gamma\lambda_z^2\alpha^2 U,
\end{aligned} \tag{6.47}$$

where $V^* = \alpha V$ and

$$
\begin{aligned}
&\psi_1 = \frac{2(h + r^2)}{r^3 \lambda_z}, \qquad \psi_2 = \mathcal{B}_{r\theta r\theta} + \lambda_z^2, \qquad \psi_3 = -\frac{3(5h - r^2)}{r^5 \lambda_z}, \\
&\psi_4 = \frac{h + r^2 + r^2 \lambda_z^3}{r^3 \lambda_z}, \qquad \psi_5 = -\frac{3(-5h + r^2)}{r^6 \lambda_z}, \\
&\psi_6 = -\frac{\lambda_z^2}{r^2} - \gamma^2 \lambda_z^2 + \frac{1}{(h - r^2)\lambda_z} - p'', \qquad \psi_7 = \frac{h + r^2}{r^3 \lambda_z}, \\
&\psi_8 = -\frac{\mathcal{B}_{\theta r \theta r}}{r^2} - \frac{p'}{r}.
\end{aligned}
\tag{6.48}
$$

We mention here that α appears through α^2 in equations (6.47).

Following the same approach in Fu et al. (2016), we expand $U(r, \alpha)$ and $V^*(r, \alpha)$ in the form

$$
U(r, \alpha) = U_0(r) + \alpha^2 U_1(r) + \dots, \qquad V^*(r, \alpha) = V_0^*(r) + \alpha^2 V_1^*(r) + \dots.
\tag{6.49}
$$

Also, the boundary conditions are expanded similarly. By substituting equation (6.49) into equation (6.47), and equating the coefficients of α^0 and α^2 to zero, we find that

$$
\frac{d}{dr} \frac{1}{r} \frac{d}{dr} r \zeta(r) \frac{d}{dr} \frac{1}{r} \frac{d}{dr} r U_0(r) = 0, \qquad \frac{d}{dr} \frac{\zeta(r)}{\zeta'(r)} \frac{d}{dr} \frac{1}{r} V_0^*(r) = 0,
\tag{6.50}
$$

where $\zeta(r) = \mathcal{B}_{r\theta r\theta}(r) = (-h + r^2)\mu/(r^2 \lambda_z)$. Thus, the general solutions can be obtained easily and are given by

$$
U_0(r) = c_1 r + c_2 \frac{1}{r} + c_3 \kappa_1(r) + c_4 \kappa_2(r), \quad V_0^*(r) = c_5 r + c_6 r \log[\zeta(r)],
\tag{6.51}
$$

where c_i (i=1, ..., 6) are constants of integration and

$$\kappa_1(r) = \frac{1}{r}\int_a^r t \int_a^t \frac{s}{\zeta(s)}ds\,dt, \quad \kappa_2(r) = \frac{1}{r}\int_a^r t \int_a^t \frac{1}{s\zeta(s)}ds\,dt. \qquad (6.52)$$

By substituting these solutions into the leading-order boundary conditions of equations (6.20), we note that the coefficients c_3, c_4 and c_6 must vanish while c_1, c_2 and c_5 are arbitrary.

At order α^2, we find that the expressions for the general solutions of U and V^* take the form

$$U_1(r) = d_1 r + d_2\frac{1}{r} + d_3\kappa_1(r) + d_4\kappa_2(r) + c_1\kappa_3(r) + c_2\kappa_4(r) + c_5\kappa_5(r),$$
$$V_1^*(r) = d_5 r + d_6 r\,\log[\zeta(r)] + c_5\kappa_6(r) + c_1\kappa_7(r) + c_2\kappa_8(r), \qquad (6.53)$$

where d_i (i=1, ..., 6) are constants and $\kappa_i(r)$ (i=3, ..., 8) are particular integrals defined by

$$\kappa_3(r) = \frac{1}{r}\int_a^r y \int_a^y \frac{1}{x\zeta(x)}\int_a^x t \int_a^t \omega_1(s)ds\,dt\,dx\,dy,$$
$$\kappa_4(r) = \frac{1}{r}\int_a^r y \int_a^y \frac{1}{x\zeta(x)}\int_a^x t \int_a^t \omega_2(s)ds\,dt\,dx\,dy,$$
$$\kappa_5(r) = \frac{1}{r}\int_a^r y \int_a^y \frac{1}{x\zeta(x)}\int_a^x t \int_a^t \omega_3(s)ds\,dt\,dx\,dy,$$
$$\kappa_6(r) = r\int_a^r \frac{\zeta'(x)}{\zeta(t)}\int_a^t \omega_4(s)ds\,dt, \qquad (6.54)$$
$$\kappa_7(r) = r\int_a^r \frac{\zeta'(x)}{\zeta(t)}\int_a^t \omega_5(s)ds\,dt,$$
$$\kappa_8(r) = r\int_a^r \frac{\zeta'(x)}{\zeta(t)}\int_a^t \omega_6(s)ds\,dt,$$

with $\omega_i(r)$ (i=1, ..., 6) given by

$$\omega_1(r) = -\frac{2h^2(2h - 3r^2)}{r^3(h - r^2)^2\lambda_z}, \quad \omega_2(r) = -\frac{2h(h - 2r^2)}{r^3(h - r^2)^2\lambda_z}, \quad \omega_3(r) = 2\gamma\lambda_z^2 r,$$

$$\omega_4(r) = -r\lambda_z^2, \quad \omega_5(r) = -2r\gamma\lambda_z^2, \quad \omega_6(r) = -\frac{2\gamma\lambda_z^2}{r}. \tag{6.55}$$

By substituting (6.51) and (6.53) into second-order boundary conditions, we obtain a matrix equation of the form $Q\boldsymbol{C}$ where Q is a 6×6 matrix which is not written for the sake of brevity, and $\boldsymbol{C}$ is the column vector obtained from the six constants $c_1, c_2, c_5, d_3, d_4, d_6$. The condition for zero to become a triple eigenvalue then requires

$$\mathrm{det}Q = 0. \tag{6.56}$$

The bifurcation condition (6.56) can be used for the cases of fixed axial force and fixed axial length. We then verify that the bifurcation condition $\mathrm{det}Q = 0$ is graphically equivalent to $J(P, F) = 0$ when we plot these two curves in the (λ_a, λ_z)-plane. We can then conclude that the bifurcation condition for localized bulging in a twisted tube is given by $J(P, F) = 0$.

6.7   Effect of torsion

After deriving the bifurcation condition, we now focus on studying the effects of torsion on localized bulging. The cases of fixed axial force and fixed axial stretch will be investigated separately. In this section the bifurcation condition (6.15) will be solved
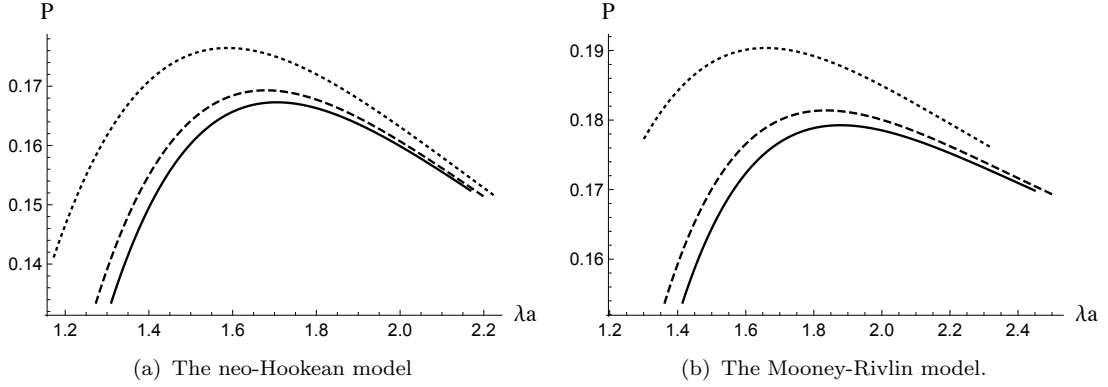
(a) The neo-Hookean model

(b) The Mooney-Rivlin model.

Figure 6.4: The pressure P as a function of λ_a for different values of M_0, $A = 0.8$, and $F = 0$. Solid, dashed, and dotted lines correspond to $M_0 = 0, 0.3, 0.6$, respectively.

when both the neo-Hookean and Mooney-Rivlin material models are used. From now on, we set $B = 1$ without loss of generality. In the case of the neo-Hookean model, we assume that the shear modulus $\mu = 1$. Also, we assume that $\mu_1 = 0.9$ and $\mu_2 = 0.1$ for the Mooney-Rivlin material model. Localized bulging may disappear with different values of μ_1 and μ_2.

6.7.1 Fixed axial force

It is well known that localized bulging would take place when the internal pressure P attains its maximum for the case of fixed resultant axial force F, see Fu et al. (2016). In order to illustrate this correspondence, we first specify A and M_0 and then solve $F = F_0$ numerically to express λ_z in terms of λ_a, where F_0 is a constant. Thus, the connection between P and λ_a can be obtained using equation (6.9). So, the

pressure as a function of the circumferential stretch curve is shown in Figure (6.4) for different values of M_0. As expected, the critical point (λ_z, λ_a) at which the pressure reaches its maximum is indeed the intersection point when we draw the contour plots of $J(P, F) = 0$ and $F = 0$ in the (λ_z, λ_a)-plane. Obviously, the pressure maximum increases along with the increasing of the twisting moment M_0, although the value of the principal stretches λ_z and λ_a decrease. This is also true for different values A and F_0 although not shown. This is presented in detail in Table (6.1) for the neo-Hookean model.

M_0	0.1	0.2	0.3	0.4	0.5	0.6	0.7	0.8
λ_a	1.7024	1.6940	1.6795	1.6581	1.6284	1.5882	1.5324	1.4492
λ_z	1.1773	1.1758	1.1732	1.1695	1.1645	1.1581	1.1501	1.1399
P_{max}	0.1675	0.1681	0.1693	0.1709	0.1733	0.1764	0.1807	0.1867
γ	0.0374	0.0755	0.1154	0.158	0.205	0.2588	0.3242	0.4131

Table 6.1: The corresponding critical values of the stretches, pressure maximum, and γ when localized bulging occurs for different M_0 and $F = 0$.

The N-shaped curves of the pressure against the circumferential stretch λ_a, or the pressure against the volume, are observed for the majority of material models with a local maximum and a local minimum. This observation is also consistent with experimental results (Wang et al., 2019). However, this feature disappears when the neo-Hookean and Mooney-Rivlin models are used.
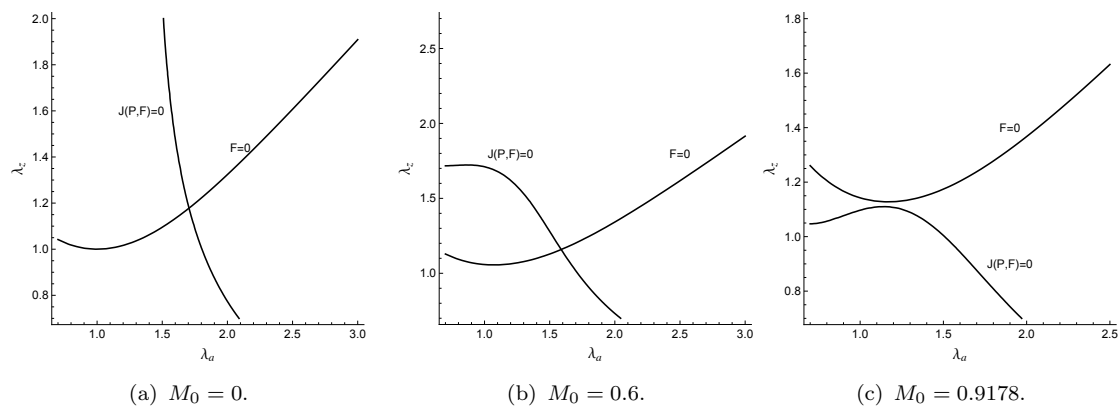
Figure 6.5: The bifurcation condition curves and $F = 0$ for different values of M_0 when the neo-Hookean model is used.
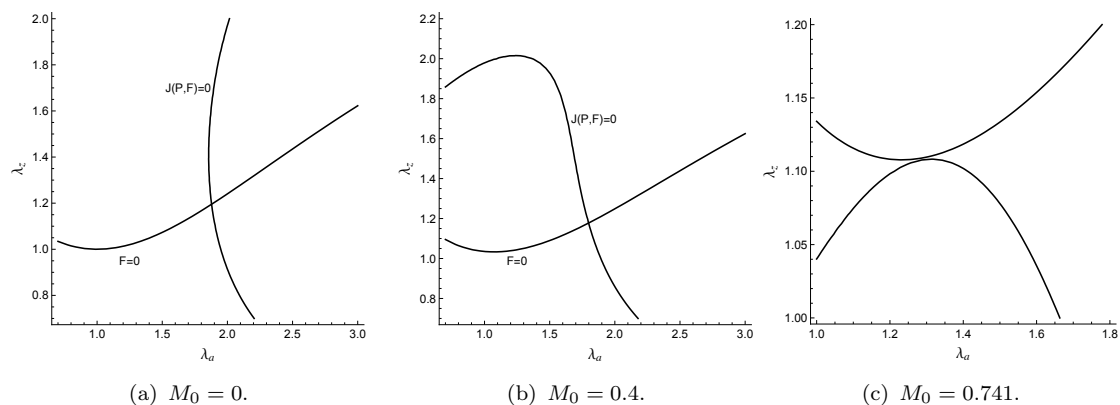
Figure 6.6: The bifurcation condition curves and $F = 0$ for different values of M_0 when the Mooney-Rivlin model is used.

Now, we can use the bifurcation condition (6.15) to determine the critical value of M_{0cr} at which localized bulging may become impossible. We first specify the inner radius by $A = 0.8$ and investigate the effect of M_0. Figures (6.5) and (6.6) show that as M_0 is increased from zero, localized bulging may appear until M_0 reaches a critical

131

Figure 6.7: The pressure P as a monotonic function of λ_a when localized bulging becomes impossible in the case of fixed axial force and for the neo-Hookean model.

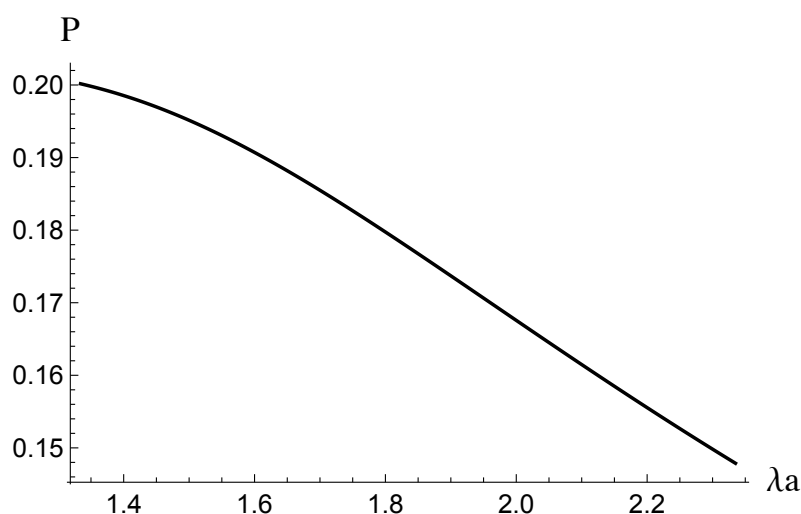value after which the bifurcation condition $J(P, F) = 0$ and $F = 0$ do not have any intersection. In this case, the pressure is a monotonic function of λ_a; see for example Figure (6.7). We also observe that when F_0 is increased, the critical value of M_{0cr} to prevent localized bulging is decreased. For instance, when $F_0 = 0.5$, we find that the corresponding critical value M_{0cr} for avoiding localized bulging is 0.7984 for the neo-Hookean model.

Finally, we consider the effects of wall thickness on the initiation of the bulge. Without torsion, we note that localized bulging occurs when the resultant axial force is zero for the neo-Hookean and Mooney-Rivlin models, no matter how thick the tube is. Therefore, we focus our attention on determining the critical value M_{0cr} above which localized bulging will not form. Figure (6.8) and Figure (6.9) show that as the thickness of tube is increased, meaning A is decreased, the critical value M_{0cr} to remove bulging

132

(a) $M_{0cr} = 0.0556, A = 0.99.$

(b) $M_{0cr} = 0.5066, A = 0.9.$

(c) $M_{0cr} = 0.723, A = 0.85.$

(d) $M_{0cr} = 1.255, A = 0.7.$

Figure 6.8: The critical values M_{0cr} at which the curves $J(P, F) = 0$ and $F = 0$ have no intersections for the various A for the neo-Hookean model.

(a) $M_{0cr} = 0.045$, $A = 0.99$.

(b) $M_{0cr} = 0.411$, $A = 0.9$.

(c) $M_{0cr} = 0.585$, $A = 0.85$.
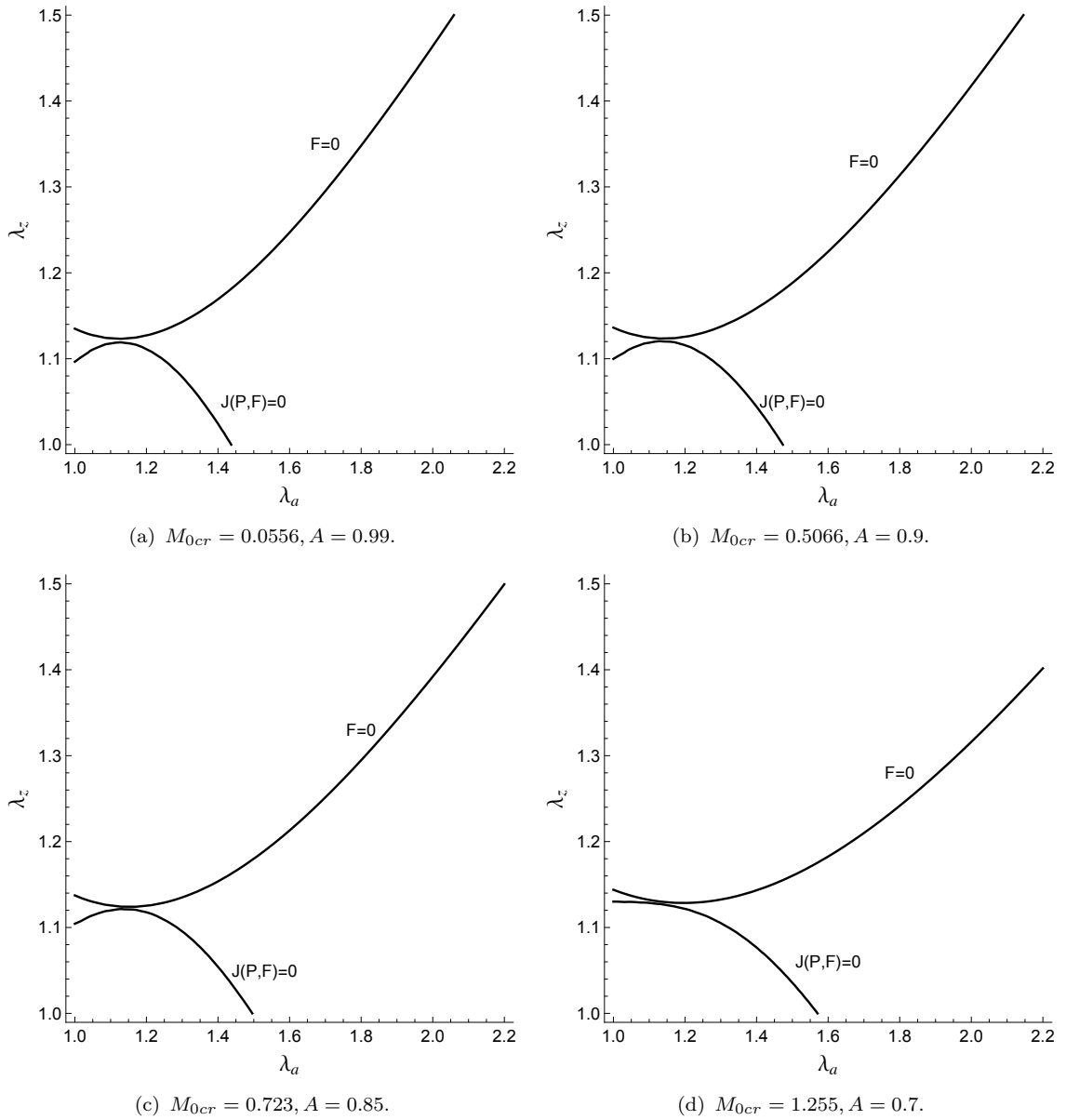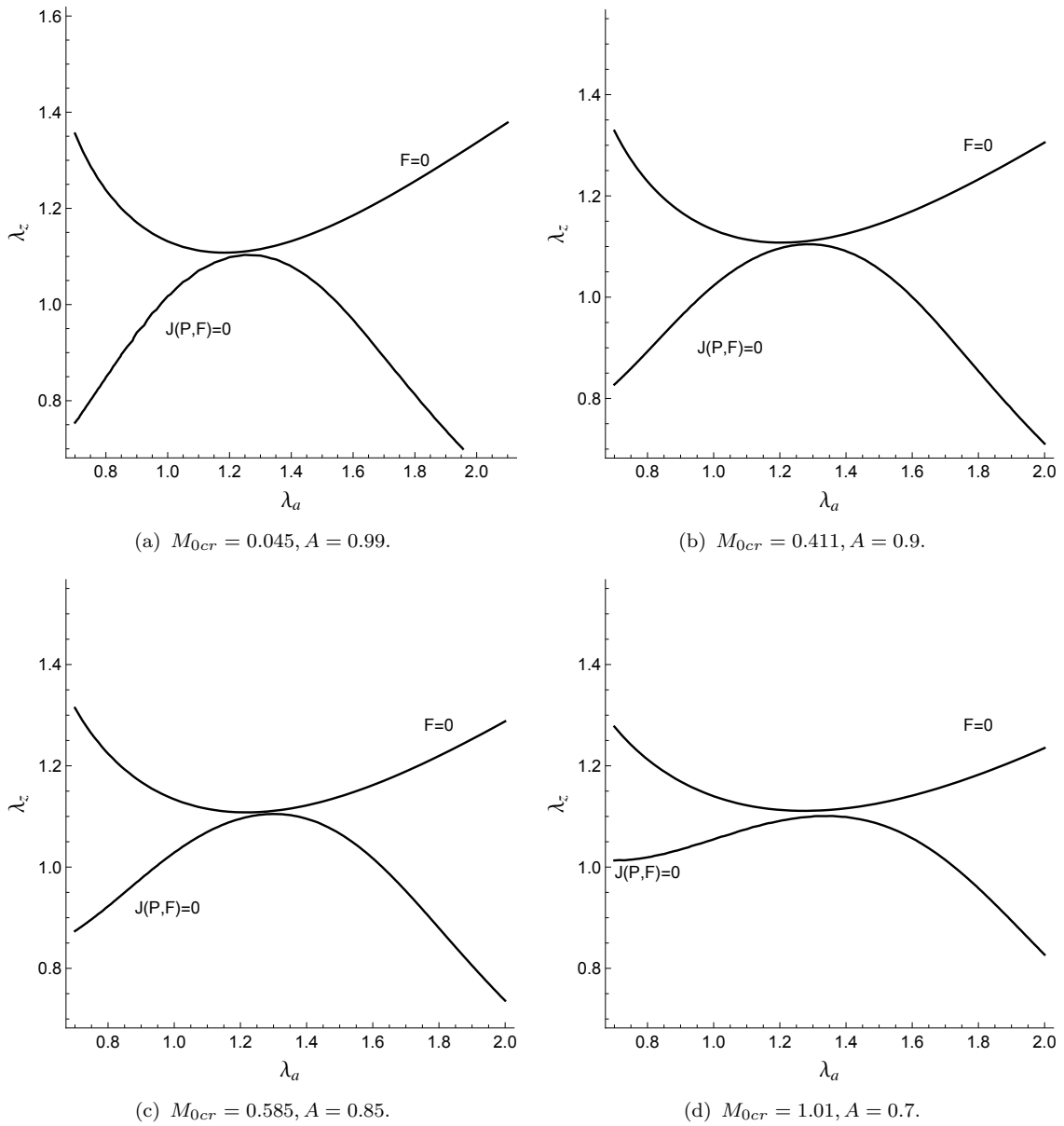
(d) $M_{0cr} = 1.01$, $A = 0.7$.

Figure 6.9: The critical values M_{0cr} at which the curves $J(P, F) = 0$ and $F = 0$ have no intersections for different values of A for the Mooney-Rivlin model.
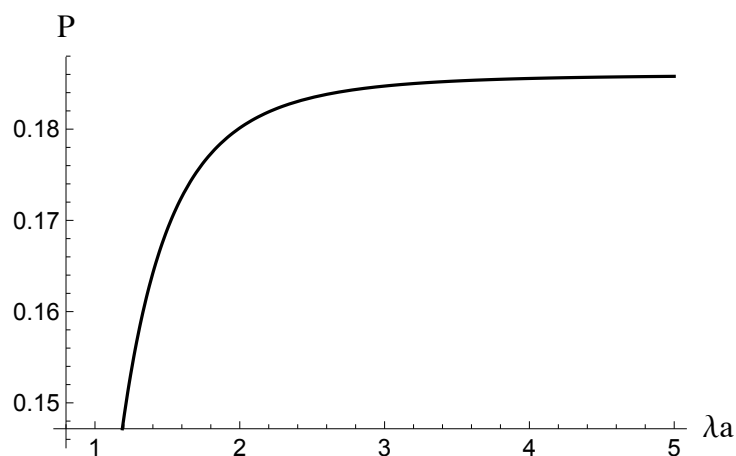
Figure 6.10: The pressure P againest the circumferential stretch λ_a in the case of fixed axial stretch when the neo-Hookean model is used where $M_0 = 0.6$, $A = 0.8$, and $\lambda_{z0} = 1.2$.

formation is increased. It is clear that adding a small twisting moment to the thin-walled tube has a significant effect on localized bulging. Thus, the critical value of M_0 to avoid localized bulging in thick-walled tubes is higher than the critical value of M_0 in thin-walled tubes. We mention that, when $M_0 < M_{0cr}$, the two curves $J(P, F) = 0$ and $F = 0$ have an intersection.

6.7.2 Fixed axial stretch

The pressure is a monotonic function of λ_a in the case of fixed axial stretch λ_z for some material models as mentioned in Chapter 4 ; see Figure (6.10). Hence, localized bulging may occur if $J(P, F) = 0$ and $\lambda_z = \lambda_{z0}$ have an intersection, where λ_{z0} is a constant. In Figures (6.11) and (6.12), we draw the contour plots of $J(P, F) = 0$ when $A = 0.8$ and $M_0 = 0, 0.6$, respectively. In the absence of torsion, it is known
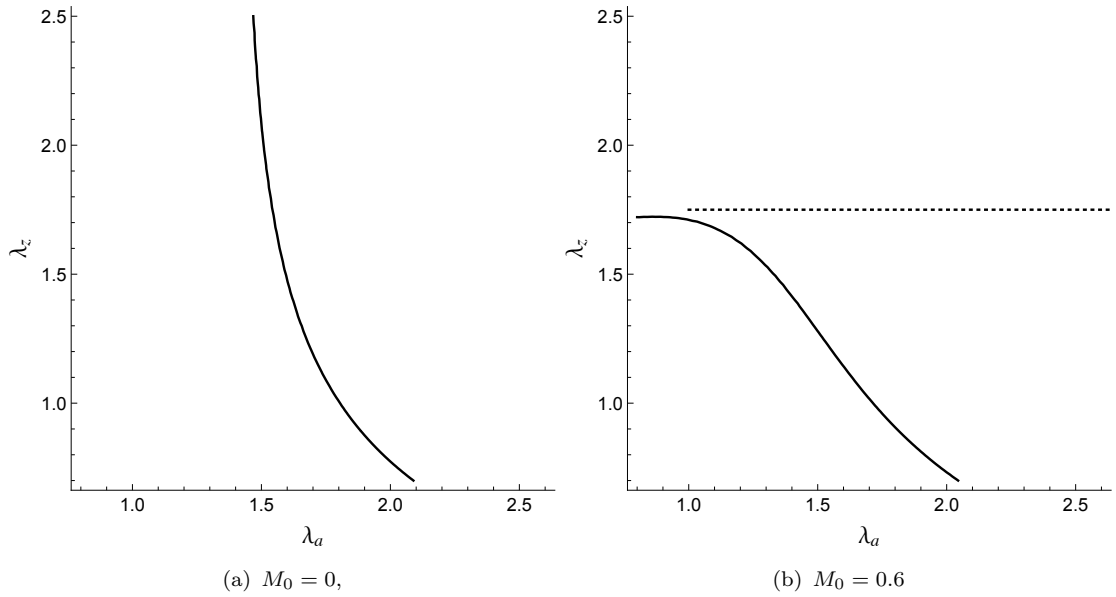
135

(a) $M_0 = 0$,

(b) $M_0 = 0.6$

Figure 6.11: The bifurcation curves for the neo-Hookean model when $A = 0.8$.

that localized bulging can occur for any isotropic material in the case of fixed axial stretch. However, this does not hold true when the torsion is present. The right plot of Figure (6.11) shows that localized bulging becomes impossible when $M_0 = 0.6$ and $\lambda_z \geq 1.74$ for the neo-Hookean model. In the case of the Mooney-Rivlin material, localized bulging becomes impossible when $M_0 = 0.6$ and $\lambda_z \geq 1.36$.

As mentioned previously, the bifurcation condition $J(P, F) = 0$ can be used for two loading types. Therefore, the bifurcation condition curves in Figures (6.8) and (6.9) can be utilized for fixed axial stretch case. So, it can also be seen that localized bulging will never occur if the tube is first uniformly stretched by $\lambda_{z0} \geq 1.15$ and then twisted by $M_0 = 0.5$ for instance; see Figure (6.8) (b). Note that increasing F_0 for the first case has similar effect when we increasing λ_{z0} for the second case.

(a) $M_0 = 0$,

(b) $M_0 = 0.6$
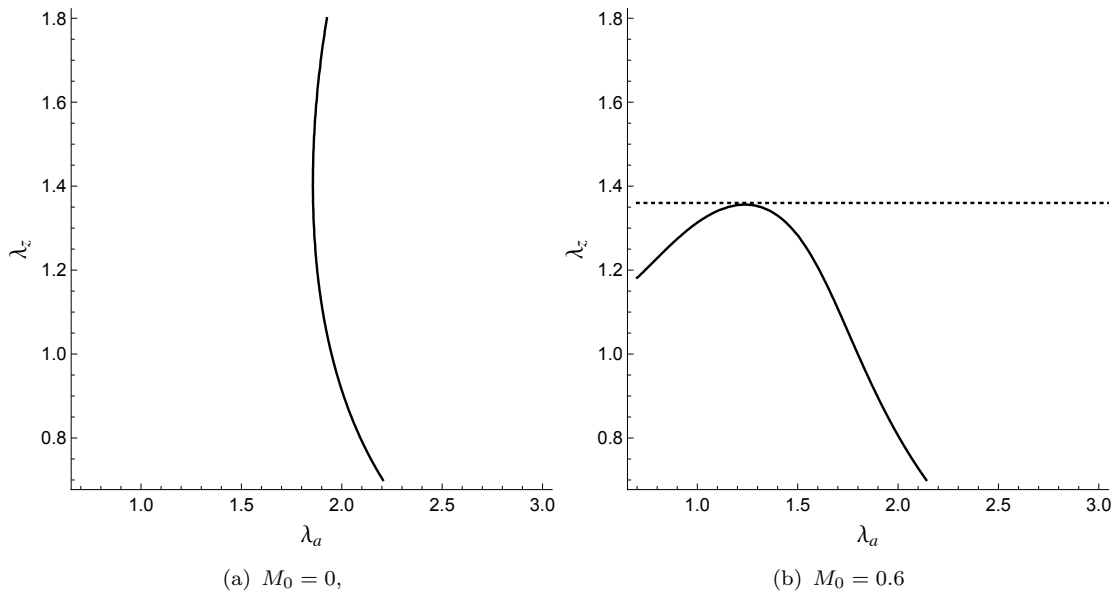
Figure 6.12: The bifurcation curves for the Mooney-Rivlin model when $A = 0.8$.

(a) $A = 0.99$.

(b) $A = 0.8$.
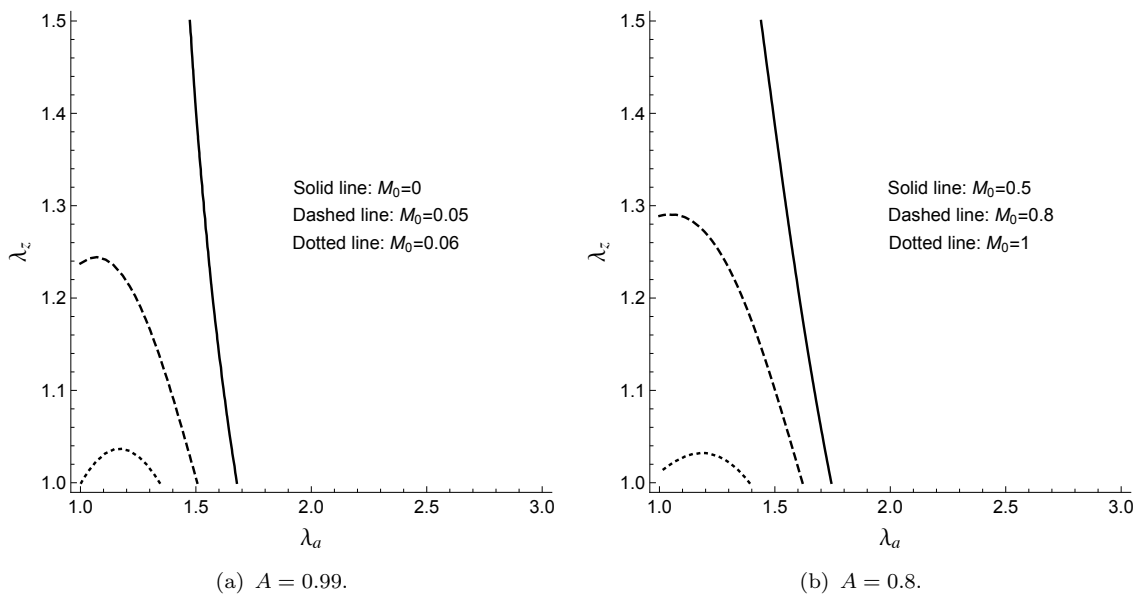
Figure 6.13: Evolution of the bifurcation condition $J(P, F) = 0$ with respect to M_0 for the neo-Hookean model.

(a) $A = 0.99$.

(b) $A = 0.8$.
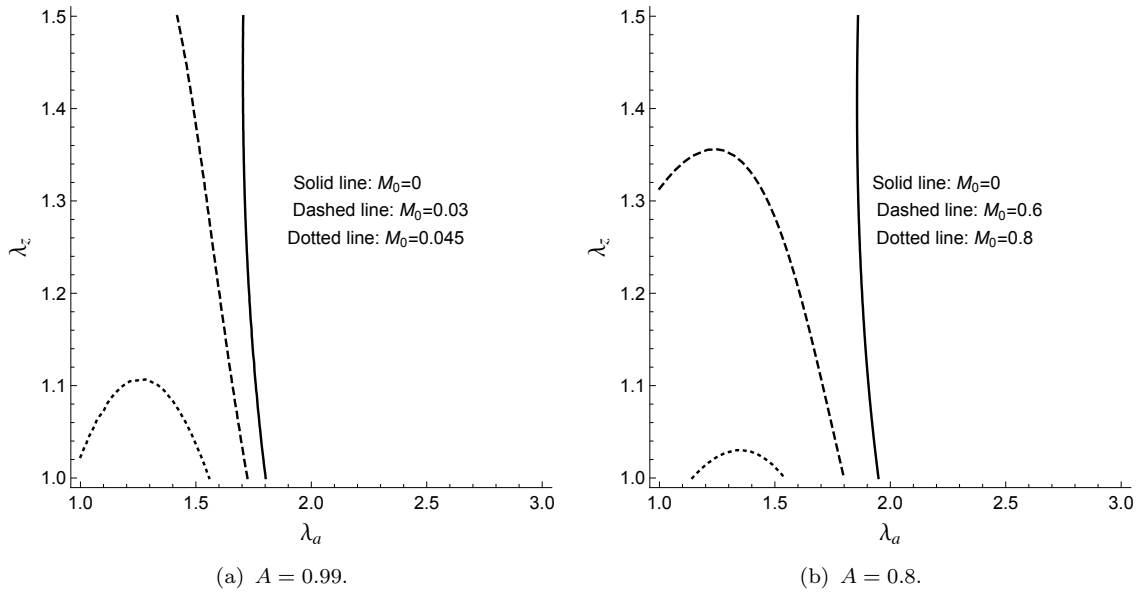
Figure 6.14: Evolution of the bifurcation condition $J(P, F) = 0$ with respect to M_0 for the Mooney-Rivlin model.

By varying the inner radius A, we may study the effect of thickness, since we fix $B = 1$. For the neo-Hookean model, Figure (6.13) shows that as M_0 is increased, the bifurcation condition $J(P, F) = 0$ curve moves down until it reaches a certain critical value in which the $J(P, F) = 0$ curve disappears. For instance, if $A = 0.99$, then localized bulging is unlikely to take place when $M_0 \geqslant 0.07$. Furthermore, the bifurcation curves for the Mooney-Rivlin model are illustrated in Figure (6.14), and a similar feature is observed.

6.8   Bifurcation condition for wrinkling

When a tube is subject to axial load, internal pressure and torsion, wrinkling may be observed due to compressive stresses. Since we are interested in localized bulging only, we assume that the amount of twist is small to avoid the possibility of wrinkling. Thus, wrinkling regions will be determined, in this section, by solving the eigenvalue problem derived earlier.

In parallel with section 6.4, we first look for a solution of the form

$$[v, w] = [V(r), W(r)] \ \sin(\alpha \ z),$$
$$[u, p^*] = [U(r), P(r)] \ \cos(\alpha \ z),$$

(6.57)

where $\alpha = 2n\pi/(\lambda_z L)$ is the axial wave number and n is the axial mode number. Similarly, the components of the incremental nominal stress tensor are given by

$$\hat{S}_{0rr} = \frac{1}{r} S_{0rr}(r) \ \cos(\alpha \ z),$$
$$\left[\hat{S}_{0r\theta}, \hat{S}_{0rz} \right] = \left[\frac{1}{r} S_{0r\theta}(r), \frac{1}{r} S_{0rz}(r) \right] \ \sin(\alpha \ z).$$

(6.58)

It follows that

$$\frac{d\boldsymbol{z}(r)}{dr} = \frac{1}{r}(\mathbf{G_3} - \boldsymbol{z}\mathbf{G_1} - \boldsymbol{z}\mathbf{G_2}\boldsymbol{z} + \mathbf{G_4}\boldsymbol{z}).$$

(6.59)
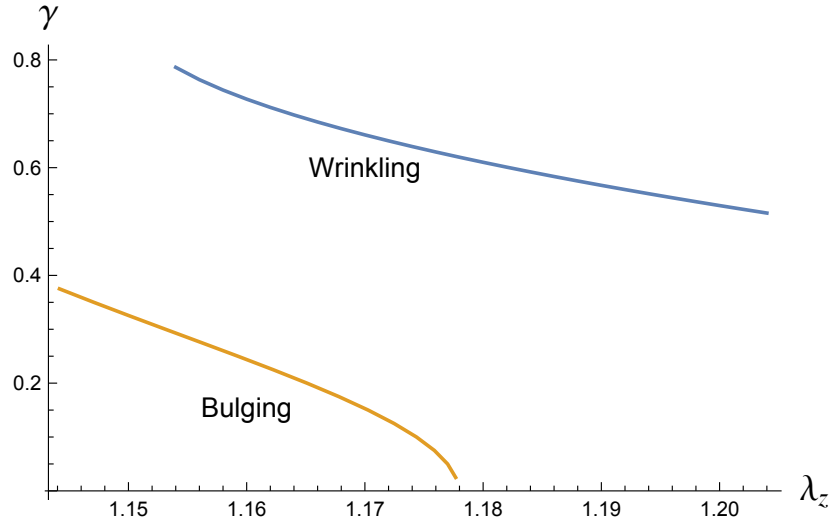
Figure 6.15: The relation between the torsion γ and the axial stretch λ_z in the case of fixed axial force when $L = 5$.

where $\mathbf{G_1}, \mathbf{G_2}, \mathbf{G_3}$, and $\mathbf{G_4}$ are not written here for the sake of brevity. In this case, the boundary conditions (6.20) are given by

$$\mathbf{z}(b) = 0, \quad \text{on} \quad r = b, \tag{6.60}$$

$$\det \left[\mathbf{z}(a) - P \begin{pmatrix} -1 & 0 & -\alpha\, a \\ 0 & -1 & 0 \\ -a\, \alpha & 0 & 0 \end{pmatrix} \right] = 0, \quad \text{on} \quad r = a. \tag{6.61}$$

We present numerical results for the two cases by assuming that $B = \mu = 1$ and $A = 0.8$. We may set the axial mode number $n = 1$ and vary the length L. In the case of fixed axial force, Figure (6.15) shows the relation between the torsion and the axial stretch λ_z where λ_a has been eliminated using $F = 0$. It seems that the value
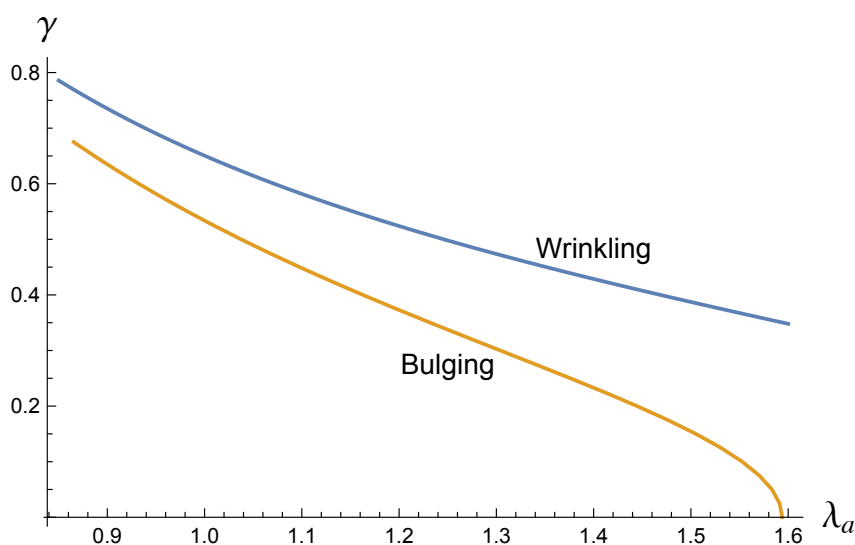
Figure 6.16: The relation between the torsion γ and the circumferential stretch λ_a in the case of fixed axial stretch $\lambda_z = 1.5$ when $L = 5$.

of γ required for the wrinkling solution is higher than the value of γ required for the bulging solution. The bulging curve is obtained by using $J(P, F) = 0$ and $F = 0$. The same feature also holds for fixed axial stretch λ_z; see Figure (6.16).

6.9   Conclusion

We have shown that when the twisting moment M is fixed, the bifurcation condition for localized bulging of a twisted tube under the combined action of internal pressure P and axial force F is simply the vanishing of the Jacobian of P and F. Moreover, in the case of fixed resultant axial force, we find that the critical pressure corresponding to the onset of localized bulging is increased as the twisting moment is increased, although the values of the principal stretches λ_z and λ_a are decreased. The critical

values of the twisting moment at which localized bulging may not occur are obtained in the cases of fixed resultant axial force and fixed axial stretch. The effects of wall thickness of the twisted tube on localized bulging are studied. In particular, it is shown that the effect of torsion on localized bulging is significant in thin tubes.

Generally speaking, the same procedure can be applied to study localized bulging for other material models. However, we may have some difficulties through the calculations. For instance, when we use the Gent material model, it is difficult to integrate equation (6.7) analytically. Therefore, a numerical approach is needed.

Chapter 7

Conclusions

In this thesis, we have studied the effect of rotation, multi-layering and torsion on localized bulging in hyperelastic tubes. Firstly, the bifurcation condition for localized bulging of a cylinder and tube is derived under the effect of rotation. Illustrative numerical results are presented using the Ogden and Gent material models. Although the numerical results are mostly given for $A = 0.8$, our simple representation of the bifurcation condition can be used to evaluate the effects of wall thickness and dependence on the material model in a straightforward manner if required. We remark that the bifurcation condition derived is only a necessary condition for localized bulging to occur. Strictly speaking, whether localized bulging can actually take place at the critical value of rotation can only be established by a weakly nonlinear analysis.

In chapter 4, we have focussed on localized bulging in a bilayer tube composed of an incompressible Gent material model. By considering a bilayer tube where one layer

cannot bulge, we determined several critical values marking the transitions between bulging and no bulging ranges. In any engineering situation where bulging formation should be eliminated, for instance, the design of Anaconda wave-energy extraction device Bucchi and Hearn (2013), the current study could provide useful insights. Furthermore, we provide a deeper understanding of the relation between the stretching ability and localized bulging of a tube. Actually, they are a pair of contradiction, which means that a tube has a higher stretching ability is easier to bulge. Our study extends the current understanding of localized bulging in a hyperelastic tube of arbitrary thickness (Fu et al., 2016; Wang and Fu, 2018) to layered structures.

In chapter 5, we have studied the effect of the modulus ratio and the constitutive model on the bulging initiation. This work supports the viewpoint that aneurysm becomes possible in human arteries with age or pathological change since a lower critical volume ration v_{cr} is attained if the inner layer is stiffening. Indeed, it is precisely true that the innermost layer (intima) stiffens more than other layers in human arteries with age (Kohn et al., 2015).

In chapters 4 and 5, we have assumed that the bilayer tube is made of an isotropic elastic material. Our study can be extended to the case when the bilayer tube is helically reinforced by two families of identical fibres. As demonstrated in a recent study for a single layer tube (Wang and Fu, 2018), it is expected that the fibres will have a drastic effect on localized bulging. To be more precise, using fibre-reinforcement can be a very effective method to construct anti-bulging tubes.

The main contribution of chapter 6 is to study the effect of torsion on the onset of localized bulging. It is shown that the torsion has a significant effect on localized bulging. We note that the pressure against the volume does not have a minimum, which contradicts the experimental observations. Thus, the neo-Hookean and the Mooney-Rivlin material models seem to be inappropriate for modelling bulge initiation and propagation. We, therefore, wish to extend this research to other more appropriate material models.

Finally, we mention that it is enough to use an infinitely long tube to carry out all theoretical analyses since the end effects only act as a minor factor and can be treated as an imperfection as long as the ratio L/B is greater than or equal to 30. Therefore, an infinitely long tube can be used to capture most features of localized bulging.

References

J. E. Adkins and R. S. Rivlin. Large elastic deformations of isotropic materials IX. The deformation of thin shells. *Philosophical Transactions of the Royal Society of London. Series A, Mathematical and Physical Sciences*, 244(888):505–531, 1952.

H. Alexander. The tensile instability of an inflated cylindrical membrane as affected by an axial load. *International Journal of Mechanical Sciences*, 13(2):87–95, 1971.

A. A. Alhayani, J. Rodríguez, and J. Merodio. Competition between radial expansion and axial propagation in bulging of inflated cylinders with application to aneurysms propagation in arterial wall tissue. *International Journal of Engineering Science*, 85:74–89, 2014.

V. Balbi and P. Ciarletta. Helical buckling of thick-walled, pre-stressed, cylindrical tubes under a finite torsion. *Mathematics and Mechanics of Solids*, 20(6):625–642, 2015.

S. V. Biryukov. Impedance method in the theory of elastic surface waves. *Soviet Physics Acoustics*, 31(5):350–354, 1985.

References

A. Bucchi and G. E. Hearn. Delay or removal of aneurysm formation in the anaconda wave energy extraction device. *Renewable energy*, 55:104–119, 2013.

P. Chadwick. *Continuum Mechanics: Concise Theory and Problems.* Courier Corporation, 1999.

P. Chadwick, C. F. Creasy, and V. G. Hart. The deformation of rubber cylinders and tubes by rotation. *The Journal of the Australian Mathematical Society*, 20(1):62–96, 1977.

E. Chater and J. W. Hutchinson. On the propagation of bulges and buckles. *Journal of applied mechanics*, 51(2):269–277, 1984.

M. Destrade and G. Saccomandi. *Waves in nonlinear pre-stressed materials*, volume 495. Springer Science & Business Media, 2007.

Y. B. Fu and A. T. Il'Ichev. Localized standing waves in a hyperelastic membrane tube and their stabilization by a mean flow. *Mathematics and Mechanics of Solids*, 20(10):1198–1214, 2015.

Y. B. Fu and R. W. Ogden. *Nonlinear Elasticity: Theory and Applications.* Cambridge University Press, 2001.

Y. B. Fu and Y. X. Xie. Stability of localized bulging in inflated membrane tubes under volume control. *International Journal of Engineering Science*, 48(11):1242–1252, 2010.

Y. B. Fu and Y. X. Xie. Effects of imperfections on localized bulging in inflated membrane tubes. *Philosophical Transactions of the Royal Society A: Mathematical, Physical and Engineering Sciences*, 370(1965):1896–1911, 2012.

Y. B. Fu, S. Pearce, and K. Liu. Post-bifurcation analysis of a thin-walled hyperelastic tube under inflation. *International Journal of Non-Linear Mechanics*, 43(8):697–706, 2008.

Y. B. Fu, G. A. Rogerson, and Y. T. Zhang. Initiation of aneurysms as a mechanical bifurcation phenomenon. *International Journal of Non-Linear Mechanics*, 47(2): 179–184, 2012.

Y. B. Fu, J. L. Liu, and G. S. Francisco. Localized bulging in an inflated cylindrical tube of arbitrary thickness–the effect of bending stiffness. *Journal of the Mechanics and Physics of Solids*, 90:45–60, 2016.

Y. B. Fu, L. Dorfmann, and Y. Xie. Localized necking of a dielectric membrane. *Extreme Mechanics Letters*, 21:44–48, 2018.

Y. C. Fung. Elasticity of soft tissues in simple elongation. *American Journal of Physiology-Legacy Content*, 213(6):1532–1544, 1967.

T. C. Gasser, R. W. Ogden, and G. A. Holzapfel. Hyperelastic modelling of arterial layers with distributed collagen fibre orientations. *Journal of the royal society interface*, 3(6):15–35, 2005.

A. Gent. *Engineering with rubber: how to design rubber components*. Hanser Publications, 2001.

A. N. Gent. A new constitutive relation for rubber. *Rubber chemistry and technology*, 69(1):59–61, 1996.

A. N. Gent and R. S. Rivlin. Experiments on the mechanics of rubber II: The torsion, inflation and extension of a tube. *Proceedings of the Physical Society. Section B*, 65 (7):487, 1952.

P. B. Gonçalves, D. Pamplona, and S. R. X. Lopes. Finite deformations of an initially stressed cylindrical shell under internal pressure. *International Journal of Mechanical Sciences*, 50(1):92–103, 2008.

A. E. Green and J. E. Adkins. *Large elastic deformations and non-linear continuum mechanics*. Clarendon Press, 1960.

A. E. Green and W. Zerna. *Theoretical elasticity*. Courier Corporation, 1992.

Z. Guo, J. Gattas, S. Wang, L. Li, and F. Albermani. Experimental and numerical investigation of bulging behaviour of hyperelastic textured tubes. *International Journal of Mechanical Sciences*, 115:665–675, 2016.

M. El Hamdaoui, J. Merodio, R. W. Ogden, and J. Rodríguez. Finite elastic deformations of transversely isotropic circular cylindrical tubes. *International Journal of Solids and Structures*, 51(5):1188–1196, 2014.

M. Haragus and G. Iooss. *Local bifurcations, center manifolds, and normal forms in infinite-dimensional dynamical systems.* Springer Science & Business Media, 2010.

D. M. Haughton and R. W. Ogden. Bifurcation of inflated circular cylinders of elastic material under axial loading I. Membrane theory for thin-walled tubes. *Journal of the Mechanics and Physics of Solids*, 27(3):179–212, 1979a.

D. M. Haughton and R. W. Ogden. Bifurcation of inflated circular cylinders of elastic material under axial loading II. Exact theory for thick-walled tubes. *Journal of the Mechanics and Physics of Solids*, 27(5-6):489–512, 1979b.

D. M. Haughton and R. W. Ogden. Bifurcation of finitely deformed rotating elastic cylinders. *The Quarterly Journal of Mechanics and Applied Mathematics*, 33(3): 251–266, 1980a.

D. M. Haughton and R. W. Ogden. Bifurcation of rotating circular cylindrical elastic membranes. In *Mathematical Proceedings of the Cambridge Philosophical Society*, volume 87, pages 357–376. Cambridge University Press, 1980b.

D. M. Haughton and R. W. Ogden. Bifurcation of rotating thick-walled elastic tubes. *Journal of the Mechanics and Physics of Solids*, 28(1):59–74, 1980c.

A. G. Holzapfel, T. C. Gasser, and R. W. Ogden. A new constitutive framework for arterial wall mechanics and a comparative study of material models. *Journal of elasticity*, 61(1-3):1–48, 2000.

G. A. Holzapfel. *Nonlinear Solid Mechanics: A Continuum Approach for Engineering.* Wiley, Chichester, 2000.

C. O. Horgan and G. Saccomandi. A description of arterial wall mechanics using limiting chain extensibility constitutive models. *Biomechanics and modeling in mechanobiology*, 1(4):251–266, 2003.

L. Hornỳ, M. Netušil, and T. Voňavková. Axial prestretch and circumferential distensibility in biomechanics of abdominal aorta. *Biomechanics and modeling in mechanobiology*, 13(4):783–799, 2014.

L. Hornỳ, M. Netušil, and Z. Horák. Limit point instability in pressurization of anisotropic finitely extensible hyperelastic thin-walled tube. *International Journal of Non-Linear Mechanics*, 77:107–114, 2015.

J. W. Hutchinson and K. W. Neale. Neck propagation. *Journal of the Mechanics and Physics of Solids*, 31(5):405–426, 1983.

A. T. Il'Ichev and Y. B. Fu. Stability of aneurysm solutions in a fluid-filled elastic membrane tube. *Acta Mechanica Sinica*, 28(4):1209–1218, 2012.

L. M. Kanner and C. O. Horgan. Elastic instabilities for strain-stiffening rubber-like spherical and cylindrical thin shells under inflation. *International Journal of Non-Linear Mechanics*, 42(2):204–215, 2007.

K. Kirchgässner. Wave-solutions of reversible systems and applications. *Journal of Differential Equations*, 45(1):113–127, 1982.

J. C. Kohn, M. C. Lampi, and C. A. Reinhart-King. Age-related vascular stiffening: causes and consequences. *Frontiers in genetics*, 6:112, 2015.

A. D. Kydoniefs. Finite axisymmetric deformations of an initially cylindrical elastic membrane enclosing a rigid body. *The Quarterly Journal of Mechanics and Applied Mathematics*, 22(3):319–331, 1969.

S. Kyriakides and C. D. Babcock. Experimental determination of the propagation pressure of circular pipes. *Journal of Pressure Vessel Technology*, 103(4):328–336, 1981.

S. Kyriakides and Y. C. Chang. On the inflation of a long elastic tube in the presence of axial load. *International journal of solids and structures*, 26(9-10):975–991, 1990.

S. Kyriakides and Y. C. Chang. The initiation and propagation of a localized instability in an inflated elastic tube. *International Journal of Solids and Structures*, 27(9): 1085–1111, 1991.

Y. Liu, Y. Ye, A. Althobaiti, and Y. Xie. Prevention of localized bulging in an inflated bilayer tube. *International Journal of Mechanical Sciences*, 153:359–368, 2019.

A. Mallock. Note on the instability of india-rubber tubes and balloons when distended by fluid pressure. *Proceedings of the Royal Society of London*, 49(296-301):458–463, 1891.

R. Mangan and M. Destrade. Gent models for the inflation of spherical balloons. *International Journal of non-linear mechanics*, 68:52–58, 2015.

G. Mao, T. Li, Z. Zou, S. Qu, and M. Shi. Prestretch effect on snap-through instability of short-length tubular elastomeric balloons under inflation. *International Journal of Solids and structures*, 51(11-12):2109–2115, 2014.

J. Merodio and R. W. Ogden. Extension, inflation and torsion of a residually stressed circular cylindrical tube. *Continuum Mechanics and Thermodynamics*, 28(1-2):157–174, 2016.

M. Mooney. A theory of large elastic deformation. *Journal of applied physics*, 11(9):582–592, 1940.

A. N. Norris and A. Shuvalov. Wave impedance matrices for cylindrically anisotropic radially inhomogeneous elastic solids. *The Quarterly Journal of Mechanics & Applied Mathematics*, 63(4):401–435, 2010.

R. W. Ogden. Large deformation isotropic elasticity. on the correlation of theory and experiment for incompressible rubberlike solids. *Proceedings of the Royal Society of London. A. Mathematical and Physical Sciences*, 326(1567):565–584, 1972.

R. W. Ogden. *Non-linear elastic deformations*. Courier Corporation, 1997.

D. C. Pamplona and D. Mota. Numerical and experimental analysis of inflating a circular hyperelastic membrane over a rigid and elastic foundation. *International Journal of Mechanical Sciences*, 65(1):18–23, 2012.

D. C. Pamplona, P. B. Goncalves, and S. R. X. Lopes. Finite deformations of cylindrical membrane under internal pressure. *International journal of mechanical sciences*, 48 (6):683–696, 2006.

J. C. Patterson and J. M. Hill. The stability of a solid rotating neo-hookean cylinder. *Mechanics Research Communications*, 4(1):69–74, 1977.

S. Pearce. Effect of strain-energy function and axial prestretch on the bulges, necks and kinks forming in elastic membrane tubes. *Mathematics and Mechanics of Solids*, 17(8):860–875, 2012.

S. Pearce and Y. B. Fu. Characterization and stability of localized bulging/necking in inflated membrane tubes. *IMA journal of applied mathematics*, 75(4):581–602, 2010.

E. Pucci and G. Saccomandi. A note on the gent model for rubber-like materials. *Rubber chemistry and technology*, 75(5):839–852, 2002.

J. S. Ren, J. W. Zhou, and X. Yuan. Instability analysis in pressurized three-layered fiber-reinforced anisotropic rubber tubes in torsion. *International Journal of Engineering Science*, 49(4):342–353, 2011.

R. S. Rivlin. Large elastic deformations of isotropic materials. I. Fundamental concepts. *Philosophical Transactions of the Royal Society of London. Series A, Mathematical and Physical Sciences*, 240(822):459–490, 1948.

R. S. Rivlin. Large elastic deformations of isotropic materials VI. Further results in the theory of torsion, shear and flexure. *Philosophical Transactions of the Royal Society of London. Series A, Mathematical and Physical Sciences*, 242(845):173–195, 1949.

J. Rodríguez and J. Merodio. A new derivation of the bifurcation conditions of inflated cylindrical membranes of elastic material under axial loading. application to aneurysm formation. *Mechanics Research Communications*, 38(3):203–210, 2011.

P. Seshaiyer and J. D. Humphrey. On the potentially protective role of contact constraints on saccular aneurysms. *Journal of biomechanics*, 34(5):607–612, 2001.

A. J. M. Spencer. Continuum mechanics, 1980.

A. N. Stroh. Dislocations and cracks in anisotropic elasticity. *Philosophical magazine*, 3(30):625–646, 1958.

A. N. Stroh. Steady state problems in anisotropic elasticity. *Journal of Mathematics and Physics*, 41(1-4):77–103, 1962.

L. A. Taber. *Nonlinear theory of elasticity: applications in biomechanics.* World Scientific, 2004.

N. Varatharajan and A. DasGupta. Study of bifurcation in a pressurized hyperelastic membrane tube enclosed by a soft substrate. *International Journal of Non-Linear Mechanics*, 95:233–241, 2017.

N. Varatharajan and A. DasGupta. Spectral stability of the bifurcation state of an arterial model with perivascular soft tissues. *Mechanics Research Communications*, 91:7–12, 2018.

J. Wang and Y. Fu. Effect of double-fibre reinforcement on localized bulging of an inflated cylindrical tube of arbitrary thickness. *Journal of Engineering Mathematics*, 109(1):21–30, 2018.

J. Wang, A. Althobaiti, and Y. B. Fu. Localized bulging of rotating elastic cylinders and tubes. *Journal of Mechanics of Materials and Structures*, 12(4):545–561, 2017.

S. Wang, Z. Guo, L. Zhou, L. Li, and Yibin Y. B. Fu. An experimental study of localized bulging in inflated cylindrical tubes guided by newly emerged analytical results. *Journal of the Mechanics and Physics of Solids*, 124:536–554, 2019.

T. Wang, F. Xu, Y. Huo, and M. Potier-Ferry. Snap-through instabilities of pressurized balloons: Pear-shaped bifurcation and localized bulging. *International Journal of Non-Linear Mechanics*, 98:137–144, 2018.

Stephen Wolfram. *Mathematica: a system for doing mathematics by computer.* Addison-Wesley, 1991.

Y. Ye, Y. Liu, A. Althobaiti, and Y. Xie. Localized bulging in an inflated bilayer tube of arbitrary thickness: Effects of the stiffness ratio and constitutive model. *International Journal of Solids and Structures*, 176:173–184, 2019.

References

O. H. Yeoh. Characterization of elastic properties of carbon-black-filled rubber vulcanizates. *Rubber chemistry and technology*, 63(5):792–805, 1990.

W. L. Yin. Non-uniform inflation of a cylindrical elastic membrane and direct determination of the strain energy function. *Journal of Elasticity*, 7(3):265–282, 1977.

L. Zhou, S. Wang, L. Li, and Y. Fu. An evaluation of the gent and gent-gent material models using inflation of a plane membrane. *International Journal of Mechanical Sciences*, 146:39–48, 2018.